8-1-2013

Analysis of the Effects of Severe Voltage Unbalance on the DC Bus of a Variable Frequency Drive and DC Bus Passive Filtering Harmonic Mitigation

Olusola Fawole
University of Wisconsin-Milwaukee

ANALYSIS OF THE EFFECTS OF SEVERE VOLTAGE UNBALANCE ON THE DC BUS OF A VARIABLE FREQUENCY DRIVE AND DC BUS PASSIVE FILTERING HARMONIC MITIGATION

By

Olusola Fawole

A Thesis Submitted in

Partial Fulfillment of the

Requirements for the Degree of

Master of Science

in Engineering

at

The University of Wisconsin-Milwaukee

August 2013

ANALYSIS OF THE EFFECTS OF SEVERE VOLTAGE UNBALANCE ON THE DC BUS OF A VARIABLE FREQUENCY DRIVE AND DC BUS PASSIVE FILTERING HARMONIC MITIGATION

By

Olusola Fawole

The University of Wisconsin-Milwaukee, 2013
Under the Supervision of Dr. David Yu

The power quality of a distribution system can greatly effect the way devices connected to that power source operate. Sometimes one poor power quality characteristic can lead to another poor power quality characteristic. In the case presented in this paper, severe voltage unbalance at the input of a variable frequency drive leads to increased harmonic content in the power distribution system and the devices under operation. This paper addresses, in particular, the effects of severe voltage unbalance on the DC bus of a 6-pulse variable frequency drive. The steady-state balanced voltage harmonic behavior of the DC bus is analyzed along with standard filtering techniques used to mitigate the characteristic harmonics on the DC bus. The steady-state severe unbalanced voltage harmonic behavior of the DC bus is then analyzed and additional filtering techniques are then introduced to mitigate the non-characteristic harmonics on the DC bus that were produced by the severe voltage unbalance. Simulations of the balanced and unbalanced conditions mentioned above are presented in MATLAB. Bode plots of the 6-pulse converter are then analyzed to measure the frequency response of the system under these conditions and the Fast Fourier Transform of different signals in the system are generated to graphically represent the harmonics in the system. Finally, experimental results will show the successful application of the filtering techniques, presented in this paper, on a 6-pulse variable frequency drive under severe voltage unbalance.

Table of Contents

List of Figures

List of Tables

Introduction

A power distribution system is often plagued by harmonics. Harmonics are undesired currents and voltages on a power distribution system that lead to poor power quality. These undesired currents and voltages are caused by non-linear loads. Non-linear loads simply mean the voltage waveform and current waveform do not share a linear relationship. The effects of harmonics on electronics on a power distribution system with poor power quality can be further worsen by the presence of steady state voltage unbalance. Steady state voltage unbalance typically arise from single phase equipment connected to a three phase distribution. Figure 1 shows 90% of U.S. distribution systems contain less than 3% voltage unbalance and 2% contain greater than 3% unbalance [9]. Systems that have more than 3% voltage unbalance are considered to be severely unbalanced in this paper.

One major contributor to harmonics on a power distribution system is a Variable Frequency Drive (VFD). VFD's use a three stage AC/DC, DC bus, DC/AC process to intelligently control an AC motor. The AC/DC stage is where the non-linear relationship develops between the voltage and current, which lead to harmonics on the power distribution system. Under the effects of voltage unbalance, the AC/DC stage of the VFD can enter into single phase operation. Under this mode of operation, a dominant second order harmonic emerges in the DC bus of the VFD. Since the VFD

uses a voltage source inverter topology, it is particularly important the DC bus remain as steady as possible. A steadier DC bus voltage leads to better motor performance and less torque pulsations during motor operation. The presence of a large second harmonic on the DC bus will impede the stability of the DC bus.

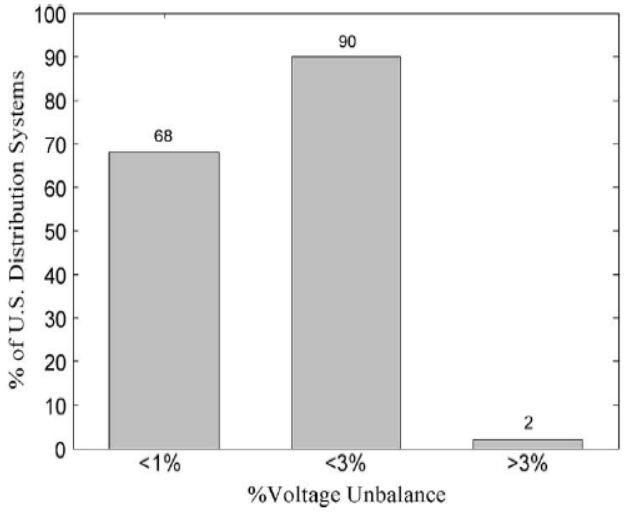

Figure 1: Voltage Unbalance Percentage in U.S. Distribution Systems

0.1 Aim and Objective

The general aim of this paper is to investigate the effects of severe voltage unbalance on the DC bus of a VFD and to also see the effects of passive filters on the DC bus of the VFD. The objectives of this paper are as follows,

1. Present parameters used to measure harmonics in power distribution systems.

2. Present Bode plots of the DC bus with and without passive filters on the DC bus.

3. Implement a model in Simulink® to simulate a VFD operating a motor under sever voltage unbalance conditions with and without passive filters on the DC bus.

4. Create an experimental set up to simulate a VFD operating a motor under severe voltage unbalance conditions with and without passive filters on the DC bus.

0.2 Chapter Outlines

Chapter 1: *The Basics of Harmonics* - Presents the basic calculations used to quantify harmonics

Chapter 2: *Problem Statement and Proposed Solution* - Presents the problem statement and the proposed solution investigated in this paper

Chapter 3: *Simulation* - Presents simulations of the different filter configurations on combination with different voltage conditions

Chapter 4: *Experimentation* - Presents an experimental set up of the different filtering configurations in combination with different voltage conditions

Chapter 5: *Experimentation and Simulation Results Comparison* - Presents an explanation for any discrepancies between experimental and simulation data

Chapter 6: *Conclusion* - Explains the correlation between the simulation and experimental results

Chapter 1

The Basics of Harmonics

1.1 Fourier Analysis

One of the most effective mathematical tools used in the study of power systems harmonics is the Fourier Series analysis. This tool allows any periodic waveform to be expressed as the sum of its individual harmonic components at different frequencies. Any periodic wave can be expressed as the following Fourier expansion,

$$f(t) = A_0 + \sum_{h=1}^{\infty} [A_h \cos(h\omega_0 t) + B_h \sin(h\omega_0 t)] \tag{1.1.1}$$

This equation can be simplified to,

$$f(t) = A_0 + \sum_{h=1}^{\infty} C_h \cos(h\omega_0 t + \psi_h) \tag{1.1.2}$$

The coefficients are defined as follows,

$$A_0 = \frac{1}{T} \int_0^T f(t) dt$$

$$A_h = \frac{2}{T} \int_0^T f(t) \cos(h\omega_0 t) dt$$

$$B_h = \frac{2}{T} \int_0^T f(t) \sin(h\omega_0 t) dt$$

$$C_h = \sqrt{A_h^2 + B_h^2}$$

$$\psi_h = \tan^{-1}(\frac{A_h}{B_h})$$

Equation (1.1.1) can be simplified based on the type of symmetry displayed by the waveform. For waveforms that display odd symmetry, that is when $f(-t) = -f(t)$, the cosine term goes to zero in equation (1.1.1). For waveforms that display even symmetry, that is when $f(-t) = f(t)$, the sine term now goes to zero in Equation (1.1.1). For waveforms that display half-wave symmetry, that is when $f(t^+_-\frac{T}{2}) = -f(t)$, the DC component goes to zero and there are no even harmonics in our Fourier expansion. An example of an odd waveform is shown in Figure 1.1.

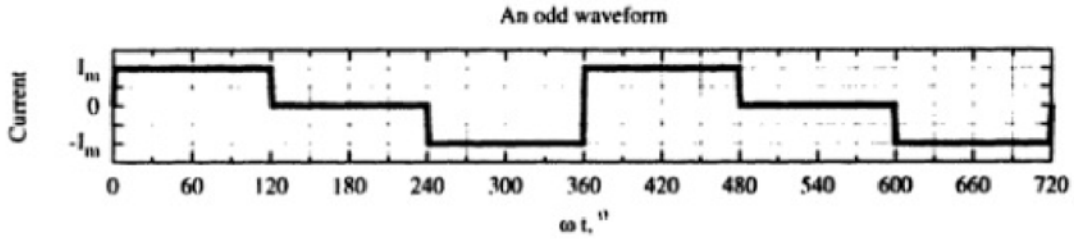

Figure 1.1: Example of an odd waveform

After simplifying the Fourier expansion for the odd waveform above and solving for the coefficients, the Fourier series is shown below.

$$f(t) = \sum_{h=1}^{\infty} \frac{I_m}{\pi h}[2 - \cos(\frac{2\pi h}{3}) - \cos(\frac{4\pi h}{3})] \sin(h\omega_0 t)$$

This series can be simplified to,

$$f(t) = \sum_{\substack{h=1 \\ h\neq 3,6,9,12,...}}^{\infty} 3\frac{I_m}{\pi h} \sin(h\omega_0 t)$$

The MATLab plot in Figure 1.2 shows the waveforms for different series. From the plots we can see that the waveforms better resembles the original waveform when we

increase the number of harmonic orders.

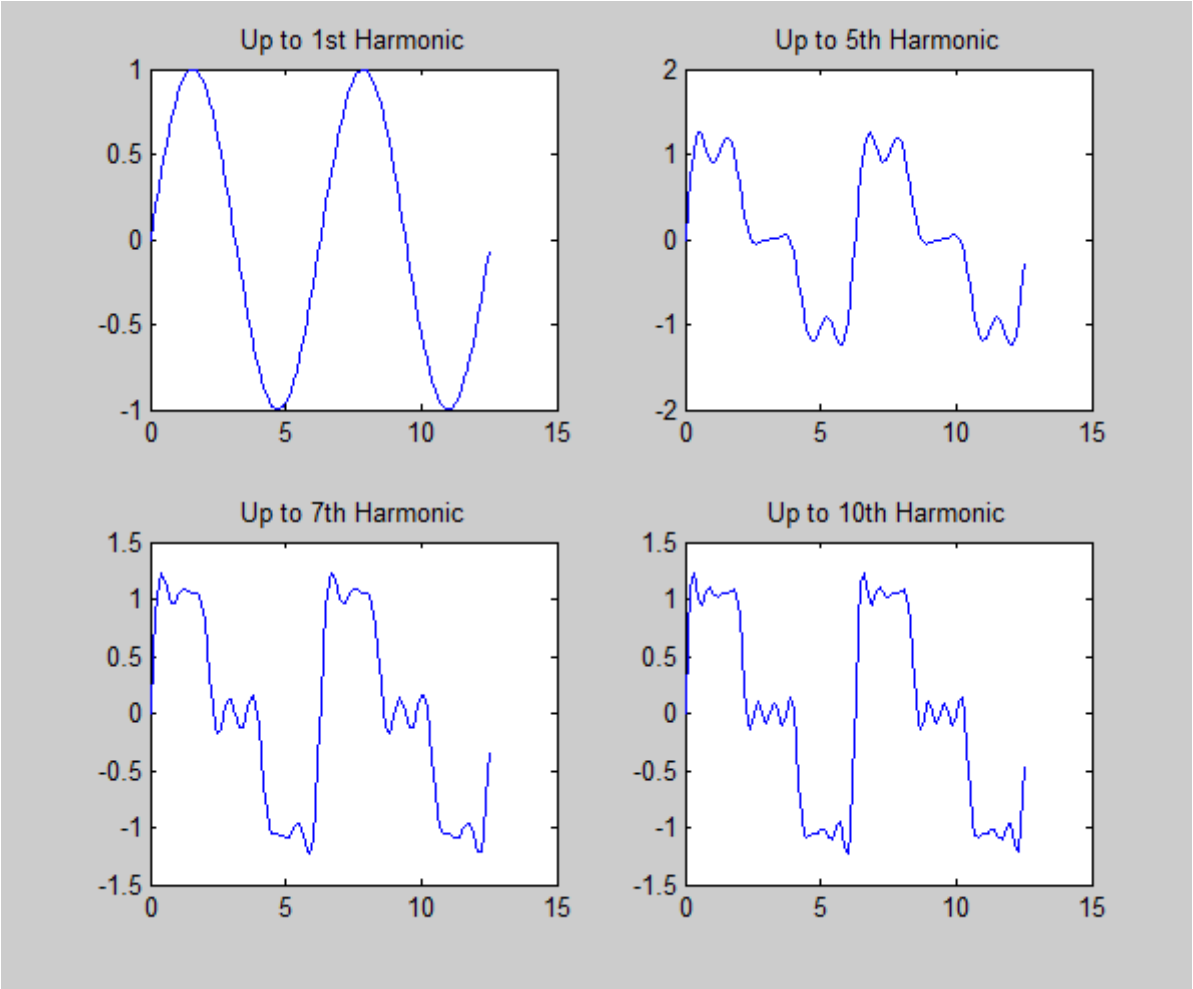

Figure 1.2: Odd waveform expressed in terms of harmonics

1.2 Voltage Unbalance

One major cause of steady state voltage unbalance are single phase loads in a three phase system. This happens quite often in rural electric power systems with long distribution lines and large urban power systems where heavy single phase demands, such as lighting loads, are imposed by large commercial facilities [3]. Another cause of voltage unbalance are single phase traction and electric transit and railroad systems. Unless proper design steps are taken, these systems can cause considerable voltage unbalance. Additionally, asymmetrical transformer winding impedances, open wye and open delta transformer banks, asymmetrical transmission impedances possibly caused by incomplete transposition of transmission lines, and blown fuses on three phase capacitor banks, are all possible causes of power system voltage unbalance.Percent voltage unbalance is defined in Equation 1.2.1.

$$\%Unbalance = \frac{|V_{avg} - V_{\Phi}|}{V_{avg}} \cdot 100\% \tag{1.2.1}$$

$$V_{avg} = \frac{V_a + V_b + V_c}{3} \tag{1.2.2}$$

Where V_{Φ} is the maximum or minimum amplitude of the three phase input RMS voltages (V_a, V_b, V_c), while V_{avg} is the average voltage amplitude.

It becomes increasingly difficult to compensate for voltage unbalance when the unbalance is continually varying as with large industrial loads. Additionally, when variable frequency drives are employed for cost savings, the customer load can vary continually with large hourly variations. If, for example, a large number of single phase VFD's are employed, then the results can be continually varying unbalanced loads. The combination of VFD's and single phase non-linear switch mode power

supply based loads such as computers, can lead to unbalance levels of distortion between phases [14].

1.3 Phase Sequence

In a three phase system that is balanced, the individual frequency harmonic components will either be entirely positive sequence, entirely negative sequence, or entirely zero sequence. To demonstrate this characteristic, the Fourier expansion of a three phase system is shown below.

$$\begin{aligned} v_a(t) = {} & V_1\cos(\omega_o t) + V_2\cos(2\omega_o t) + V_3\cos(3\omega_o t) \\ & + V_4\cos(4\omega_o t) + V_5\cos(5\omega_o t) + V_6\cos(6\omega_o t) \\ & + V_7\cos(7\omega_o t) + \ldots \end{aligned} \tag{1.3.1}$$

$$\begin{aligned} v_b(t) = {} & V_1\cos(\omega_o t - 120^o) + V_2\cos(2\omega_o t - 240^o) + V_3\cos(3\omega_o t - 360^o) \\ & + V_4\cos(4\omega_o t - 480^o) + V_5\cos(5\omega_o t - 600^o) + V_6\cos(6\omega_o t - 720^o) \\ & + V_7\cos(7\omega_o t - 840^o) + \ldots \\ = {} & V_1\cos(\omega_o t - 120^o) + V_2\cos(2\omega_o t + 120^o) + V_3\cos(3\omega_o t) \\ & + V_4\cos(4\omega_o t - 120^o) + V_5\cos(5\omega_o t + 120^o) + V_6\cos(6\omega_o t) \\ & + V_7\cos(7\omega_o t - 120^o) + \ldots \end{aligned} \tag{1.3.2}$$

$$\begin{aligned} v_c(t) = {} & V_1\cos(\omega_o t + 120^o) + V_2\cos(2\omega_o t + 240^o) + V_3\cos(3\omega_o t + 360^o) \\ & + V_4\cos(4\omega_o t + 480^o) + V_5\cos(5\omega_o t + 600^o) + V_6\cos(6\omega_o t + 720^o) \\ & + V_7\cos(7\omega_o t + 840^o) + \ldots \\ = {} & V_1\cos(\omega_o t + 120^o) + V_2\cos(2\omega_o t - 120^o) + V_3\cos(3\omega_o t) \\ & + V_4\cos(4\omega_o t + 120^o) + V_5\cos(5\omega_o t - 120^o) + V_6\cos(6\omega_o t) \\ & + V_7\cos(7\omega_o t + 120^o) + \ldots \end{aligned} \tag{1.3.3}$$

Table 1.1: Phase voltage sequence for the first 15 harmonics of a 3-phase system

Harmonic Order	1	2	3	4	5	6	7	8	9	10	11	12	13	14	15
Sequence	+	-	0	+	-	0	+	-	0	+	-	0	+	-	0

If the fundamental harmonics in Equations (1.3.1), (1.3.2), and (1.3.3) were looked at individually, it can be seen that this harmonic contains only positive sequence components. If the second harmonic is looked at individually, it can be seen that this component only contains negative sequence components, if the third harmonic is looked at individually, it can be seen that this component only contains zero sequence components. The phasor diagrams for the phase sequence of the first three harmonics are shown in Figure 1.3. This pattern continues every three harmonic orders, so the

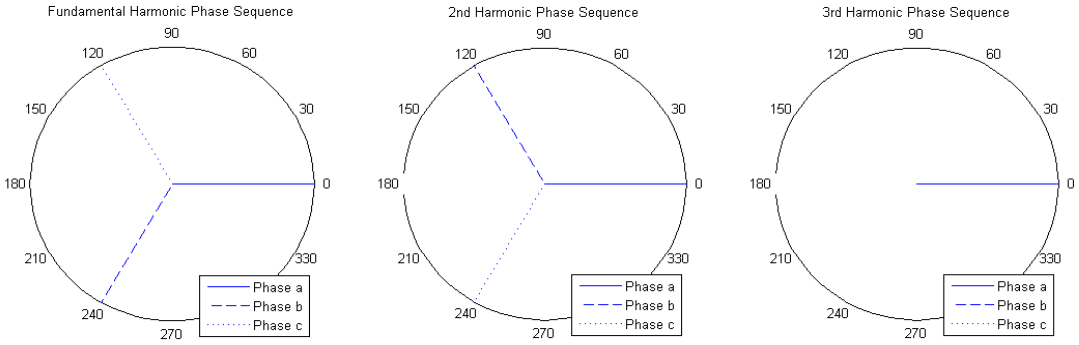

Figure 1.3: Phasor diagram of first three harmonics

1^{st}, 4^{th}, 7^{th} ... harmonic order contain only positive sequence components, the 2^{nd}, 5^{th}, 8^{th} ... harmonic orders contain only negative sequence components, and the 3^{rd}, 6^{th}, 9^{th} ..., or triplen harmonic orders contain only zero sequence components. Table 1.1 shows the phase sequence for the first 15 harmonic orders. From the phase voltage equations defined earlier, the phase to phase voltage equations can be derived. For

instance, for a wye connected system, the line to line voltage can be defined as follows,

$$\begin{aligned} v_{ab}(t) &= v_a(t) - v_b(t) \\ &= \sqrt{3}[V_1 \cos(\omega_o t + 30^o) + V_2 \cos(2\omega_o t - 30^o) \\ &\quad + V_4 \cos(4\omega_o t + 30^o) + V_5 \cos(5\omega_o t - 30^o) \\ &\quad + V_7 \cos(7\omega_o t + 30^o) + \ldots] \end{aligned} \tag{1.3.4}$$

1.4 Harmonic Indices

Harmonics are a sinusoidal component of a period and frequency that is an integer multiple of the fundamental frequency [2]. Thus, if a system has a fundamental frequency of f_o, then the frequency of the h^{th} harmonic order will be $h \times f_o$. Harmonics are used to describe distorted sine waves that are associated with voltages and currents. There are several important indices used to describe the effects of harmonics on a power system. The most commonly used, and maybe the most important, indices are the total harmonic distortion (THD) of the current and voltage. In order to define the total harmonic current and voltage distortion, the Fourier expansion form of the current and voltage must first be expressed as shown in Equations (1.4.1) and (1.4.2).

$$i(t) = \sum_{h=1}^{\infty} I_h \cos(h\omega_o t + \phi_h) \tag{1.4.1}$$

$$v(t) = \sum_{h=1}^{\infty} V_h \cos(h\omega_o t + \phi_h) \tag{1.4.2}$$

Note that any periodic wave form has a root sum square (RMS) value described by Equation (1.4.3).

$$F_{rms}^2 = \frac{1}{T}\int_0^T f^2(t)dt = \frac{1}{2}\sum_{h=1} F_h^2 = \sum_{h=1} F_{h,rms}^2 \tag{1.4.3}$$

Application of Equation (1.4.3) to Equations (1.4.1) and (1.4.2) yield the RMS values for current and voltage shown in Equations (1.4.4) and (1.4.5) respectively.

$$I_{rms} = \sqrt{\sum_{h=1}^{\infty} I_{h,rms}^2} \tag{1.4.4}$$

$$V_{rms} = \sqrt{\sum_{h=1}^{\infty} V_{h,rms}^2} \tag{1.4.5}$$

The total harmonic distortion for current and voltage are now defined in terms of the RMS values for current and voltage in Equations (1.4.6) and (1.4.7).

$$THD_I = \frac{1}{I_1}\sqrt{\sum_{h=2}^{\infty} I_h^2} = \sqrt{(\frac{I_{rms}}{I_{1rms}})^2 - 1} \tag{1.4.6}$$

$$THD_V = \frac{1}{V_1}\sqrt{\sum_{h=2}^{\infty} V_h^2} = \sqrt{(\frac{V_{rms}}{V_{1rms}})^2 - 1} \tag{1.4.7}$$

The THD_I and THD_V are the ratio of the RMS values of the harmonics to the RMS value of the fundamental component. This index measures the deviation of the wave form from an ideal sine wave, or in other words, if the THD is zero then the sine wave is purely at the fundamental frequency. Another important measure to take notice of is the harmonic distortion at a given harmonic order for current and voltage can be defined as $\frac{I_h}{I_1}$ and $\frac{V_h}{V_1}$.

Another important index used in the measure of power system harmonics is the total demand distortion (TDD) shown in Equation (1.4.8).

$$TDD = \frac{1}{I_L}\sqrt{\sum_{h=2}^{\infty} I_h^2} \tag{1.4.8}$$

Where the I_L is the maximum demand load current (typically 15 or 30 minute demand) at the fundamental frequency at the point of common coupling (PCC), which

is typically located at the secondary of the utility distribution transformer, calculated as the maximum demands for the previous twelve months [2].

A very important index used in the measure of system harmonics is the distortion power factor and its effects on the true power factor. In power systems, the power factor quantifies how efficiently the load utilizes the current it draws from an AC power system [5]. In systems where load(s) are linear, the only power factor to consider is the displacement power factor. Thus, the true power factor for a system with only linear loads is given in Equation (1.4.9).

$$PF_{true} = \frac{P}{S} = \frac{P}{\sqrt{P^2 + Q^2}} = \frac{\frac{V_1}{\sqrt{2}}\frac{I_1}{\sqrt{2}}\cos(\theta_1 - \phi_1)}{\frac{V_1}{\sqrt{2}}\frac{I_1}{\sqrt{2}}} = \cos(\theta_1 - \phi_1) = PF_{disp} \quad (1.4.9)$$

For systems that contain current and voltage harmonics, the real power P for all harmonics have to be taken into account and the apparent power S for all harmonics have to be taken into account. The real power is shown in Equations (1.4.10) through (1.4.12).

$$P = \frac{1}{T}\int_0^T p(t)dt \quad (1.4.10)$$

$$= \frac{1}{2}\sum_{h=1}^{\infty} V_h I_h \cos(\theta_h - \phi_h) \quad (1.4.11)$$

$$= \frac{1}{2}\sum_{h=1}^{\infty} V_{h,rms} I_{h,rms} \cos(\theta_h - \phi_h) \quad (1.4.12)$$

The apparent power is shown in Equations (1.4.13) through (1.4.16).

$$S = V_{rms} I_{rms} \quad (1.4.13)$$

$$= \sqrt{\sum_{h=1}^{\infty} V_{h,rms}^2 I_{h,rms}^2} \quad (1.4.14)$$

$$= V_{1,rms} I_{1,rms} \sqrt{1 + THD_V^2}\sqrt{1 + THD_I^2} \quad (1.4.15)$$

$$= S_1 \sqrt{1 + THD_V^2}\sqrt{1 + THD_I^2} \quad (1.4.16)$$

In the scenario with the additional harmonics included, the true power factor becomes the product of the displacement power factor (PF_{disp}) and the distortion power factor (PF_{dist}) as shown in Equations (1.4.17) through (1.4.19).

$$PF_{true} = \frac{P}{S} = \frac{P}{V_{1,rms} I_{1,rms} \sqrt{1 + THD_V^2} \sqrt{1 + THD_I^2}} \tag{1.4.17}$$

$$= \frac{P}{S_1} \cdot \frac{1}{V_{1,rms} I_{1,rms} \sqrt{1 + THD_V^2} \sqrt{1 + THD_I^2}} \tag{1.4.18}$$

$$= PF_{disp} \cdot PF_{dist} \tag{1.4.19}$$

The distortion power factor describes how the harmonic distortion of the load current decreases the average power transfers between the source and the load. To take this idea one step further, distortion power can be found once the reactive power Q is known. Equations (1.4.20) and (1.4.21) define Q.

$$Q = \frac{1}{2} \sum_{h=1}^{\infty} V_h I_h \sin(\theta_h - \phi_h) \tag{1.4.20}$$

$$= \frac{1}{2} \sum_{h=1}^{\infty} V_{h,rms} I_{h,rms} \sin(\theta_h - \phi_h) \tag{1.4.21}$$

The distortion power D can now be defined as shown in Equation (1.4.22).

$$D^2 = S^2 - (P^2 + Q^2) \tag{1.4.22}$$

An index that is also closely monitored is the crest factor for both current and voltage. The current crest factor (CCF) and voltage crest factor (VCF) are shown in Equations (1.4.23) and (1.4.24) respectively.

$$CCF = \frac{1}{I_1} \sum_{h=2} I_h \tag{1.4.23}$$

$$VCF = \frac{1}{V_1} \sum_{h=2} V_h \tag{1.4.24}$$

The crest factor index is important in the selection of the circuit components [1]. For instance, two loads can have the same RMS values for current, but different peak

current values as shown in Figure 1.4. The red and blue waveforms have same RMS values, however the peak values vary.

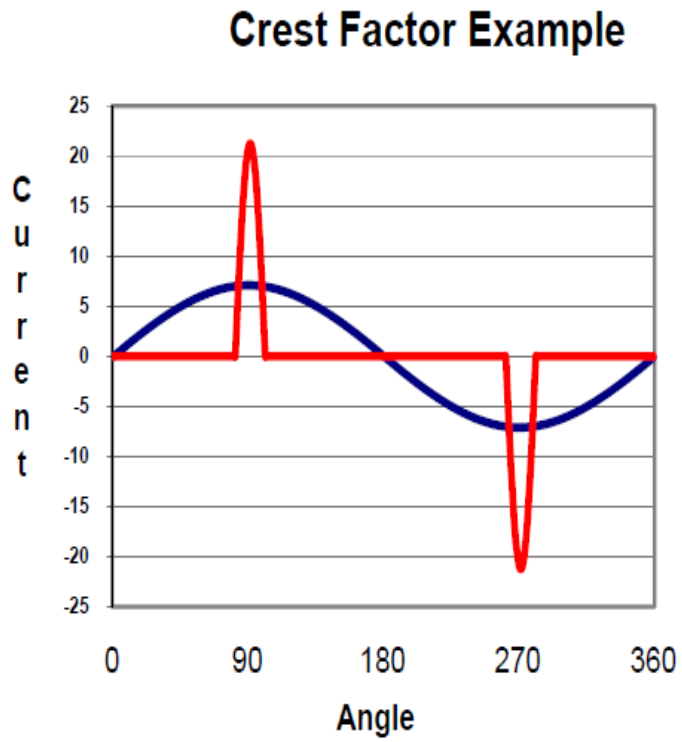

Figure 1.4: Equivalent RMS currents with different peak values

A final index worth mentioning is the telephone interference factor (TIF). Harmonics generate telephone interference through inductive coupling [15]. The telephone interference factor for current and voltage are shown in Equations (1.4.25) and (1.4.26).

$$TIF_I = \frac{1}{I_{rms}} \sqrt{\sum_{h=1}^{\infty} (T_h I_h)^2} \tag{1.4.25}$$

$$TIF_V = \frac{1}{V_{rms}} \sqrt{\sum_{h=1}^{\infty} (T_h V_h)^2} \tag{1.4.26}$$

Where T_h is a weighting that accounts for the audio and inductive coupling effects

at the h^{th} harmonic order. In practice, this distortion index is typically expressed as the product of the TIF values and the RMS current or RMS voltage. They are referred to as the IT product and the VT product. The IT and VT values are shown in Equations (1.4.27) and (1.4.28).

$$IT = \sqrt{\sum_{h=1}^{\infty}(T_h I_h)^2} \tag{1.4.27}$$

$$VT = \sqrt{\sum_{h=1}^{\infty}(T_h V_h)^2} \tag{1.4.28}$$

1.5 Harmonics and Circuit Elements

In the study of harmonics, it is important to note the effects of harmonics on passive circuit elements. This section will look at the effects of harmonics on certain parameters for resistors, inductors, and capacitors.

The power in a resistor is defined in Equation (1.5.1).

$$P_R = \frac{1}{2}\sum_{h=1}^{\infty} V_h I_h = \frac{1}{2}\sum_{h=1}^{\infty} I_h^2 R_h = \frac{1}{2}\sum_{h=1}^{\infty}\frac{V_h^2}{R_h} \tag{1.5.1}$$

The power in the resistor in terms of THD voltage and current are shown in Equations (1.5.2) and (1.5.3) respectively.

$$P_R = \frac{1}{2R}\sum_{h=1}^{\infty} V_h^2 = \frac{V_1^2}{2R}(1 + THD_V^2) = P_{R1}(1 + THD_V^2) \tag{1.5.2}$$

$$P_R = \frac{R}{2}\sum_{h=1}^{\infty} I_h^2 = \frac{I_1^2 R}{2}(1 + THD_I^2) = P_{R1}(1 + THD_I^2) \tag{1.5.3}$$

The per unit value of power in a resistor is defined in Equations (1.5.4) and (1.5.5) in terms of THD voltage and THD current.

$$P_{Rp.u.} = \frac{P_R}{P_{R1}} = 1 + THD_V^2 = \sum_{h=1}^{\infty} V_{hp.u.}^2 \tag{1.5.4}$$

$$P_{Rp.u.} = \frac{P_R}{P_{R1}} = 1 + THD_I^2 = \sum_{h=1}^{\infty} I_{hp.u.}^2 \tag{1.5.5}$$

From Equations (1.5.4) and (1.5.5), it is important to note that the total harmonic distortion for voltage and current are equal for a resistive circuit element.

For inductive loads, the power in an inductor Q_L is defined in Equation (1.5.6).

$$Q_L = \frac{1}{2}\sum_{h=1}^{\infty} V_h I_h = \sum_{h=1}^{\infty} V_{h,rms} I_{h,rms} \tag{1.5.6}$$

The fundamental and harmonic voltage across the inductor are defined in Equation (1.5.7) and (1.5.8) respectively.

$$V_1 = j2\pi f_0 L I_1 \tag{1.5.7}$$

$$V_h = j2\pi f_0 L I_h \tag{1.5.8}$$

From Equations (1.5.7) and (1.5.8) the per unit value for the voltage can be defined, as shown in Equation (1.5.9).

$$\frac{V_h}{V_1} = h\frac{I_h}{I_1} \tag{1.5.9}$$

Equation (1.5.9) can be used to define the per unit value of the reactive power $\frac{Q_L}{Q_1}$ in terms of the harmonic voltages or the harmonic currents as shown in Equation (1.5.10).

$$\frac{Q_L}{Q_1} = \frac{\frac{1}{2}\sum_{h=1}^{\infty} V_h I_h}{\frac{1}{2} V_1 I_1} = \sum_{h=1}^{\infty} h(\frac{I_h}{I_1})^2 = \sum_{h=1}^{\infty} \frac{1}{h}(\frac{V_h}{V_1})^2 \tag{1.5.10}$$

The per unit reactive power $Q_{Lp.u.}$ in terms of per unit current and per unit voltage is shown in Equation (1.5.11).

$$Q_{Lp.u.} = \sum_{h=1}^{\infty} h I_{hp.u.}^2 = \sum_{h=1}^{\infty} \frac{V_{hp.u.}^2}{h} \tag{1.5.11}$$

For a capacitive load, the reactive power Q_C in the capacitor is defined in Equation (1.5.12).

$$Q_C = -\frac{1}{2}\sum_{h=1}^{\infty} V_h I_h = -\sum_{h=1}^{\infty} V_{h,rms} I_{h,rms} \tag{1.5.12}$$

The negative sign in Equation (1.5.12) comes from the loading convention used in this particular analysis. The fundamental and harmonic voltages across the capacitor are shown in Equations (1.5.13) and (1.5.14).

$$V_1 = \frac{I_1}{j2\pi f_0 C} \tag{1.5.13}$$

$$V_h = \frac{I_h}{j2\pi h f_0 C} \tag{1.5.14}$$

The per unit voltage values can be defined from Equations (1.5.13) and (1.5.14) as shown in Equation (1.5.15).

$$\frac{V_h}{V_1} = \frac{1}{h}\frac{I_h}{I_1} \tag{1.5.15}$$

Equation (1.5.15) can be used to define the per unit value of the reactive power $\frac{Q_C}{Q_1}$ in terms of the harmonic voltages or the harmonic currents as shown in Equation (1.5.16).

$$\frac{Q_C}{Q_1} = \frac{-\frac{1}{2}\sum_{h=1}^{\infty} V_h I_h}{-\frac{1}{2} V_1 I_1} = \sum_{h=1}^{\infty} h(\frac{V_h}{V_1})^2 = \sum_{h=1}^{\infty} \frac{1}{h}(\frac{I_h}{I_1})^2 \tag{1.5.16}$$

The per unit value for the reactive $Q_{Cp.u.}$ can now be defined in terms of the per unit value for current and voltage as shown in Equation (1.5.17).

$$Q_{Cp.u.} = \sum_{h=1}^{\infty} \frac{I_{hp.u.}^2}{h} = \sum_{h=1}^{\infty} h V_{hp.u.}^2 \tag{1.5.17}$$

1.6 Harmonic Resonance

In power systems, a large portion of consideration is given towards the selection of passive circuit elements due to their effects on system harmonics. One major phenomenon that can have potentially destructive effects on the system is harmonic resonance. Harmonic resonance can produce large current and voltage spikes on the system, which can cause the operation of protective devices or the failure of equipment

[12]. Circuits that contain both capacitors and inductors have one or more natural resonant frequencies [6]. A resonant condition occurs when the inductive reactance and capacitive reactance become equal in an electrical system. The damage to the system occurs when one of the natural resonant frequencies occur at or near a system harmonic frequency. There are two main types of resonant conditions and they are series resonance and parallel resonance. Based on this definition for resonance in an RLC circuit, the angular resonance frequency can be defined as shown in Equation (1.6.1).

$$X_{Lr} = \omega_r L = X_{Cr} = \frac{1}{\omega_r C} \Rightarrow \omega_r = \frac{1}{\sqrt{LC}} \tag{1.6.1}$$

The resonance frequency is now defined in Equation (1.6.2) based on Equation (1.6.1).

$$f_r = \frac{1}{2\pi\sqrt{LC}} = \frac{f_0}{\omega_0\sqrt{LC}} = f_0\sqrt{\frac{X_C}{X_L}} \tag{1.6.2}$$

The harmonic order at which resonance will occur is given in Equation (1.6.3).

$$h_r = \frac{f_r}{f_0} = \frac{1}{\omega_0\sqrt{LC}} \tag{1.6.3}$$

1.6.1 Series Resonance

In a series RLC circuit, the impedance is shown in Equation (1.6.4).

$$Z = R + j(X_L + X_C) \tag{1.6.4}$$

In terms of the harmonic content, the impedance can be defined as shown in Equation (1.6.5).

$$Z(h) = R + j(hX_L + \frac{X_C}{h}) \tag{1.6.5}$$

Where the magnitude of Z can be defined in Equation (1.6.6).

$$|Z(h)| = \sqrt{R^2 + (hX_L - \frac{X_C}{h})^2} \tag{1.6.6}$$

Once the RLC circuit is at resonance, the following circuit parameters can be defined. Equation (1.6.7) defines the reactance at resonance.

$$h_r X_L = \frac{X_C}{h_r} = X_r \tag{1.6.7}$$

The harmonic order at resonance is defined in Equation (1.6.8).

$$h_r = \sqrt{\frac{X_C}{X_L}} \tag{1.6.8}$$

The impedance at resonance is defined in Equation (1.6.9).

$$Z(h_r) = R \tag{1.6.9}$$

Finally the quality factor is defined in Equation (1.6.10).

$$Q = \frac{X_r}{R} \tag{1.6.10}$$

Equation (1.6.10) shows the quality factor to be the ratio of the reactance of the tuned circuit to the resistance. What Q really measures is the sharpness of the response of the tuned circuit [8]. Thus, the higher the quality factor, the sharper the circuit response at resonance.

Example 1 A series RLC circuit has the following parameters, $X_C = 1.6$, $X_L = 0.064$, and $Q = 100$, solve for the resonance harmonic, resonance reactance, resistance, and perform a frequency scan of the impedance.

Solution: Equation (1.6.8) can be used to solve for the resonance harmonic, Equation (1.6.7) can be used to solve for the resonance reactance, Equation (1.6.10) can be used to solve for the resistance and Figure 1.5 shows a frequency scan of the impedance and phase angle.

$$h_r = 5, X_r = 0.32, R = 0.0032$$

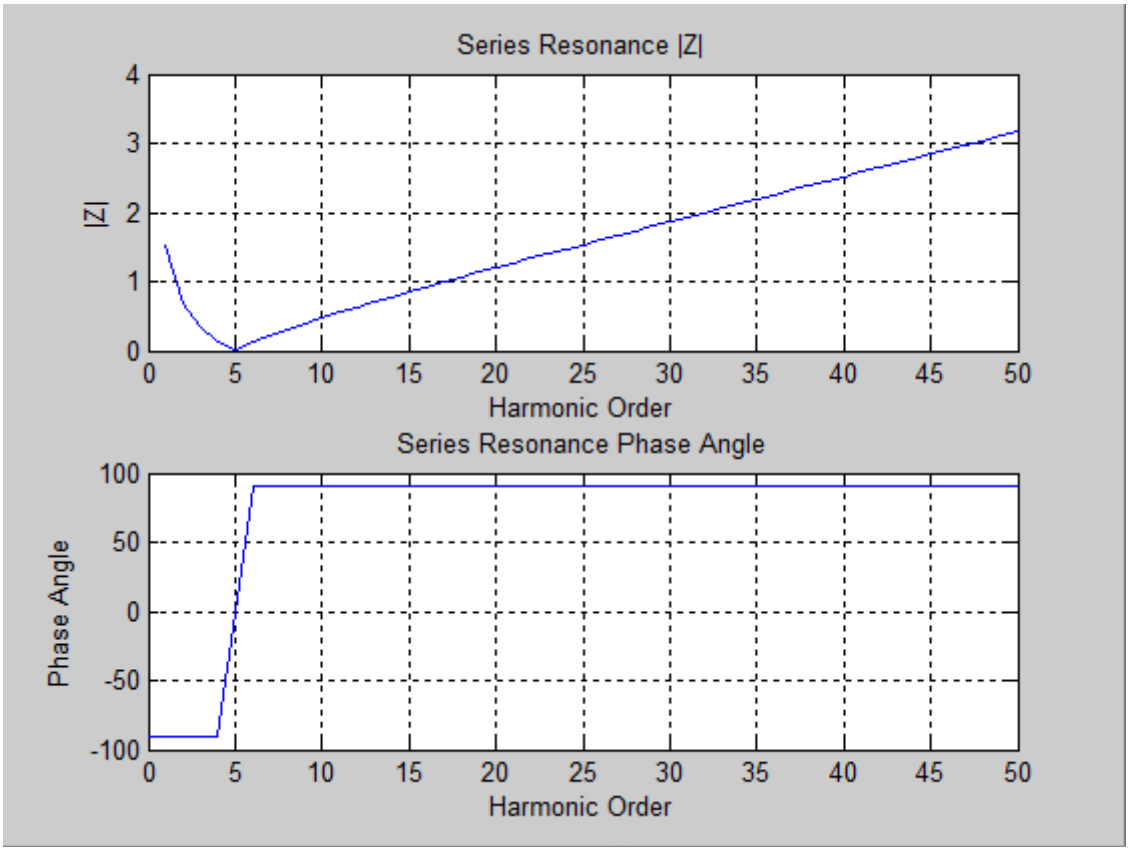

Figure 1.5: Frequency scan of the impedance and phase angle

The dip in the impedance graph shown in Figure 1.5 is an important characteristic of series resonance. Figure 1.6 shows a series resonant equivalent circuit. In this circuit, if there is a large harmonic voltage close to or at the resonant frequency, the current into the LC network will be the harmonic voltage divided by the LC network impedance, which is very close to zero. This will in turn cause a current spike at that specific harmonic order [10].

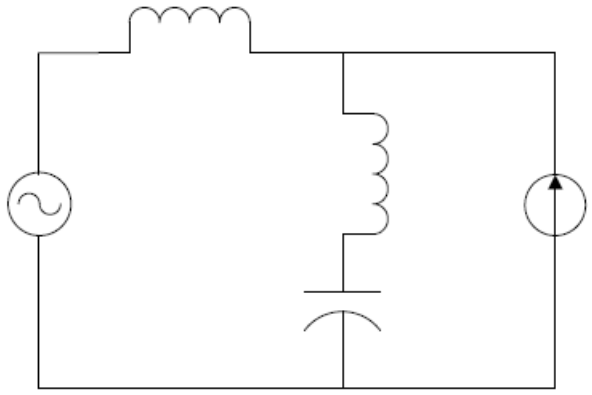

Figure 1.6: Series Resonance Equivalent Circuit

1.6.2 Parallel Resonance

For the parallel RLC circuit, the impedance is shown in Equation (1.6.11).

$$Z = \frac{R \cdot -j\frac{X_L X_C}{X_L - X_C}}{R - j\frac{X_L X_C}{X_L - X_C}} \tag{1.6.11}$$

In terms of the harmonic content, the impedance is shown in Equation (1.6.12).

$$Z(h) = \frac{-jRX_L X_C}{R(hX_L - \frac{X_C}{h}) - jX_L X_C} \tag{1.6.12}$$

The magnitude of Z can now be defined as shown in Equation (1.6.13).

$$|Z(h)| = \frac{RX_L X_C}{\sqrt{[R(hX_L - \frac{X_C}{h})]^2 + [X_L X_C]^2}} \tag{1.6.13}$$

With the RLC circuit at resonance, the following circuit parameters can be defined. The reactance at resonance is shown in Equation (1.6.14).

$$h_r X_L = \frac{X_C}{h_r} = X_r \tag{1.6.14}$$

The harmonic order at resonance is defined in Equation (1.6.15).

$$h_r = \sqrt{\frac{X_C}{X_L}} \tag{1.6.15}$$

The impedance at resonance is defined in Equation (1.6.16).

$$Z(h_r) = R \tag{1.6.16}$$

And finally, the quality factor is defined in Equation (1.6.17). It is interesting to note that the quality factor for parallel resonance is the inverse of the quality factor for series resonance.

$$Q = \frac{R}{X_r} \tag{1.6.17}$$

Example 2 A parallel RLC circuit has the following parameters, $X_C = 60$, $X_L = 0.495$, and $Q = 3$, solve for the resonance harmonic, resonance reactance, resistance, and perform a frequency scan of the impedance. *Solution:* Equation (1.6.15) can be used to solve for the resonance harmonic, Equation (1.6.14) can be used to solve for the resonance reactance, Equation (1.6.17) can be used to solve for the resistance and Figure 1.7 shows a frequency scan of the impedance and phase angle.

$$h_r = 11, X_r = 5.45, R = 16.35$$

For parallel resonance, Figure 1.7 shows that there is an impedance spike in the graph for the frequency scan at the resonance harmonic.

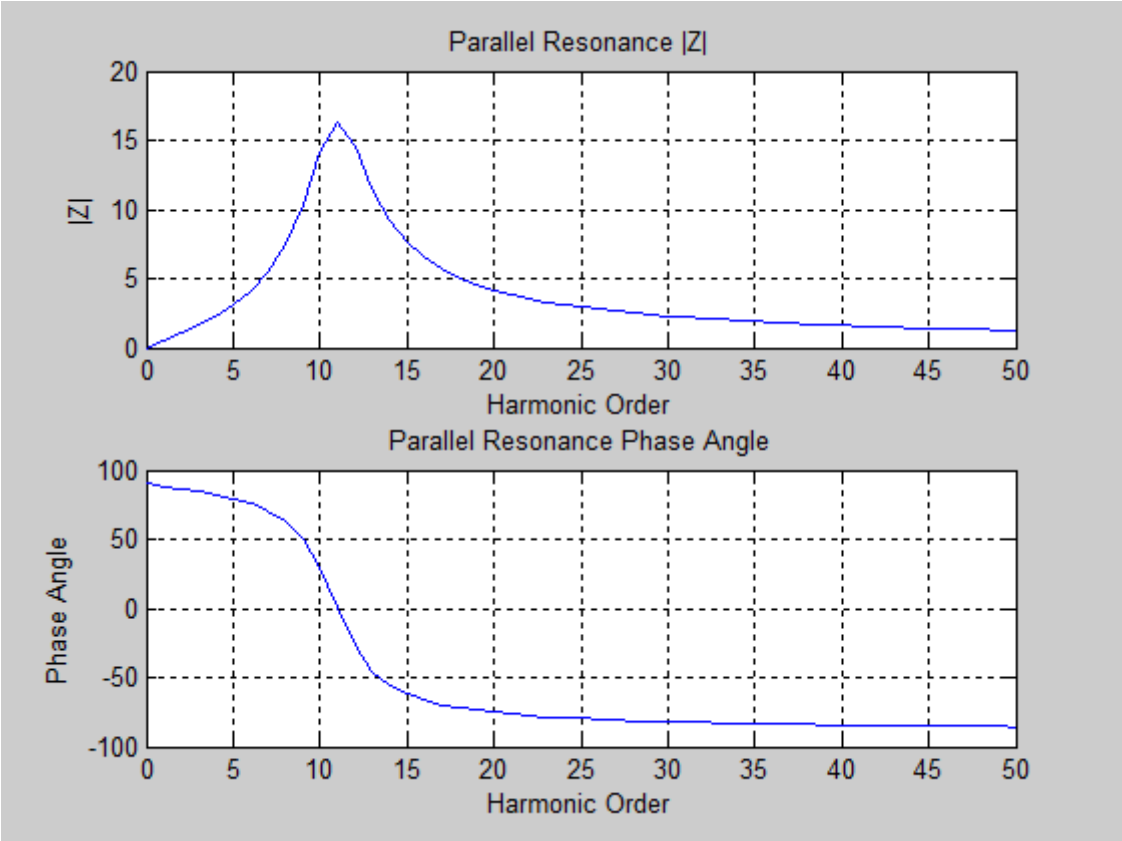

Figure 1.7: Frequency scan of the impedance and phase angle

Figure 1.8 shows a parallel resonance equivalent circuit. In this circuit, if there is a harmonic current near the resonance frequency of the circuit, there will be a spike in the voltage. This is because of the increase in impedance due to resonance and the presence of the harmonic current [10].

At this point it is important to point out that there is a direct relationship between the type of resonance (series or parallel) and the resulting frequency scan of the impedance. For series resonance the is dip in the frequency scan at that harmonic, and for parallel resonance there is a spike in the frequency scan at that harmonic.

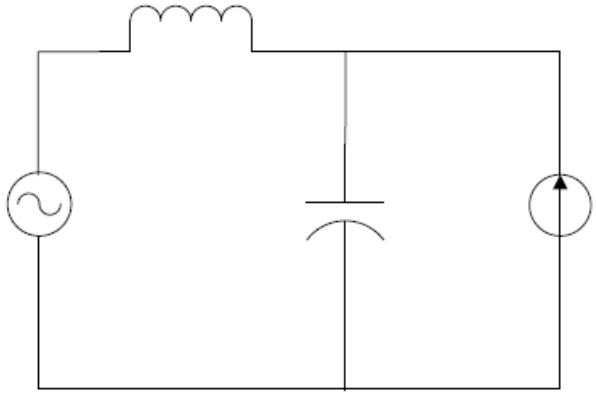

Figure 1.8: Parallel Resonance Equivalent Circuit

1.7 Bus Voltage Rise and System Resonance

Often in power systems, there is a desire to increase the voltage at a particular bus by using a capacitor bank. The bank supplies the system with reactive power and boosts the bus voltage. This section investigates the effects of bus voltage rise on the system resonance.

Figure 1.9 shows a capacitor bank being switched at bus V_{bus}.

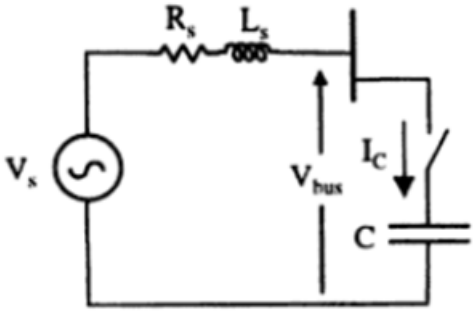

Figure 1.9: Capacitor Bank Switched at a Bus

With the switch open V_{bus} is defined by Equation (1.7.1).

$$V_{bus} = V_s \tag{1.7.1}$$

Once the switch is closed, the V_{bus} is defined in Equation (1.7.3) and (1.7.4).

$$V_C = V_{bus}^1 = V_S - (R_s + jX_s)I_C \tag{1.7.2}$$

$$= \frac{-jX_C}{Z_S - jX_C}V_S \tag{1.7.3}$$

$$= \frac{V_S}{1 - \omega_o^2 L_S C + j\omega_o C R_S} \tag{1.7.4}$$

The change in bus voltage and the magnitude of the bus voltage change are then given by Equation (1.7.5) and (1.7.6) respectively.

$$Vbus^1 - V_{bus} = (R_S + jX_S)I_C \tag{1.7.5}$$

$$\Delta V_{bus} = |V_{bus}^1| - |V_{bus}| \approx X_S|I_C| \tag{1.7.6}$$

In typical power systems applications, a load is connected at the bus, in parallel with a capacitor. The capacitor size is then based on the desired voltage rise for the system. Equation (1.7.9) and Figure 1.10 depict a straight forward way to calculate the capacitor bank size for a given system.

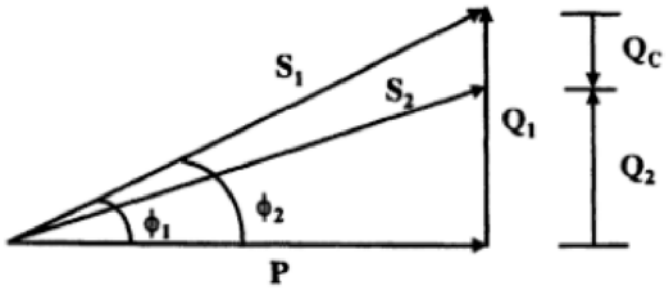

Figure 1.10: Bus voltage rise phasor diagram

$$Q_C = Q_1 - Q_2 \tag{1.7.7}$$

$$= P(\tan\phi_1 - \tan\phi_2) \tag{1.7.8}$$

$$= P[\tan(\cos^{-}1pf_1) - \tan(\cos^{-}1pf_2)] \tag{1.7.9}$$

Where P is the real power delivered by the system and absorbed by the load, Q_1 is the load reactive power, S_1 is the load apparent power, Q_2 is the system's reactive power with the capacitor bank connected, S_2 is the system's apparent power with the capacitor bank connected, pf_1 is the original power factor, and pf_2 is the improved power factor after the capacitor bank is connected. Once the capacitor bank size is determined, the effect of the capacitor bank on the system can now be analyzed. Figure 1.11 shows the Thevenin equivalent circuit for the given power system.

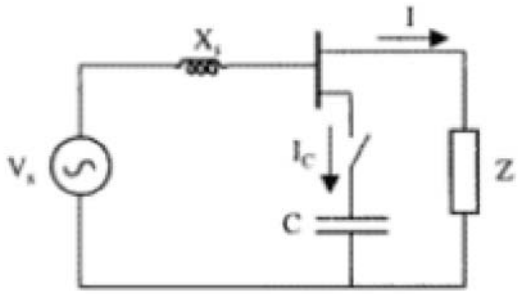

Figure 1.11: Bus voltage Thevenin equivalent circuit

Equations (1.7.10) through (1.7.13) define the reactance values for the inductor and capacitor in Figure 1.11.

$$X_S = \omega_o L_S = 2\pi f_o L_s = \frac{kV_n^2}{SCC} \tag{1.7.10}$$

The base impedance is defined as $Z_b = \frac{kV_b^2}{S_b}$. The per unit (p.u.) reactance values are

then shown in Equations (1.7.11) through (1.7.13).

$$X_{Sp.u.} = \frac{X_S}{Z_b} = \frac{\frac{kV_n^2}{SCC}}{\frac{kV_b^2}{S_b}} \tag{1.7.11}$$

$$X_{Sp.u.} = \frac{S_b}{SCC} = \frac{1}{SCC_{p.u.}} \tag{1.7.12}$$

$$X_{Cp.u.} = \frac{X_C}{Z_b} = \frac{1}{Q_{Cp.u.}} \tag{1.7.13}$$

At this point it is a good time to determine what role the resonant frequency plays in the bus voltage change. Equation (1.7.14) defines the resonant frequency of the system for a given inductor and capacitor.

$$f_r = \frac{1}{2\pi\sqrt{L_S C}} = \frac{\omega_o}{2\pi\sqrt{\frac{X_{Sp.u.}}{X_{Cp.u.}}}} = f_o\sqrt{\frac{X_{Cp.u.}}{X_{Sp.u.}}} = f_o\sqrt{\frac{SCC_{p.u.}}{Q_{Cp.u.}}} \tag{1.7.14}$$

Equation (1.7.15) now defines the harmonic order for the resonant frequency defined in Equation (1.7.14).

$$h_r = \frac{f_r}{f_o} = \sqrt{\frac{X_{Cp.u.}}{X_{Sp.u.}}} = \sqrt{\frac{SCC_{p..u.}}{Q_{Cp.u.}}} \tag{1.7.15}$$

Where f_o is the system's fundamental frequency, $SCC_{p.u.}$ is the short circuit MVA at the bus, and $Q_{Cp.u.}$ is the capacitor MVA rating. The bus voltage change can now be defined as a function of the inductance, capacitance, and fundamental frequency. Looking at Figure 1.11 for the Thevenin equivalent circuit, with the capacitor bank disconnected, the source voltage is shown in Equation (1.7.16).

$$V_S^1 = V_{bus} + jX_S I \tag{1.7.16}$$

Once the capacitor bank is reconnected, and assuming the source voltage remains constant, Equations (1.7.18) and (1.7.19) show the capacitor voltage and current values.

$$V_S^1 = V_{bus_n} + jX_S I \tag{1.7.17}$$

$$I_C = j\frac{V_C}{X_C} \tag{1.7.18}$$

$$V_C = V_{bus_n} \tag{1.7.19}$$

The bus voltage change and per unit bus voltage change are now defined in Equations (1.7.20) and (1.7.21) respectively.

$$\Delta V_{bus} = |V_{bus_n}| - |V_bus| = | - jX_S I_C| = \frac{X_S}{X_C}|V_{bus_n}| \tag{1.7.20}$$

$$\Delta V_{busp.u.} = \frac{\Delta V_{bus}}{|V_{bus_n}|} = \frac{X_S}{X_C} = \omega_o L_S C = (2\pi)^2 f_o^2 L_S C \tag{1.7.21}$$

The resonant frequency of the bus voltage change is now shown in Equation (1.7.22).

$$f_r = \frac{1}{2\pi\sqrt{L_S C}} = \frac{f_o}{\sqrt{\Delta V_{busp.u.}}} \tag{1.7.22}$$

The resonance harmonic order of the bus voltage change relationship is defined in Equations (1.7.23) and (1.7.24).

$$h_r = \frac{1}{\sqrt{\Delta V_{busp.u.}}} \tag{1.7.23}$$

$$\Delta V_{busp.u.} = \frac{1}{h_r^2} \tag{1.7.24}$$

Example 3 The circuit in Figure 1.12 was analyzed to see the effect transformer short circuit capacity and capacitor bank size on the harmonic order.

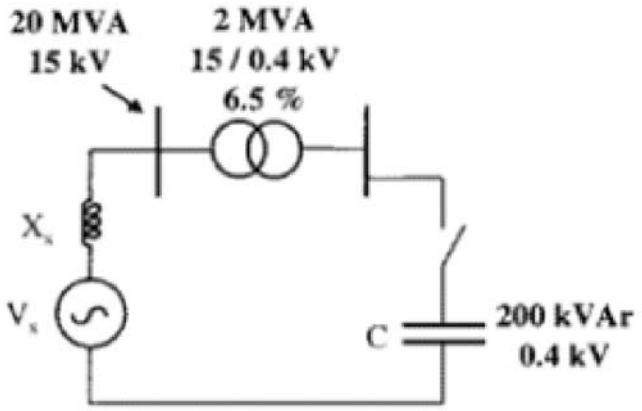

Figure 1.12: Bus voltage change circuit example

*Solution:*First the base MVA and the base line to line voltage were chosen. Second, the base current and base impendence were derived based on the MVA and line to line voltage. Then the following circuit parameter values were determined based on equations presented earlier in this paper, the transformer reactance $X_T = 0.065pu$, the total reactance referenced from the 0.4kV side of the circuit was $X_{400} = 0.165pu$, the short circuit capacity referenced from the 0.4kV side of the circuit was $SCC_{400} = 6.06pu$, the capacitor bank reactive power and reactance were $Q_C = 0.1pu$ and $X_C = 10pu$ respectively, and the resonance harmonic was determined to be $h_r = 7.785$. The frequency scan of the impedance and phase angle are presented in figure 1.13.

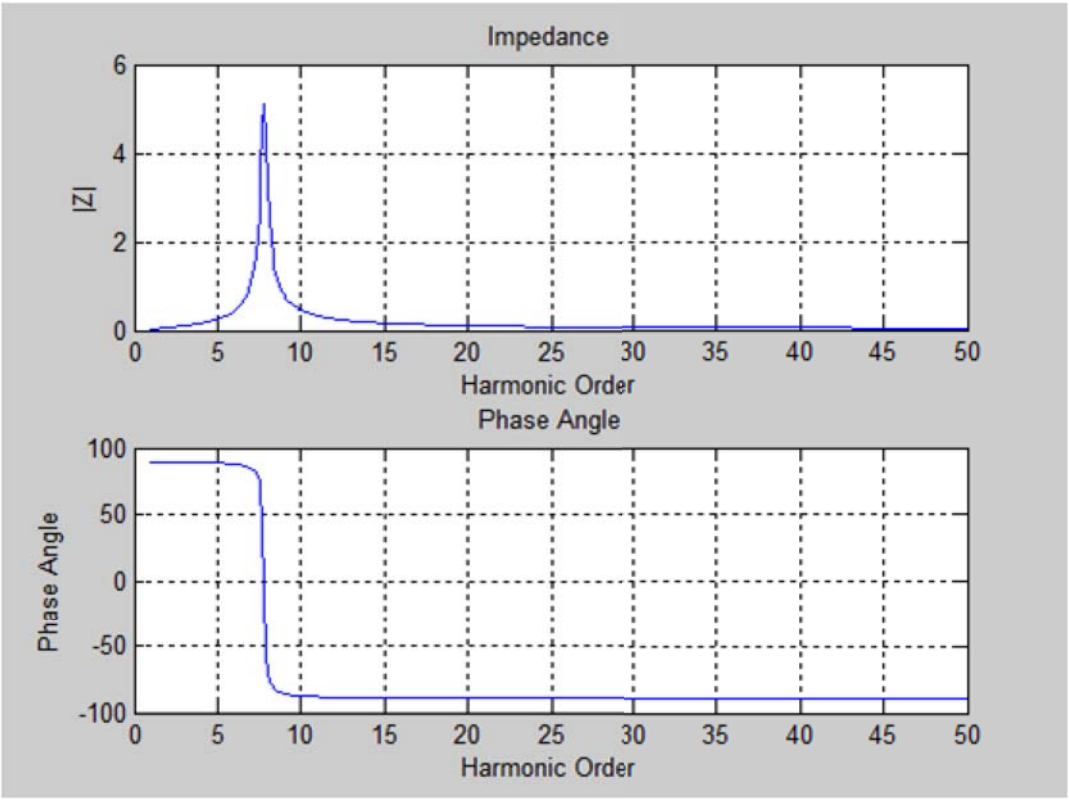

Figure 1.13: Bus voltage change circuit example

A further analysis was carried out to show the effects of varied short circuit capacities and capacitor bank reactive powers. The results are shown in Tables 1.2 and 1.3.

	$SCC = 80MVA$				
Q_C	100	200	300	400	500
h_r	14.9	10.5	8.6	7.5	6.7

Table 1.2: Resonance harmonic for constant SCC and varying reactive power

$SCC = 20MVA$					
Q_C	100	200	300	400	500
h_r	11	7.8	6.4	5.5	4.9

Table 1.3: Resonance harmonic for constant SCC and varying reactive power

A frequency scan of the impedance and phase angle was also performed on the data shown in Table 1.2 and 1.3. The results are shown in Figure 1.14 and 1.15. Two very important observations were made from the information presented in Table 1.2, Table 1.3, Figure 1.14, and Figure 1.15. One observation was, if the short circuit capacity were kept constant and the capacitor bank size was increase, then the resonance harmonic moves to a lower order. The second observation was, if the capacitor bank size was kept constant and the short circuit capacity was increased, then the resonance harmonic moved to a higher order. From the equations and example above, the inductor and capacitor values can be chosen such that the voltage change shows up at a particular harmonic frequency. This concept proves very useful when it comes to circuit component selection in the simulation and experiment that are presented in this paper.

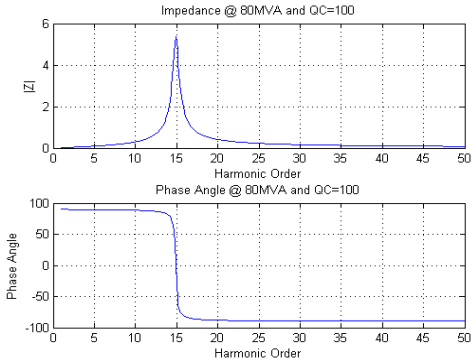

(a) Frequency scan at $SCC = 80MVA$ and $Q_C = 100kVAr$

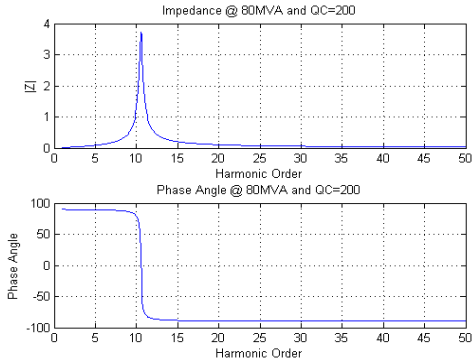

(b) Frequency scan at $SCC = 80MVA$ and $Q_C = 200kVAr$

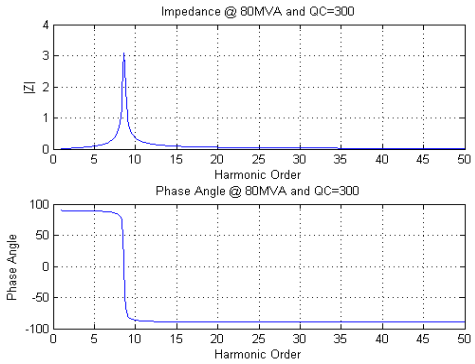

(c) Frequency scan at $SCC = 80MVA$ and $Q_C = 300kVAr$

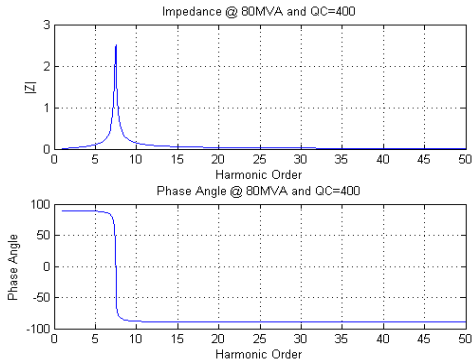

(d) Frequency scan at $SCC = 80MVA$ and $Q_C = 400kVAr$

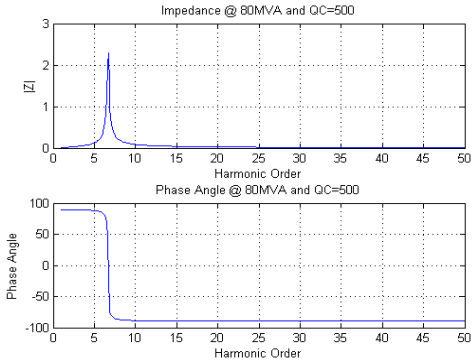

(e) Frequency scan at $SCC = 80MVA$ and $Q_C = 500kVAr$

Figure 1.14: Frequency scan for 80MVA SCC with various kVAr

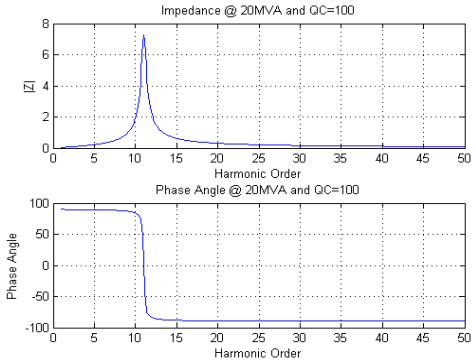

(a) Frequency scan at $SCC = 20MVA$ and $Q_C = 100kVAr$

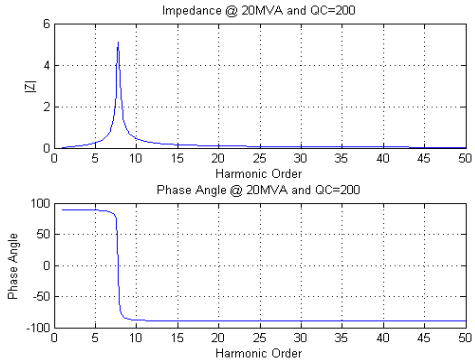

(b) Frequency scan at $SCC = 20MVA$ and $Q_C = 200kVAr$

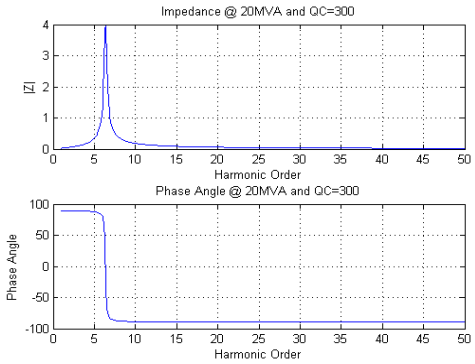

(c) Frequency scan at $SCC = 20MVA$ and $Q_C = 300kVAr$

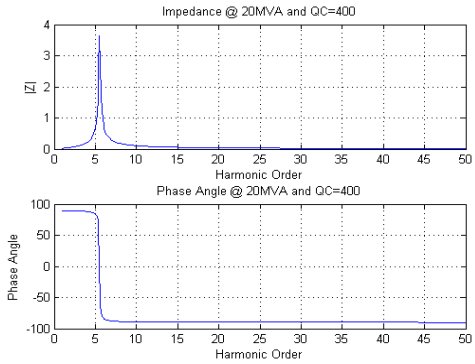

(d) Frequency scan at $SCC = 20MVA$ and $Q_C = 400kVAr$

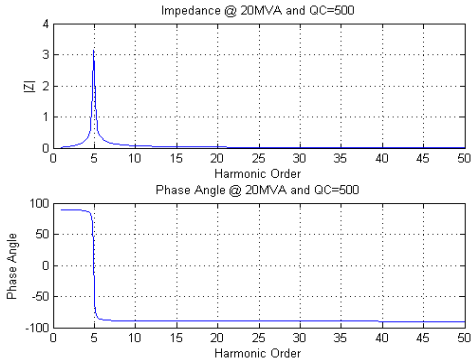

(e) Frequency scan at $SCC = 20MVA$ and $Q_C = 500kVAr$

Figure 1.15: Frequency scan for 20MVA SCC with various kVAr

1.8 Harmonic in a VFD

Power electronic converters are the interface for many large electronic loads that range from uninterruptible power supplies to motors operating at variable speeds through the use of variable frequency drives (VFD). Figure 1.16 shows a simple VFD schematic. Many converter schemes contain diode rectifier front ends and DC link capacitors that convert the incoming AC voltage to a low ripple DC voltage. The inverter section of the VFD, which typically contains Insulated Gate Bipolar Transistors (IGBT), convert the DC voltage back to variable three-phase AC. The magnetude and frequency of the pulse width modulated (PWM) inverter output control the motor speed [14].

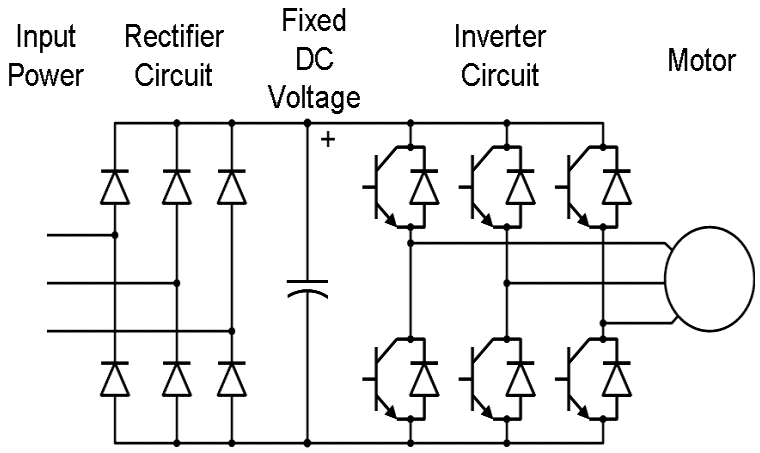

Figure 1.16: Simple VFD Schematic

Three phase diode converter front ends converters draw non-sinusoidal currents that contain odd harmonics. For converters supplied by a balanced voltage source, the input current characteristic harmonics are determined by Equation (1.8.1).

$$h = kq \pm 1 \tag{1.8.1}$$

Where h = the order of the harmonic, k = 1,2,3,..., q = number of pulses of the rectifier system.

Traditional VFD's utilize six-pulse rectifiers (q =6), which means the DC bus voltage consists of portions of the line to line AC waveform and repeats with a 60^o duration, i.e. containing six pulses in 360^o. Thus, the characteristic harmonics on the input of a VFD are h = 5, 7, 11, 13, etc.

Once the supply voltage becomes unbalanced, the input harmonics are no longer limited to the characteristic harmonics, and uncharacteristic triplen harmonics appear such as the 3^{rd} and the 9^{th}. In addition, there is a noticeable increase in the 2^{nd} harmonic on the DC bus voltage. An interesting characteristic of the input current harmonic is as the input voltage becomes more unbalanced, the input current becomes significantly more unbalanced and changes from a double-pulse waveform to a single-pulse waveform due to the asymmetric conduction of the diodes [14]. In some cases, the voltage unbalance can lead to excessive current to flow in one or two of the diodes and that can lead to overload-protection circuits tripping. In addition, the excess current can overheat diodes in the converter and decrease the life-span of the DC link capacitor.

1.9 IEEE Std. 519-1992

In industry, IEEE Std. 519-1992 is the standard for both voltage and current harmonic distortion limits in a power distribution system. IEEE Std. 519 was introduced in 1981 and was revised in 1992. It was intended to provide direction on dealing with harmonics introduced by static power converters and other non-linear loads [13].

Voltage Distortion Limits

Bus Voltage at PCC	Individual Voltage Distortion (%)	Total Voltage Distortion THD (%)
Below 69 kV	3.0	5.0
69 kV to 161 kV	1.5	2.5
161 kV and above	1.0	1.5
NOTE: High-voltage systems can have up to 2.0% THD where the cause is an HVDC terminal that will attenuate by the time it is tapped for a user.		

Figure 1.17: IEEE Std. 519-1992 Voltage Distortion Limits

Current Distortion Limits for General Distribution Systems (120 V Through 69000 V)

Maximum Harmonic Current Distortion in Percent of I_L						
Individual Harmonic Order (Odd Harmonics)						
I_{SC}/I_L	<11	11≤*h*<17	17≤*h*<23	23≤*h*<35	35≤*h*	TDD
<20*	4.0	2.0	1.5	0.6	0.3	5.0
20<50	7.0	3.5	2.5	1.0	0.5	8.0
50<100	10.0	4.5	4.0	1.5	0.7	12.0
100<1000	12.0	5.5	5.0	2.0	1.0	15.0
>1000	15.0	7.0	6.0	2.5	1.4	20.0
Even harmonics are limited to 25% of the odd harmonic limits above.						
Current distortions that result in a dc offset, e.g. half-wave converters, are not allowed.						
* All power generation equipment is limited to these values of current distortion, regardless of actual I_{sc}/I_L.						
Where I_{sc} = maximum short-circuit current at PCC. I_L = maximum demand load current (fundamental frequency component) at PCC. TDD = Total demand distortion (RSS), harmonic current distortion in % of maximum demand load current (15 or 30 min demand). PCC = Point of common coupling.						

Figure 1.18: IEEE Std. 519-1992 Current Distortion Limits

Figure 1.17 shows the IEEE Std. 519-1992 harmonic limits and Figure 1.18 shows the IEEE Std. 519-1992 harmonic limits. The harmonic current limits define the maximum amount of harmonic current the customer can inject into the system. The

utility provider is responsible for providing clean (low distortion) voltage to its customers. However, the utility provider can only do this when its customer meet the harmonic current limits.

The general purpose of IEEE Std. 519-1992 is to limit the harmonic current produced by individual customers and to limit the voltage distortion on the utility provider's voltage supply. One point of confusion in IEEE Std. 519-1992 is the Point of Common Coupling (PCC) location. The PCC is a point where another customer can be served, regardless of metering location or equipment ownership. Often in the field, facility owners will define a PCC inside the facility distribution and require providers of non-linear load equipment to meet IEEE Std. 519-1992 at these PCC's. The goal of IEEE Std. 519-1992 is to prevent one customer from causing harmonic problems for the utility or other customers.

Chapter 2

Problem Statement and Proposed Solution

2.1 Problem Statement

Harmonics are undesirable voltages and currents on a power distribution system caused by non-linear loads. This paper investigates on non-linear load in particular, a variable frequency drive. Under balanced voltage conditions, variable frequency drives exhibit typical or characteristic harmonics on the power distribution system. Under the presence of three phase voltage unbalance, the variable frequency drives exhibit non-typical or non-characteristic harmonics (in addition to characteristic harmonics) in the power distribution system. The goal of this paper will be to investigate one of the many mitigation techniques to reduce the non-characteristic harmonics introduced by the presence of voltage unbalance.

2.2 Proposed Solution

One way to reduce the non-characteristic harmonics on the power distribution system is through the use of notch filters on the DC bus of the variable frequency drive. This paper will analyze the frequency response of the system with and without the notch filters. Then the filters will be added to the DC bus to see how well they reduce harmonics on the DC bus and on the input of the variable frequency drive. Experimental and simulation data are then presented to verify the theories presented in this paper.

Chapter 3

Simulation

3.1 Fast Fourier Transform (FFT)

In prior sections of this paper, the Fourier Transform was shown to be a useful tool for periodic waveform decomposition into the sum of sine waves at different frequencies with different amplitudes. In order to implement the Fourier Transform on any periodic waveform without performing an integration of a function, a given waveform is sampled at discrete values of time and a Discrete Fourier Transform (DFT) is used to extract the power spectrum from the sampled values.

To implement a Discrete Fourier Transform, a given waveform must first be broken down into a set of N sampled discrete values. Given N, the N-point DFT of a sampled waveform, $x[n]$ can be defined as shown in equation (3.1.1)

$$X_k = \sum_{n=0}^{N-1} x[n] e^{\frac{-j2\pi nk}{N}} \tag{3.1.1}$$

The DFT is a versatile and accurate too for calculating the power spectrum of a given periodic waveform. This accuracy and versatility come at the cost of computing speed. In order to evaluate X_k, N complex multiplications and $N-1$ additions must be performed. There are N values of k, so the total number of complex operations

are shown in Equation (3.1.2) [4]

$$N \cdot N + N(N-1) = 2N^2 - N \equiv N^2 \tag{3.1.2}$$

It is important to note that the complex multiplication function is very taxing computationally since it requires four real multiplications and two real additions in order to be performed. to compensate for the large amount of complex multiplications performed, in 1965 James Cooley and John Tukey came up with the Fast Fourier Transform (FFT) [11]. The FFT is a quicker way of calculating the Discrete Fourier Transform of a given periodic waveform. The FFT algorithm requires that the number of data point be $N = 2^r$ for $r = 1, 2, \ldots$. The FFT algorithm also relies on the fact that the N-point DFT of a signal can be broken down into two tasks, each involving an $\frac{N}{2}$-point DFT. The process is repeated until a 1-point DFT is reached.

To better understand how this method for computing the FFT came about, a weighting function, W_N, is introduced as shown in Equation (3.1.3).

$$W_N = e^{\frac{-j2\pi}{N}} \tag{3.1.3}$$

The DFT equation defined earlier can now be rewritten as follows in Equation (3.1.4).

$$X_k = \sum_{n=0}^{N-1} x[n] e^{\frac{-j2\pi nk}{N}} = \sum_{n=0}^{N-1} x[n] W_N^{kn} \tag{3.1.4}$$

At this point, $x[n]$ can be broken down into an odd and even signal as depicted in Equation (3.1.5) and (3.1.6).

$$a[n] = x[2n] \qquad n=0,1,2,\ldots \tfrac{N}{2} - 1 \tag{3.1.5}$$

$$b[n] = x[2n+1] \qquad n=0,1,2,\ldots \tfrac{N}{2} - 1 \tag{3.1.6}$$

The $\frac{N}{2}$-point DFT can now be determined for $a[n]$ and $b[n]$ as shown in Equations

(3.1.7) and (3.1.8).

$$A_k = \sum_{n=0}^{\frac{N}{2}-1} a[n] e^{\frac{-j2\pi nk}{\frac{N}{2}}} \qquad k=0,1,2,\ldots \tfrac{N}{2}-1 \tag{3.1.7}$$

$$B_k = \sum_{n=0}^{\frac{N}{2}-1} b[n] e^{\frac{-j2\pi nk}{\frac{N}{2}}} \qquad k=0,1,2,\ldots \tfrac{N}{2}-1 \tag{3.1.8}$$

The FFT can then be calculated based on A_k and B_k as shown in Equation (3.1.9).

$$X_k = \begin{cases} A_k + W_N^k B_k & k = 0, 1, \ldots \frac{N}{2} - 1, \\ A_{k-\frac{N}{2}} - W_N^k B_k & k = \frac{N}{2}, \frac{N}{2}+1, \ldots, N-1. \end{cases} \tag{3.1.9}$$

The $\frac{N}{2}$-point DFT's, A_k and B_k are combine according to Equation (3.1.9) to compute the N-point DFT X_k. It is important to note that this FFT algorithm requires only $\frac{N}{2}\log_2 N$ operations rather than N^2. This greatly reduces the computing time required to calculate the Fourier Transform of the given waveform.

Using the FFT increases the speed of the calculating the N-point DFT. The speed comes at the cost of versatility, because the FFT function places some restrictions on the signal under analysis. The main restriction being the FFT function requires that there be 2^r number of data points by definition, where $r = 1, 2, 3, \ldots$. Even though using the FFT reduces calculation versatility and accuracy, the power spectrum resolution is still high enough to produce information that is very meaningful. For the purpose of this paper, the FFT Analysis Tool in Simulink® will be used as the primary FFT technique.

3.2 Bode Plot

A Bode plot is a graph of the steady state response of a linear time-invariant (LTI) system. A Bode plot can consist of up to two separate graphs. One graph plots the

magnitude or gain versus the frequency, while another graph plots the phase versus the frequency. Bode plots visually describe the system and they are one of the most commonly used concepts in linear systems theory. A term often used in conjunction with the Bode plot is it describes the *frequency response* of the system. this simply means the steady state response of the system to a sinusoid of a particular frequency.

In general, a sinusoidal function $\sin(\omega t)$ that enters a LTI system will leave the system as $A\sin(\omega t + \theta)$, where A is some gain and θ is some phase change. Figure 3.1 represents the eigenfunction input of a continuous time (CT) system.

Figure 3.1: Transfer function block diagram

Figure 3.1 shows that the output is a product of the input and $H(s)$, which is known as the transfer function. The transfer function can also be used to create the Bode plot. So the Bode plot is also a representation of the transfer function $H(s)$ evaluated along the $j\omega$-axis ($s = j\omega$).

A simple example can be used to better illustrate the mechanics behind creating a Bode plot from the system transfer function. Equation (3.2.1) represents the transfer function of a system. Table 3.1 shows the values that will be used to plot the magnitude and phase graphs of the Bode plot.

$$H(s) = \frac{1}{s + 10} \tag{3.2.1}$$

ω	$\lvert H(j\omega)\rvert$	$\angle H(j\omega)$	$20\log_{10}\lvert H(j\omega)\rvert$
0	0.1000	0.00^o	-20.00 dB
1	0.0995	-5.71^o	-20.04 dB
2	0.0981	-11.31^o	-20.17 dB
5	0.0894	-26.57^o	-20.97 dB
10	0.0707	-45.00^o	-23.01 dB
20	0.0447	-63.43^o	-26.99 dB
50	0.0196	-78.69^o	-34.15 dB
100	0.0100	-84.29^o	-40.04 dB

Table 3.1: Transfer function Bode plot values

Note that in Table 3.1 the magnitude of the $H(j\omega)$ is described by $|H(j\omega)| = \frac{|Numerator|}{|Denomonator|}$ and the phase of $H(j\omega)$ is described as $\angle H(j\omega) = \angle Numerator - \angle Denomonator$. The final column of Table 3.1 show the magnitude of the frequency response on a logarithmic scale. The log scale is used on the horizontal axis to show the frequency response over a wider range of frequencies than are available on a standard linear scale graph of the same physical space. The log scale is also used on the vertical axis of the magnitude plot to compress larger changes and emphasize small ones. On the vertical axis, the unit used to describe magnitude is the decibel dB. The decibel is described as $dB = 20log_{10}(Amplitude)$. One final advantage of log scale plots are the ease with which they can be made by hand.

An examination of Table 3.1, shows that there should be some straight lines on the log-log bode plot of the magnitude. These straight lines are the asymptotes of

the magnitude plot. The straight lines with different slopes meet at breakpoints, which are pole or zero locations. It should be noted that the phase plot changes slope at $0.1 \times breakpoint$ and $10 \times breakpoint$. At the breakpoint, the actual phase plot changes by 45^o and crosses the asymptotic approximation line. I should be noted that the actual magnitude of $(20log(-\frac{1}{\sqrt{2}}))$ or $-3dB$.

Using the transfer function presented in Equation (3.2.1), the asymptotic approximations can be used to derive the Bode plot.

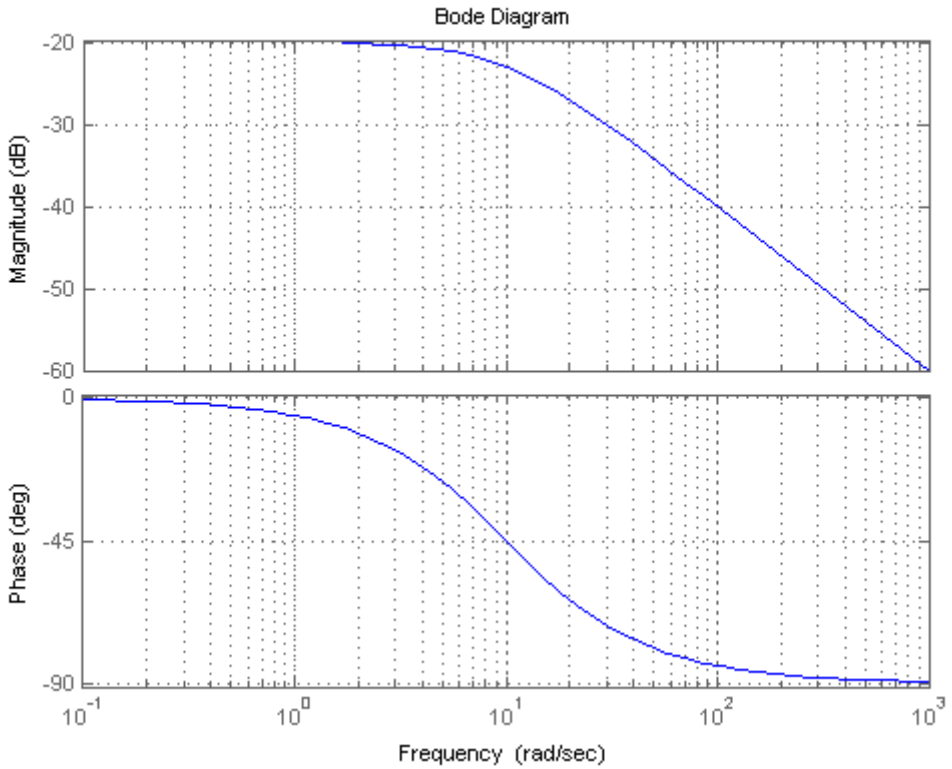

Figure 3.2: Bode plot of first order Transfer Function

Figure 3.2 shows, since $s = j\omega$, a breakpoint occurs at the pole $\omega = 10$. For $\omega < pole$, the transfer function $H(j\omega) \approx \frac{1}{10}$ or $-20dB$. For $\omega > pole$, the transfer function

$H(j\omega) \approx \frac{1}{j\omega}$ or $-20dB/decade$. In the phase plot, for $\omega < 0.1 \times pole$,$H(j\omega) \approx \frac{1}{10}$ or 0^o and for $\omega > 10 \times pole$, $H(j\omega) \approx \frac{1}{j\omega}$, or 90^o, and for $\omega = pole$, $H(j\omega) = \frac{1}{10j+10}$ or -45^o.

The transfer function plotted in Figure 3.2 only has one pole. On occasion, the transfer function will consist of multiple poles and zeros. On these occasions, the log-magnitude plot utilizes the log characteristic that the log of a product is the sum of the logs. As for the phase plot, the phase of a product (division) is the sum (difference) of the phases [7].

Another that often comes up when dealing with the Bode plot of transfer functions is how to handle complex poles and zeros. The Bode plot historically only dealt with real poles and zeros, however this does not mean complex poles and zeros can not be plotted. There are no good rule(s) of thumb for plotting transfer functions with complex poles and zeros. The best path forward is to use simulation software like MATLAB®. There are some interacting observations to be made once the plots are created through simulation software.

$$H(s) = \frac{1}{s^2 + 0.4s + 1.04} \tag{3.2.2}$$

Figure 3.3 shows the Bode plot of the transfer function in Equation 3.2.2. Its interesting to note the bump in the log-magnitude plot peaks where the product of distances to the poles is minimized; this is approximately equal to the imaginary part of the pole location if they are close to the $j\omega$-axis. Another interesting observation is, the closer the poles are to the $j\omega$-axis, the larger the bump height [7]. This bump height is typically based on there being a damping resistor in the circuit. How quickly the phase changes is also based on how high this bump is, with a high spike meaning

a quicker phase change.

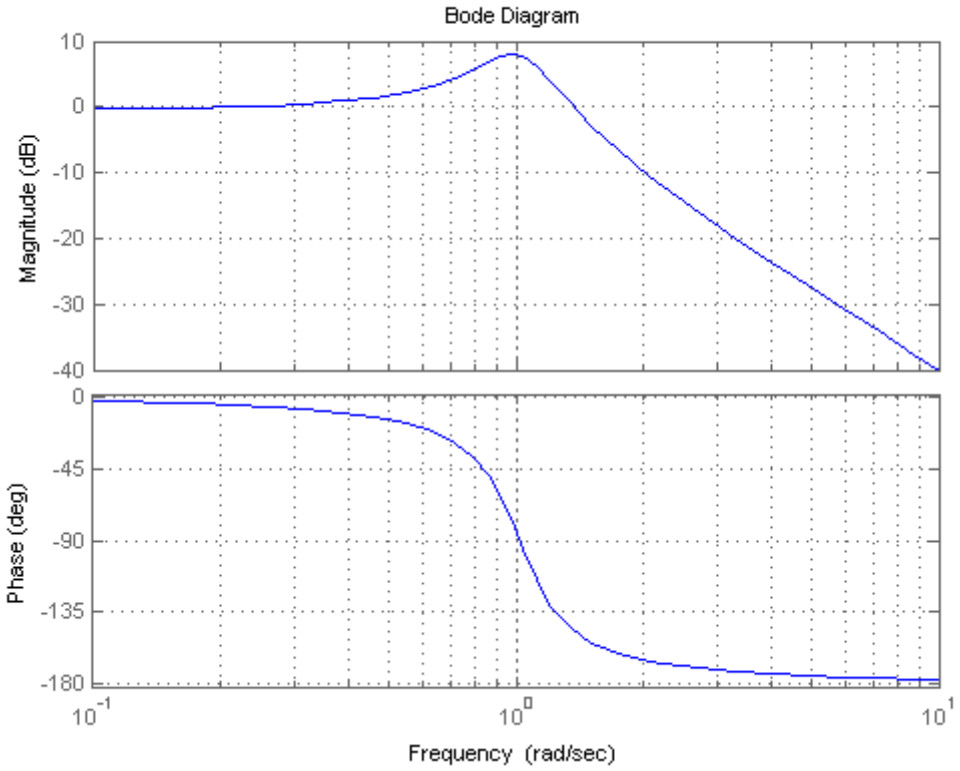

Figure 3.3: Bode plot of second order Transfer Function

3.2.1 Bode Plot of DC Bus Low Pass Filter

The Bode plot was a useful tool that helped display the frequency response of the DC bus before and after the passive filters were added. Figure 3.4 shows the low pass filter LC circuit after the rectifier of the variable frequency drive used in the simulation and experimentation portion of this paper.

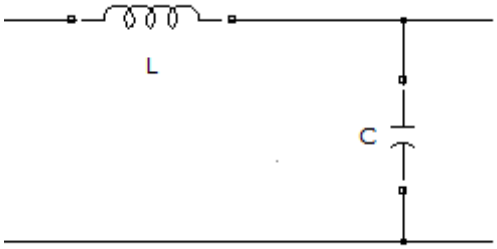

Figure 3.4: VFD Low Pass Filter Circuit

The Transfer Function for Figure 3.4 is shown in Equation (3.2.3).

$$H(s) = \frac{1}{s^2LC + 1} \tag{3.2.3}$$

The Bode plot for the Transfer Function in Equation (3.2.3) is shown in Figure 3.5, where $L = 600\mu H$ and $C = 4300\mu F$.

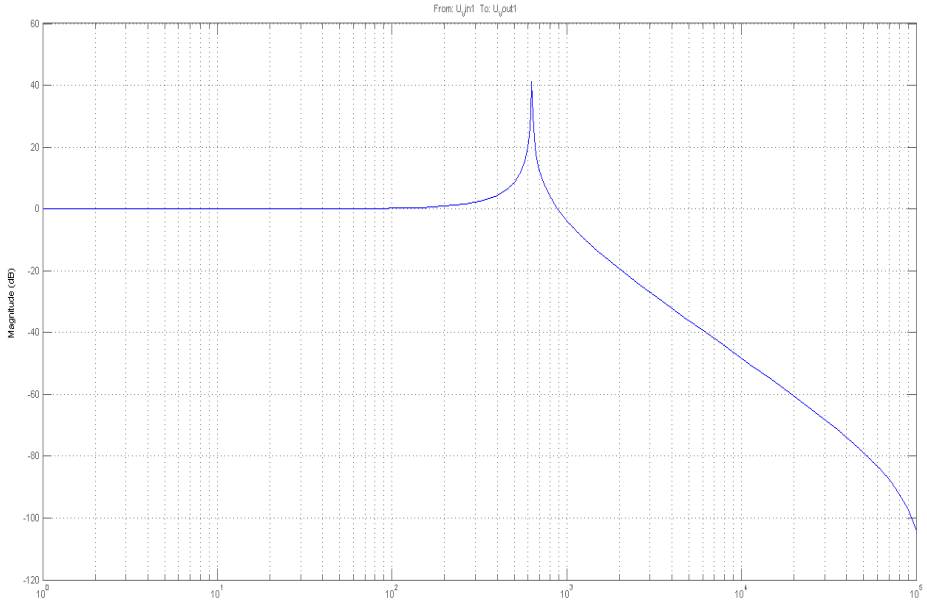

Figure 3.5: VFD Low Pass Filter Bode Plot

As discussed earlier in this paper, under balanced voltage conditions, the largest harmonic contributor is the 6^{th} harmonic and the VFD is designed to especially attenuate this harmonic. Figure 3.5 shows that the low pass filter design in the VFD DC bus has a cutoff frequency of approximately $\omega = 630\frac{rads}{sec}$ or $f = 100Hz$, which is below the 6^{th} harmonic frequency of $360Hz$. This means the low pass filter will start attenuating signals beyond the cutoff frequency of $100Hz$, which includes the $360Hz$, 6^{th} harmonic.

3.2.2 Bode Plot of DC Bus Low Pass Filter with Notch Filters

Under voltage unbalance conditions, the largest contributor to harmonics on the DC Bus is the 2^{nd} harmonic followed by the 6^{th}. So the filters added to the DC bus will target these two harmonics. Figure 3.6 shows the low pass LC circuit on the DC bus along with the 2^{nd} and 6^{th} order notch filters.

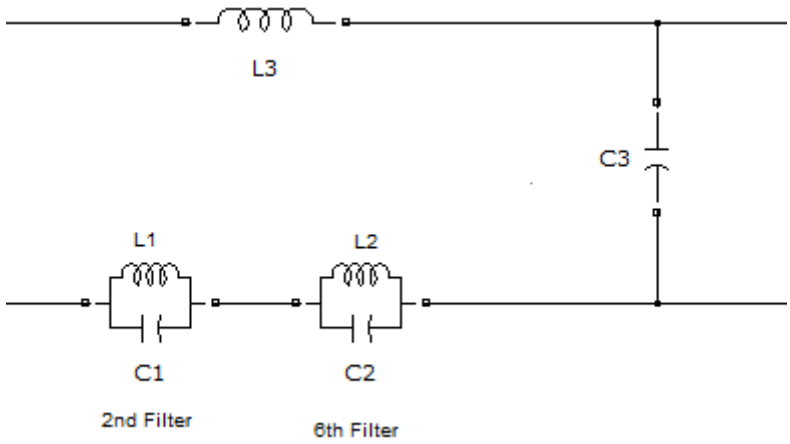

Figure 3.6: VFD Low Pass Filter Circuit with Passive DC Filters

The Transfer Function for Figure 3.6 is shown in Equation (3.2.4).

$$H(s) = \frac{As^4 + Bs^2 + 1}{Cs^6 + Ds^4 + Es^2 + 1} \tag{3.2.4}$$

Where,

$$A = [L_1C_1L_2C_2]$$
$$B = [L_1C_1 + L_2C_2]$$
$$C = [L_1C_1L_2C_2L_3C_3]$$
$$D = [C_3(L_1L_2C_2 + L_2L_1C_1 + L_2C_2L_3 + L_1L_3C_1) + (L_1C_1L_2C_2)]$$
$$E = [C_3(L_1 + L_2 + L_3) + (L_1C_1 + L_2C_2)]$$

The resonance equations presented in earlier sections were used in the design of the filter. The link choke inductor size was used as a starting point for tuning the notch filters that were added to the DC bus. The calculated circuit parameters in Figure 3.6 are $L_3 = 600\mu H$, $C_3 = 4300\mu F$, $C_1 = 978\mu F$, $L_1 = 1800\mu H$, $L_2 = 600\mu H$, $C_2 = 326\mu H$. The Bode plot for the calculated circuit parameters are shown in Figure 3.7.

Due to limited equipment availability in the experimental set up, the circuit components were chosen based on how close they were to the calculated circuit parameters. The actual circuit parameters in Figure 3.6 are, $L_3 = 600\mu H$, $C_3 = 4300\mu F$, $C_1 = 1000\mu F$, $L_1 = 1620\mu H$, $L_2 = 500\mu H$, $C_2 = 330\mu F$. The bode plot for actual circuit parameters are shown in Figure 3.8.

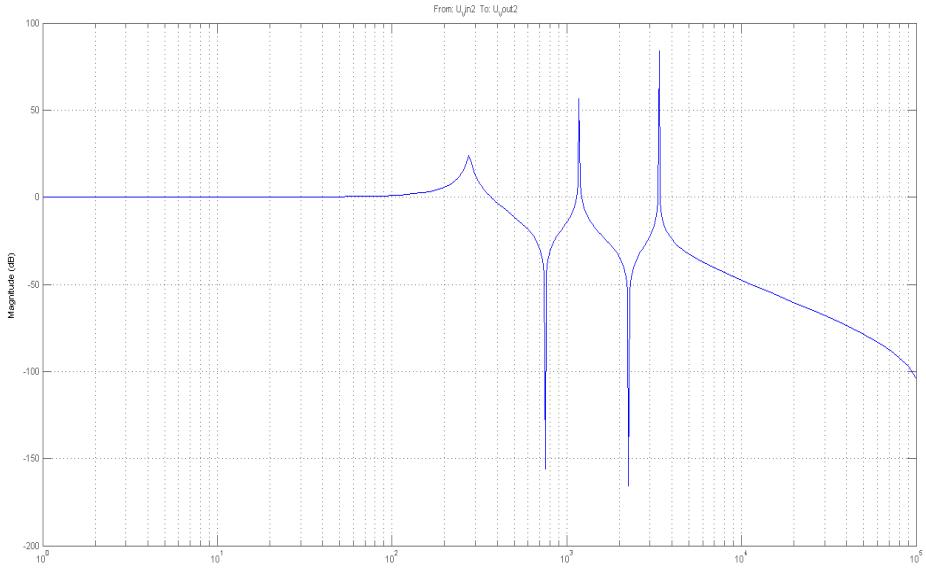

Figure 3.7: Calculated VFD Low Pass Filter Circuit with Passive DC Filters Bode Plot

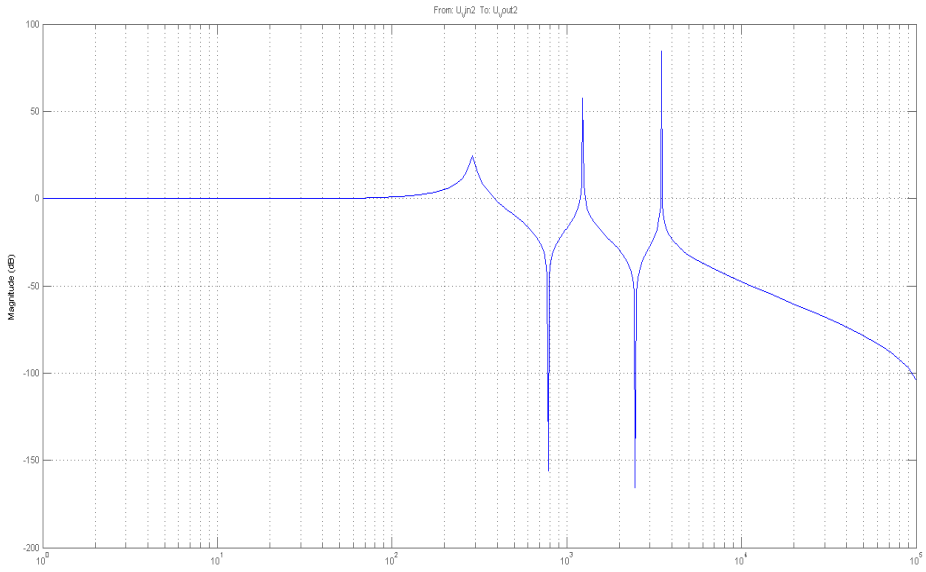

Figure 3.8: Actual VFD Low Pass Filter Circuit with Passive DC Filters Bode Plot

Table 3.2 show show some critical frequency comparisons between the calculated and actual circuit parameters.

Calculated and Actual Critical Frequencies		
Type	Calculated Component Values	Actual Component Values
Spike	$\omega = 276\frac{rads}{sec}\ (f = 43Hz)$	$\omega = 290\frac{rads}{sec}\ (f = 46Hz)$
	$\omega = 1180\frac{rads}{sec}\ (f = 188Hz)$	$\omega = 1230\frac{rads}{sec}\ (f = 196Hz)$
	$\omega = 3380\frac{rads}{sec}\ (f = 538Hz)$	$\omega = 3490\frac{rads}{sec}\ (f = 555Hz)$
Notch	$\omega = 753\frac{rads}{sec}\ (f = 120Hz)$	$\omega = 786\frac{rads}{sec}\ (f = 125Hz)$
	$\omega = 2260\frac{rads}{sec}\ (f = 360Hz)$	$\omega = 2460\frac{rads}{sec}\ (f = 392Hz)$

Table 3.2: Calculated and Actual Critical Frequencies

From Table 3.2, the cutoff frequency of the LC low pass filter portion of the VFD DC bus is at 43Hz for the calculated circuit parameters and 46Hz for the actual circuit parameters. Since the fundamental frequency is 60Hz, which is beyond the cutoff frequency, there will be some attenuation on the signal at the fundamental frequency. Table 3.2 also shows a calculated notch at 120Hz and an actual notch at 125Hz. This notch filter is used to reduce the second order harmonic. Table 3.2 also shows a calculated notch at 360Hz and an actual notch at 392Hz. this notch filter is used to further reduce the sixth order harmonic. There are also additional spikes at two frequencies in both the actual and calculated values. These spikes arise due to unwanted series resonance paths in the circuit. It is important to make sure these spikes do not occur at characteristic harmonics on the DC bus. It is a good idea to select components such that these spikes occur at non-integer multiples of the

fundamental frequency. Dividing the two actual values by the fundamental frequency yield harmonic orders of 3.3 and 9.3.

3.3 Simulation

The most common 6-pulse Variable Frequency Drive (VFD) topology is shown in Figure 3.9. Though the rectifier section utilizes a simple, cheap, and control-less design, it does contain higher harmonic distortion than other types of AC/DC converters. The rectifier operates by conducting the diodes when the AC voltage is greater than the DC link voltage. When the diodes conduct, they cause pulses of current on the DC bus. These current pulses must be handled by the DC link capacitor(s).

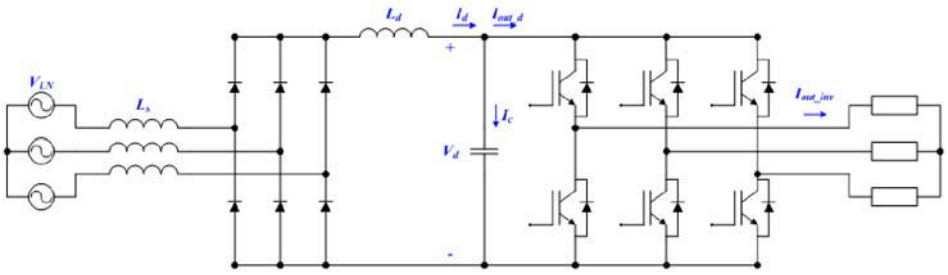

Figure 3.9: 6-Pulse VFD Topology

The first step in selecting the DC bus inductor and capacitor is to calculate the ripple current on the DC bus. To calculate the ripple current, some information must be gathered from the circuit. They include the line to line voltage (V_{LL}), the line frequency (f_{line}), the total inductance (L_{total}, includes the source and DC link inductance), and output current (I_{out}, current flowing to the inverter). Figure 3.10 better depicts the circuit parameters required to calculate the ripple current.

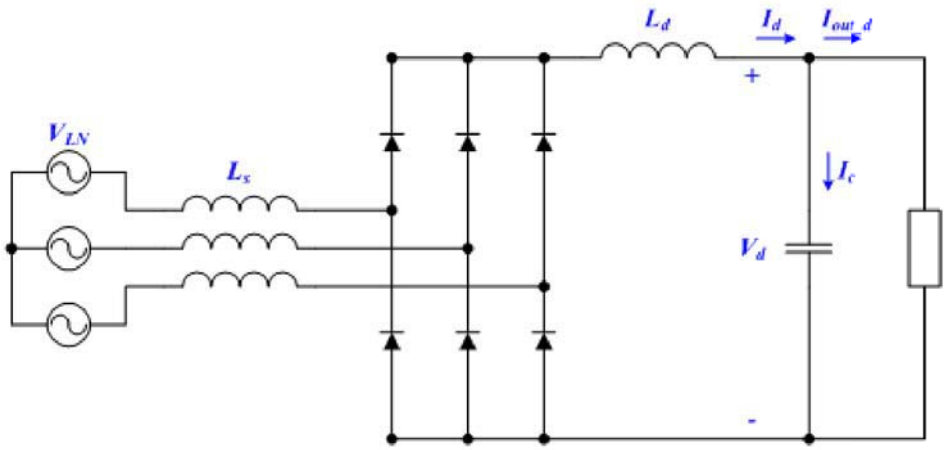

Figure 3.10: 6-Pulse Converter Section of VFD Topology

Following the path of current in the circuit show that the total impedance given in Equation (3.3.1).

$$L_{Total} = 2L_s + L_d \tag{3.3.1}$$

The percent impedance is now defined in Equation (3.3.2).

$$\%impedance = \omega \cdot L_{Total} \cdot \frac{I_{rms}}{V_{LL}} \cdot 100\% \tag{3.3.2}$$

It is interesting to note that continuous conduction occurs when $\%impedance > 1.3\%$. This means the total minimum inductance can be calculated as shown in Equation (3.3.3).

$$L_{Total\_Minimum} = \frac{1.3\%}{\omega} \cdot \frac{V_{LL}}{I_{rms}} \tag{3.3.3}$$

Under balanced conditions, Figure 3.11 shows the most significant contributor of harmonics on the DC bus is the sixth harmonic. This is the reason the inductor and capacitor on the DC bus are designed to reduce the sixth harmonic. The sixth order harmonic current on the DC bus is calculated from Equation (3.3.4).

$$i_{c\_6\_rms} = \frac{2}{35} \cdot \frac{1.35 \cdot V_{LL}}{\sqrt{2} \cdot 6 \cdot \omega \cdot L_{Total}} \tag{3.3.4}$$

The sixth order harmonic ripple current describes the peak ripple current that flows in the capacitor. The peak ripple current (I_{peak}), the ripple voltage (Δv), and the line frequency (f) can be used to calculate the size of the capacitor, as shown in Equation (3.3.5).

$$C_d = \frac{2}{\Delta v} \cdot \frac{\sqrt{2} \cdot i_{c\_6\_rms}}{6 \cdot \omega} \tag{3.3.5}$$

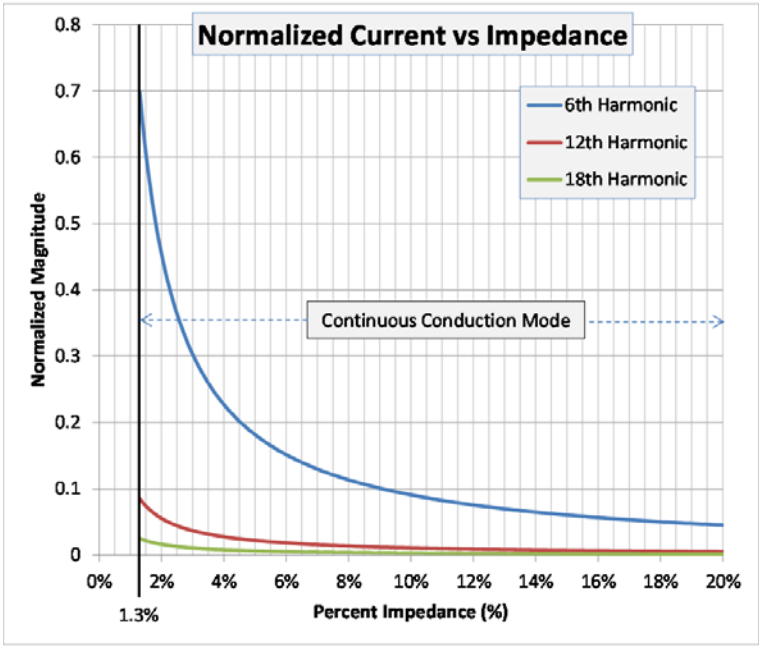

Figure 3.11: Normalized Current vs. Impedance

3.3.1 MATLAB® Simulations

This MATLAB® simulation is broken down into multiple sections. The simulations presented in those sections are based on an experimental set-up presented later in this paper. All of the simulations presented utilize a 36KVA variable frequency drive to run a 3HP motor. The drive was designed with a 600μH DC link chock inductor and a 4300μF DC bus capacitor. The transformer supplying power to the VFD is

rated at 27KVA. The first section will show readings from the system under balanced voltage conditions. The second section will show readings from the system under severe voltage unbalance conditions (> 3% voltage unbalance). Finally, the third section will show readings from the system under severe voltage unbalance conditions with passive filters on the DC bus.

3.3.2 Balanced Voltage Conditions Simulation

Figure 3.12 shows the Simulink® circuit diagram for a variable frequency drive running a motor under balanced voltage conditions.

Figures 3.13 and 3.14 show the input voltage waveform and the input current waveforms respectively. The voltage waveforms show a flat-topping effect at the top of the waveforms. These are caused by the characteristic harmonics present in the system, i.e. the 5^{th}, 7^{th}, 11^{th}, 13^{th}, etc. The current waveforms show much more severe contributions of the characteristic harmonics.

Figure 3.15 and Figure 3.16 show the THD spectrum for Vab and Ia respectively. The FFT spectrum shows the amplitude of the characteristic harmonic contributors. The spectrums also show the THD for the voltage waveform as 5.11% and the THD for the current waveform as 79.94%. Figure 3.17 and Figure 3.18 show the harmonic spectrum table for Vab and Ia respectively.

Figure 3.19 and Figure 3.20 show the harmonic spectrum graph and table for the DC bus voltage. An interesting point to note is the size of the ripple voltage which is only about 2 volts.

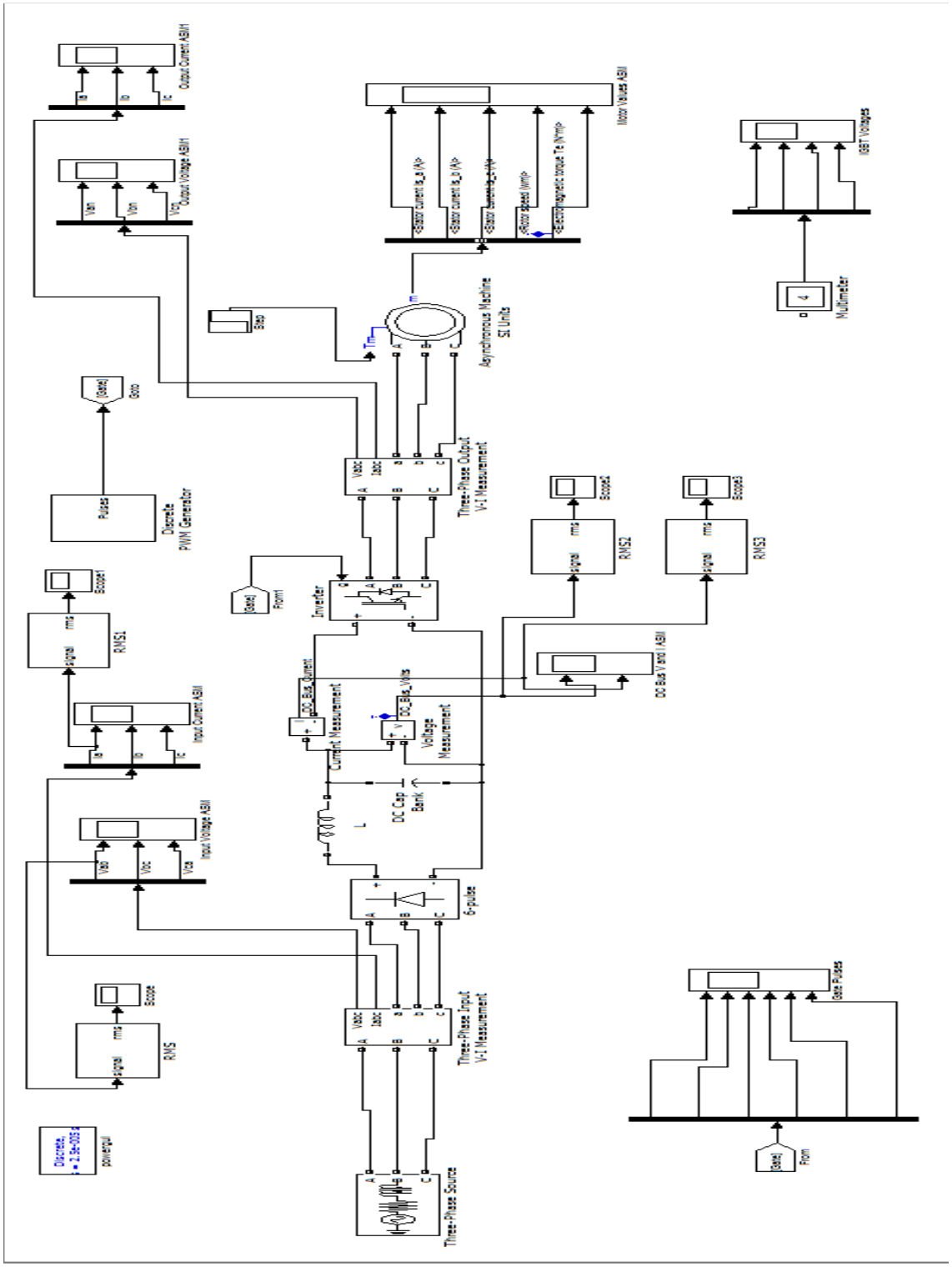

Figure 3.12: Three Phase Balanced Voltage Circuit Simulation

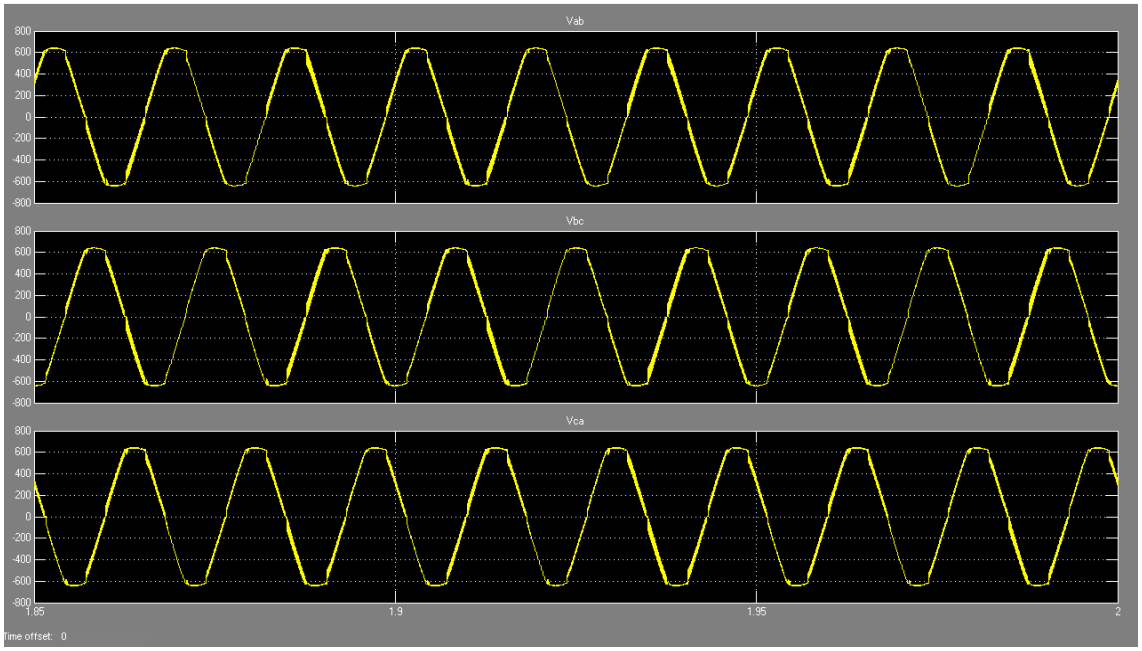

Figure 3.13: Three Phase Balanced Voltage Waveform

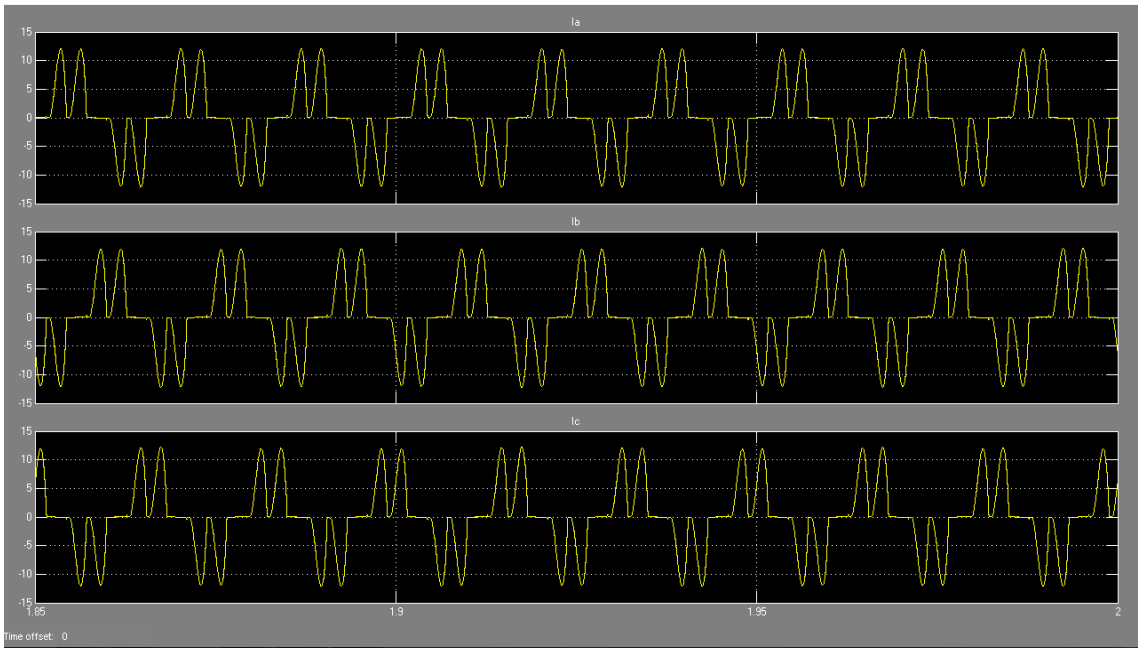

Figure 3.14: Three Phase Balanced Current Waveform

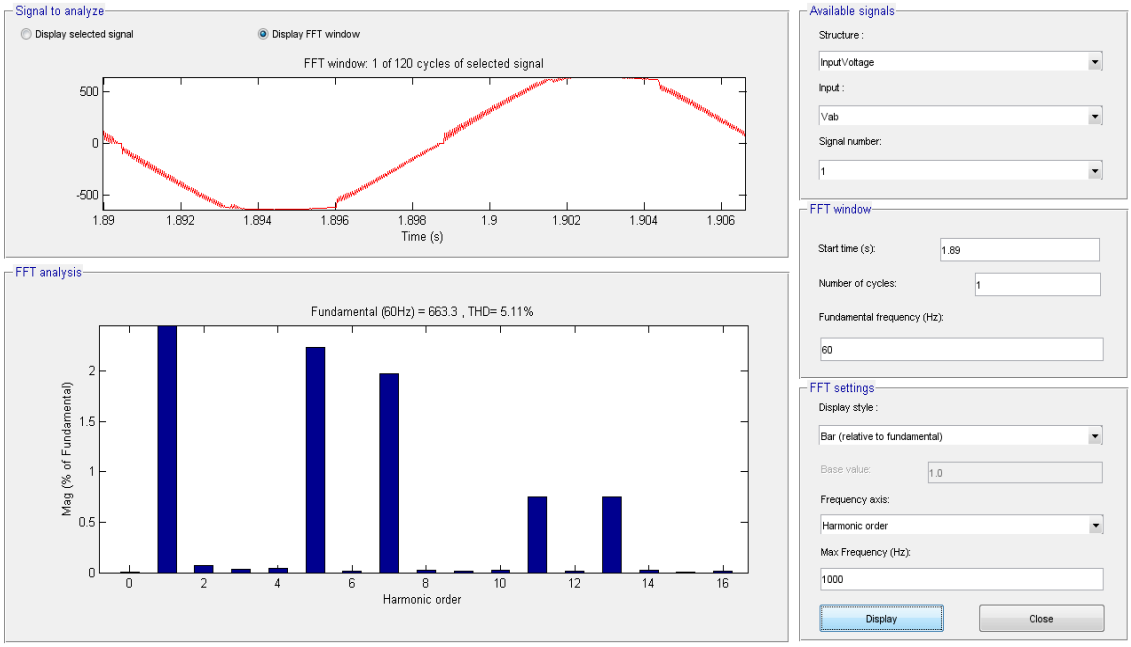

Figure 3.15: Three Phase Balanced Vab Harmonic Spectrum Graph

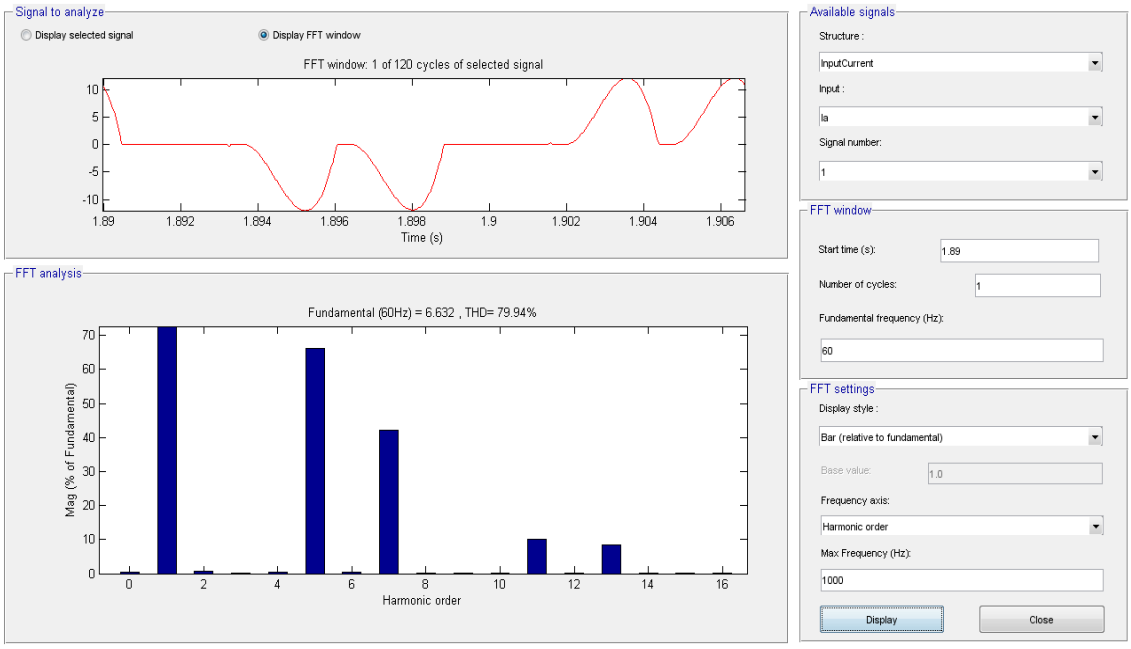

Figure 3.16: Three Phase Balanced Ia Harmonic Spectrum Graph

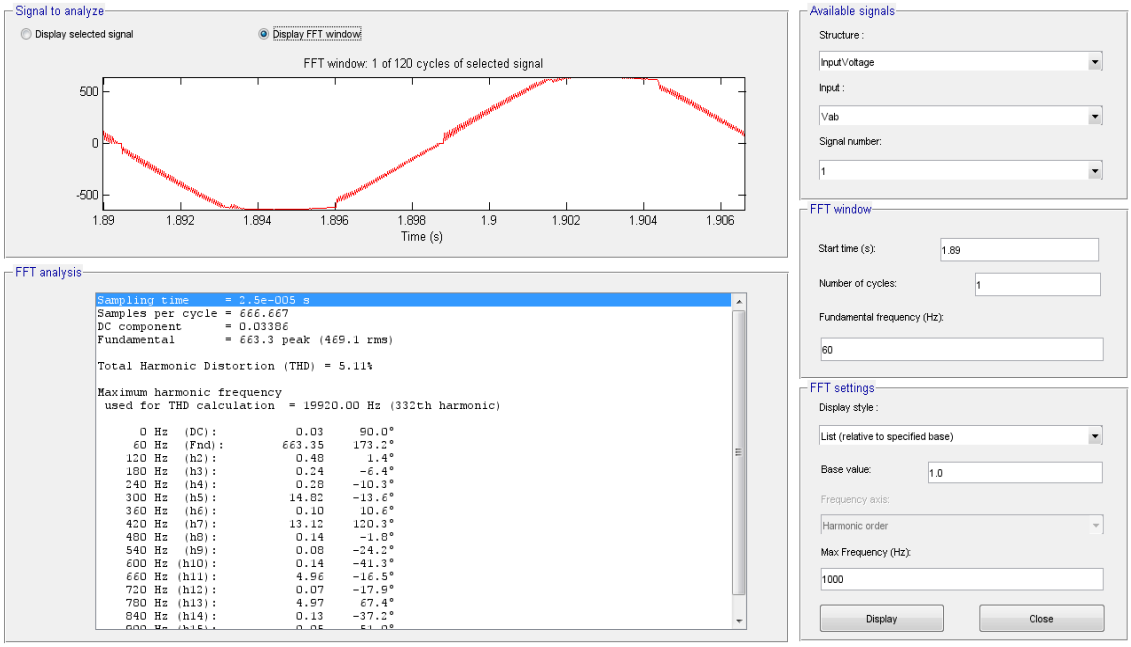

Figure 3.17: Three Phase Balanced Vab Harmonic Spectrum Table

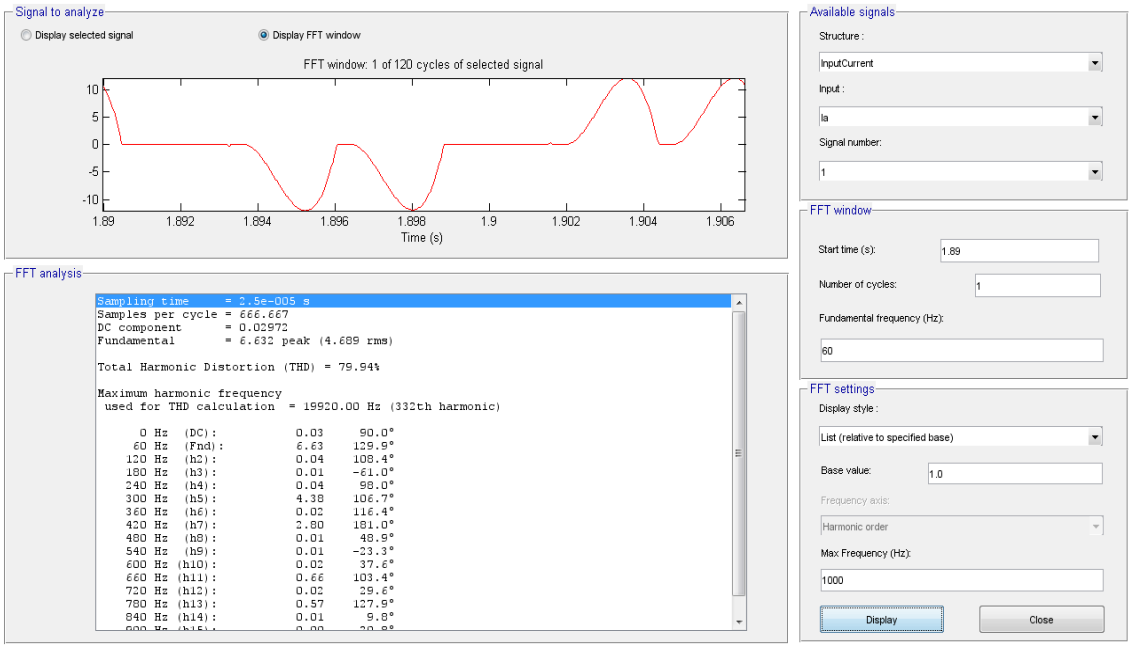

Figure 3.18: Three Phase Balanced Ia Harmonic Spectrum Table

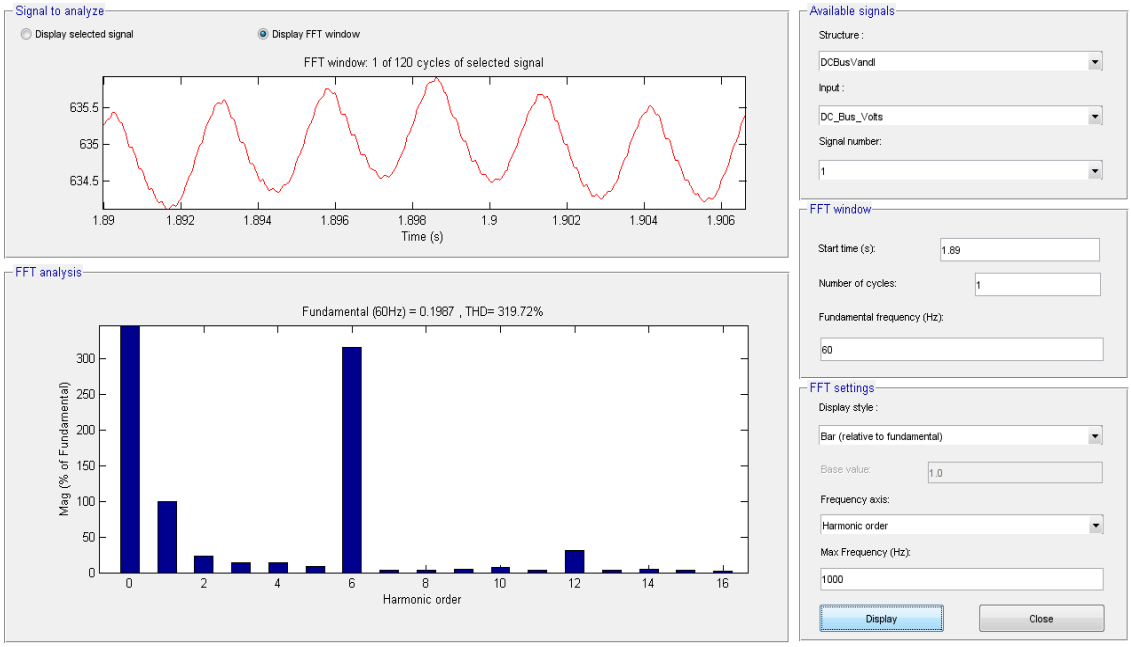

Figure 3.19: Three Phase Balanced DC Bus Voltage Harmonic Spectrum Graph

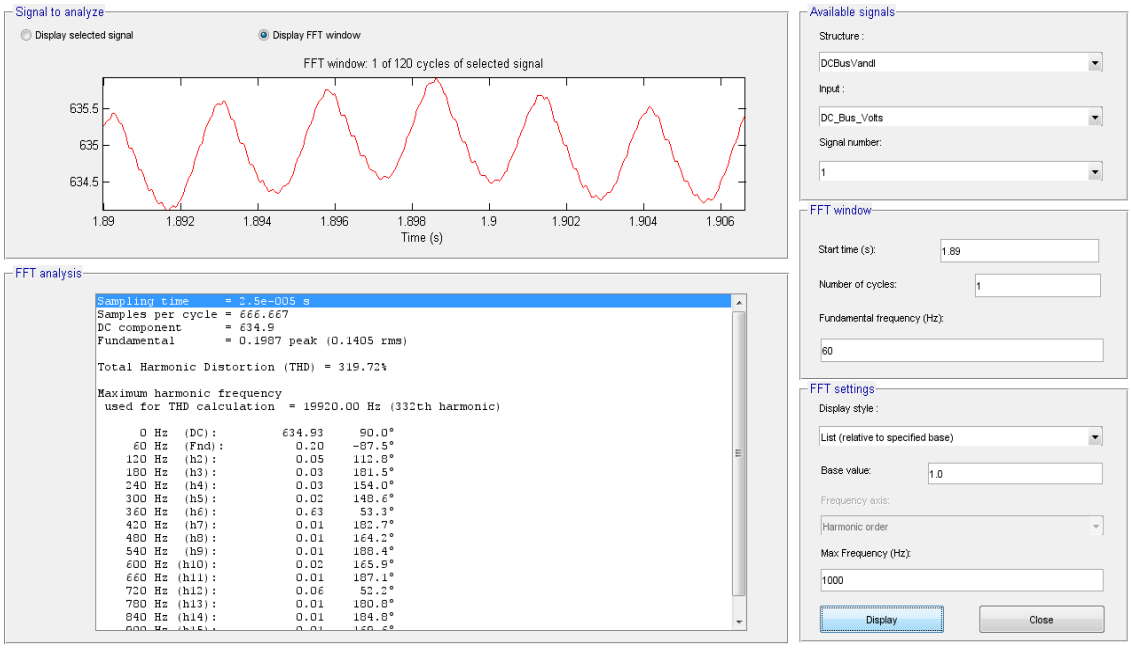

Figure 3.20: Three Phase Balanced DC Bus Voltage Harmonic Spectrum Table

3.3.3 Unbalanced Voltage Conditions Simulation

Figure 3.21 shows the Simulink® circuit diagram for the variable frequency drive running a motor under unbalanced voltage conditions. The approximate voltage unbalance on the three phase input is 3.1%.

Figure 3.22 and 3.23 show the input voltage waveform and input current waveforms respectively. The waveforms show that the voltage and current waveforms vary more from one phase to the next than in the balanced voltage condition simulation. The characteristic harmonics are still present in each phase, however the voltage and current THD's vary from one phase to the next. The THD for Vab=13.55%, Vbc=11.76%, Vca=7.31%, Ia=73.75%, Ib=33.18%, and Ic=85.69%. Figure 3.24 and 3.25 show the FFT spectrum graph and table for Vab respectively. Figure 3.26 and 3.27 show the FFT spectrum graph and table for Vbc respectively. Figure 3.28 and 3.29 show the FFT spectrum graph and table for Vca respectively. Figure 3.30 and 3.31 show the FFT spectrum graph and table for Ia respectively. Figure 3.32 and 3.33 show the FFT spectrum graph and table for Ib respectively. Figure 3.34 and 3.35 show the FFT spectrum graph and table for Ic respectively.

Figure 3.36 and 3.37 show the harmonic spectrum graph and table for the DC bus voltage. An interesting point to note here is the size of the voltage ripple which is now about 6 volts.

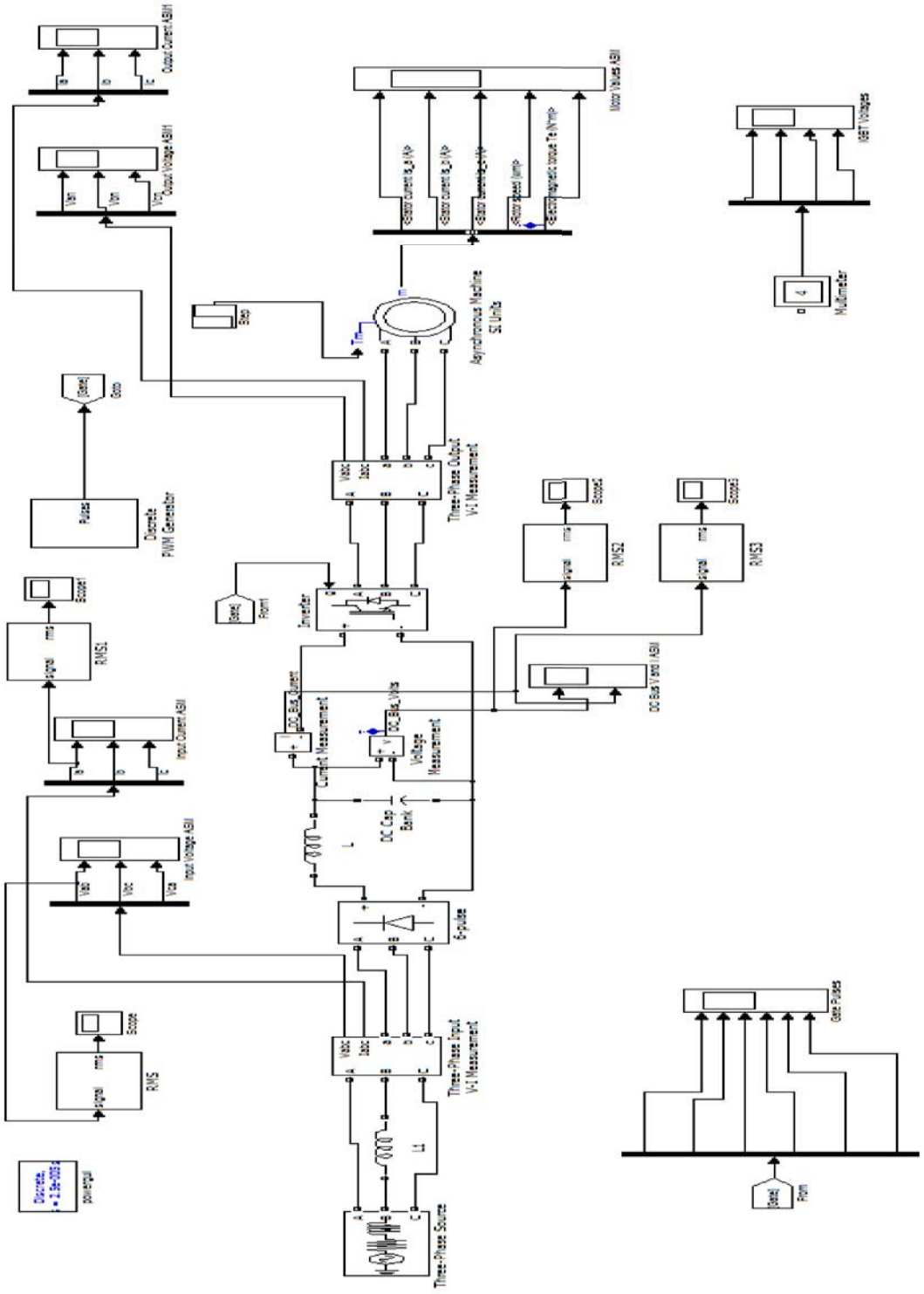

Figure 3.21: Three Phase Unbalanced Voltage Circuit Simulation

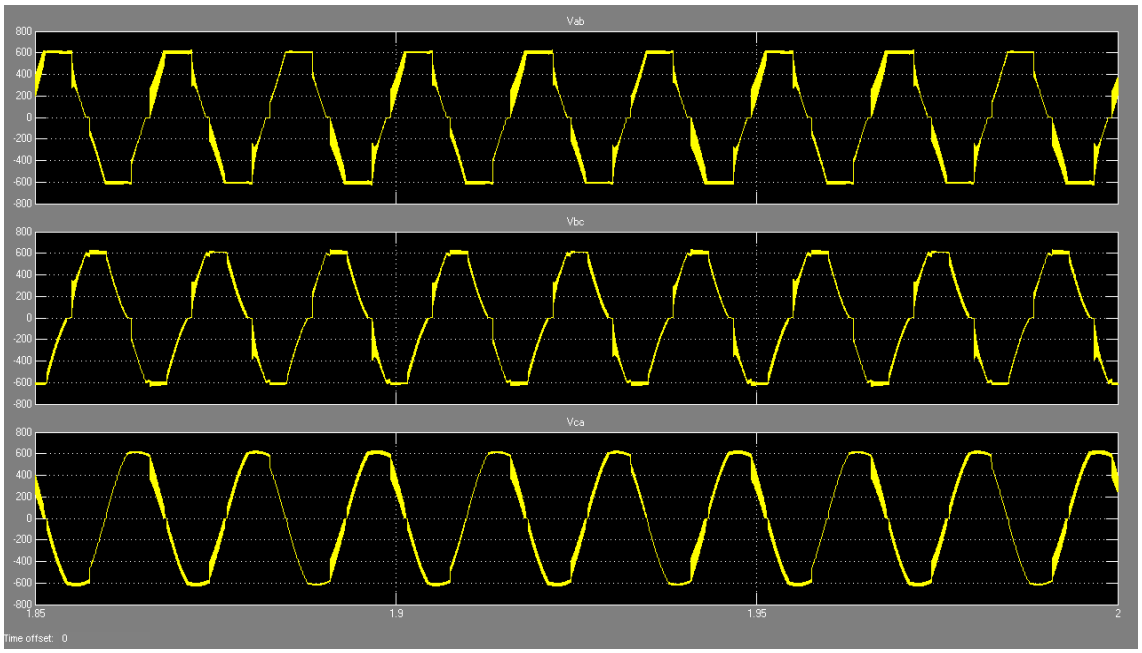

Figure 3.22: Three Phase Unbalanced Voltage Waveform

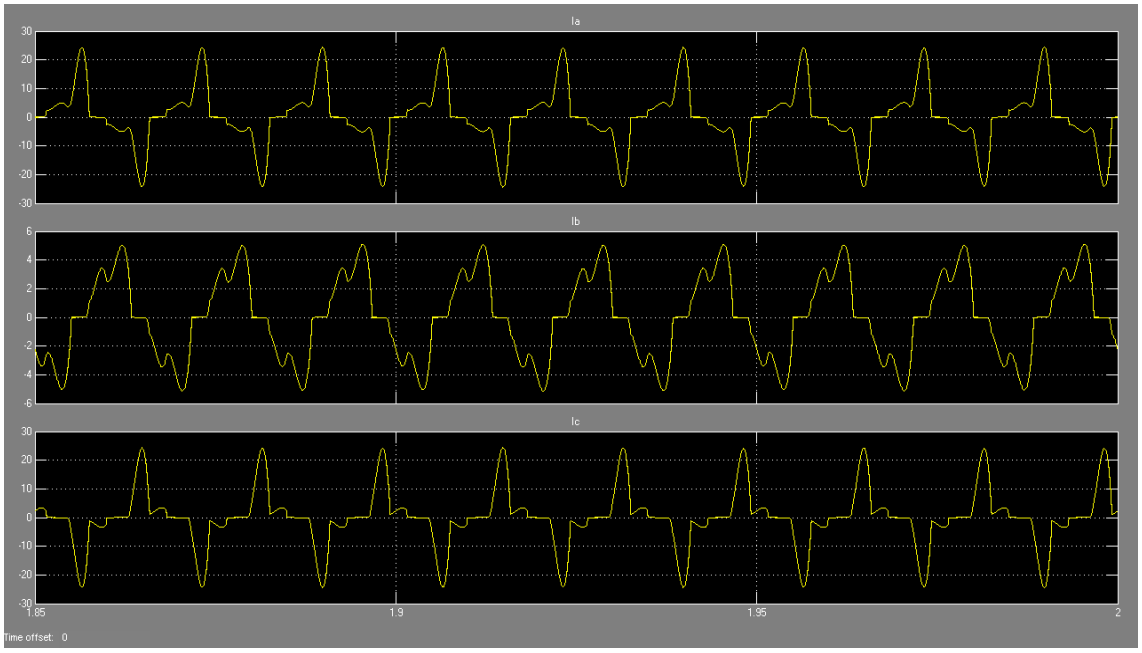

Figure 3.23: Three Phase Unbalanced Current Waveform

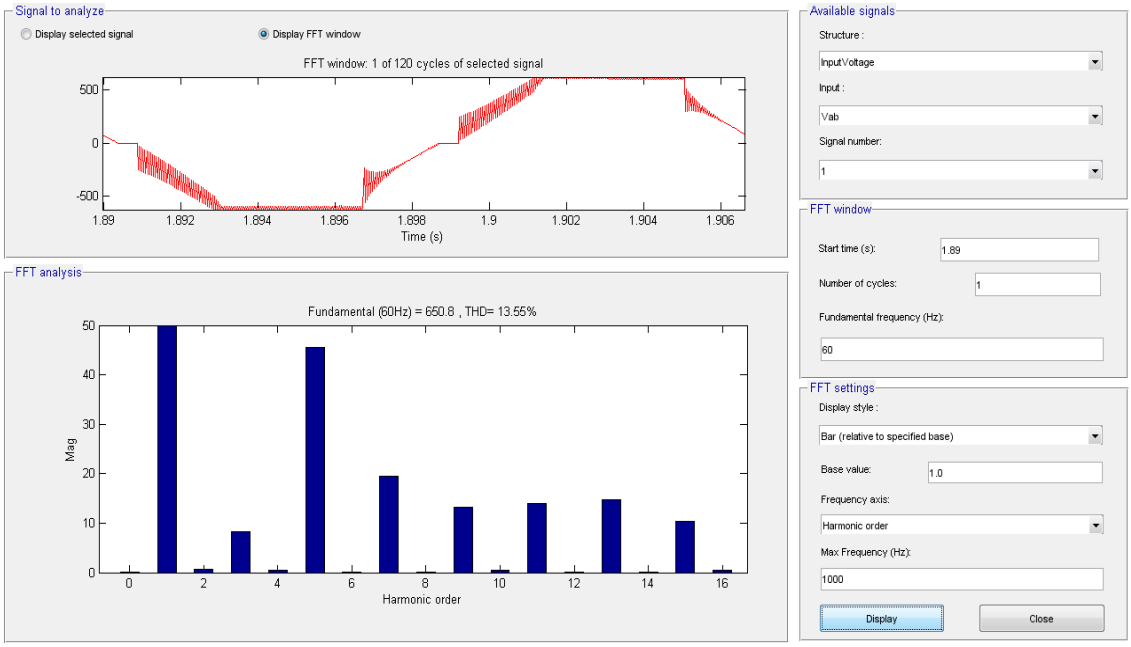

Figure 3.24: Three Phase Unbalanced Vab Harmonic Spectrum Graph

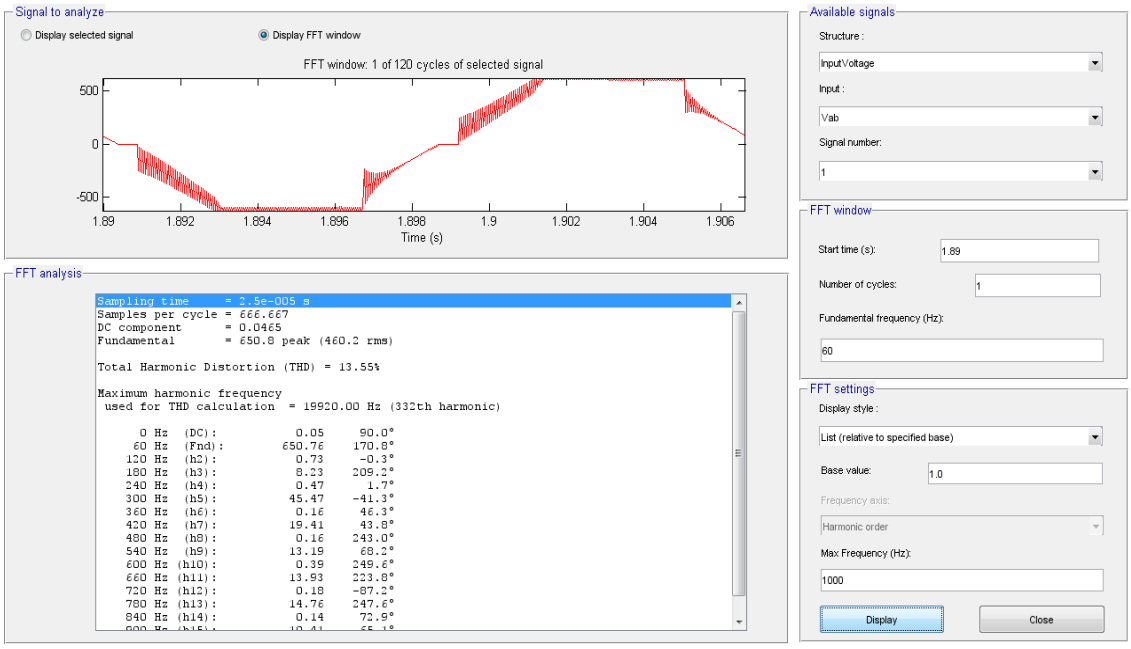

Figure 3.25: Three Phase Unbalanced Vab Harmonic Spectrum Table

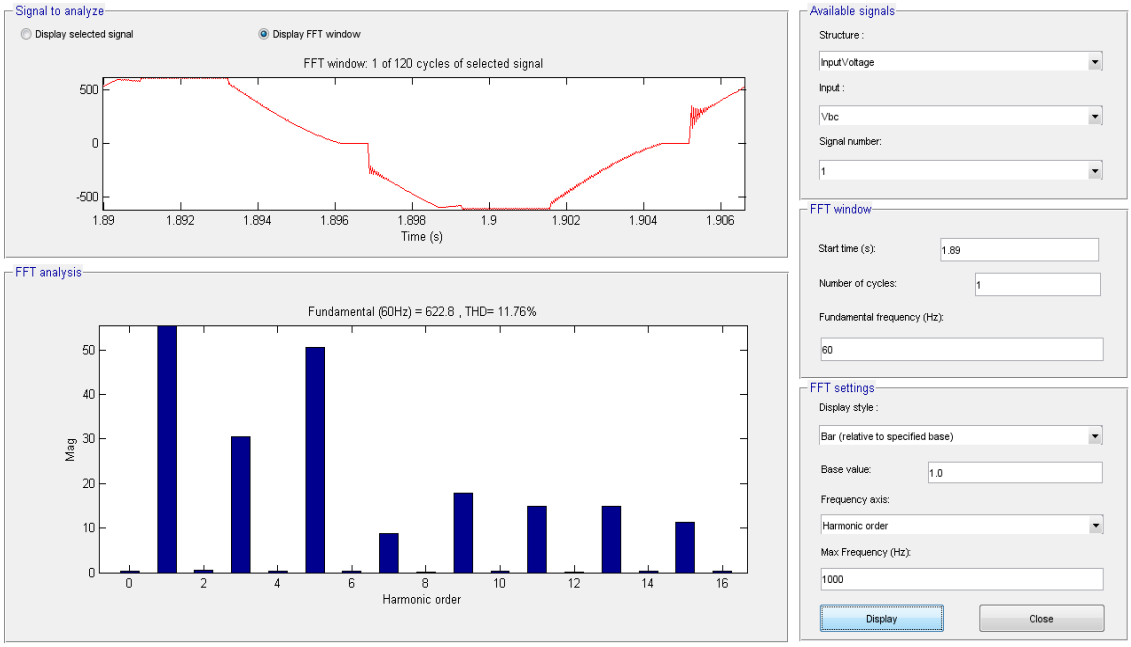

Figure 3.26: Three Phase Unbalanced Vbc Harmonic Spectrum Graph

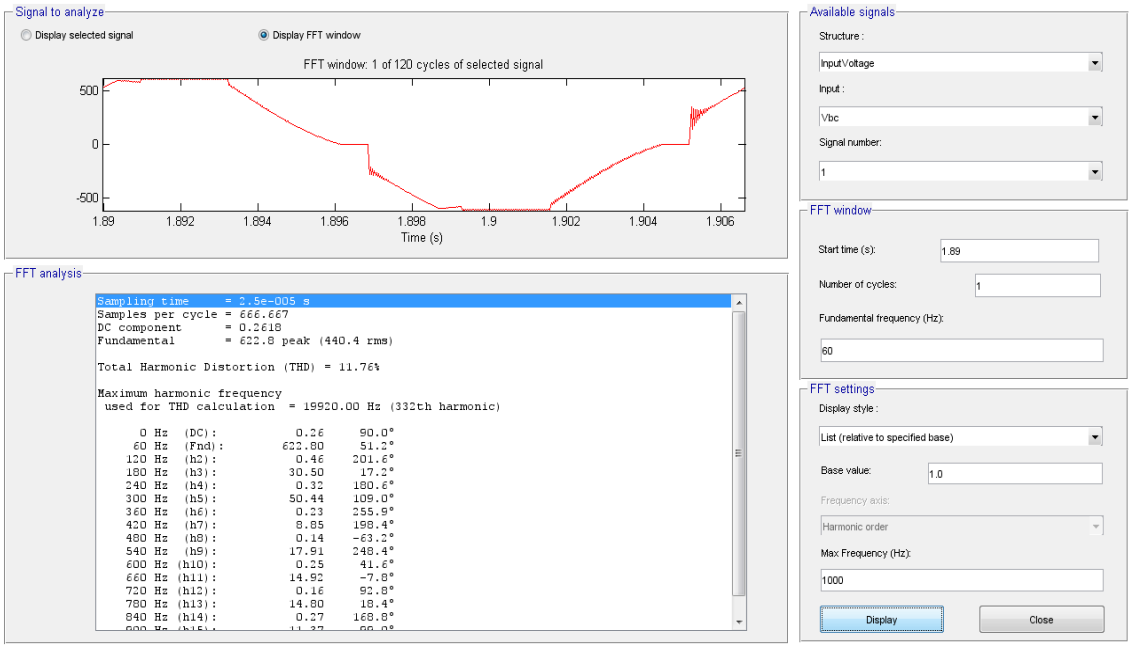

Figure 3.27: Three Phase Unbalanced Vbc Harmonic Spectrum Table

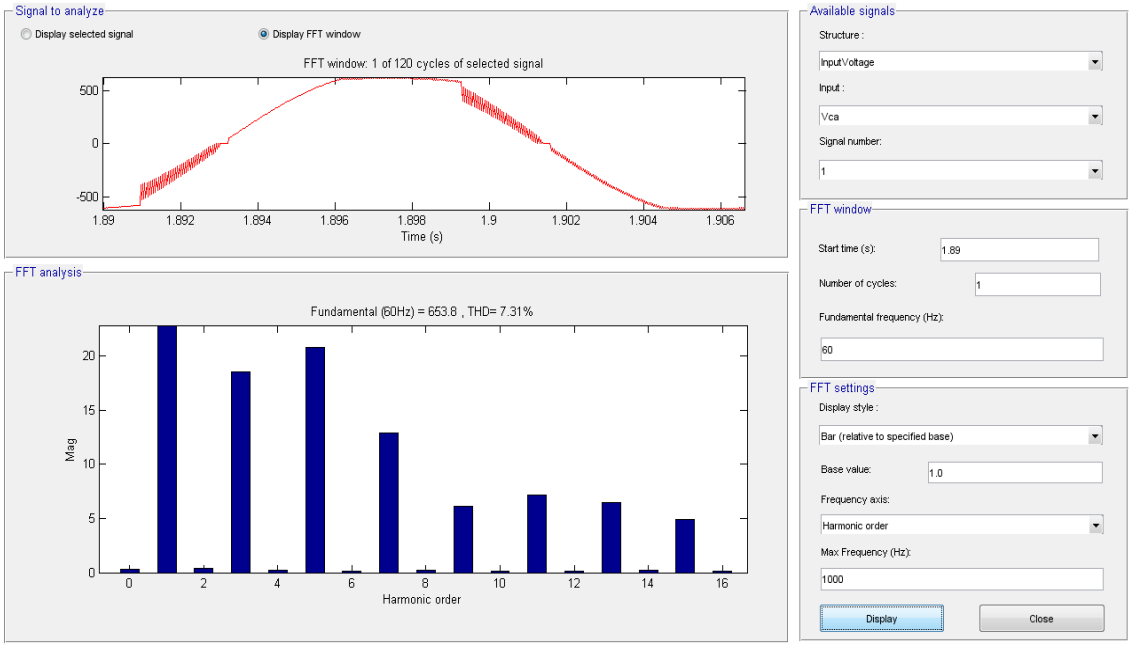

Figure 3.28: Three Phase Unbalanced Vca Harmonic Spectrum Graph

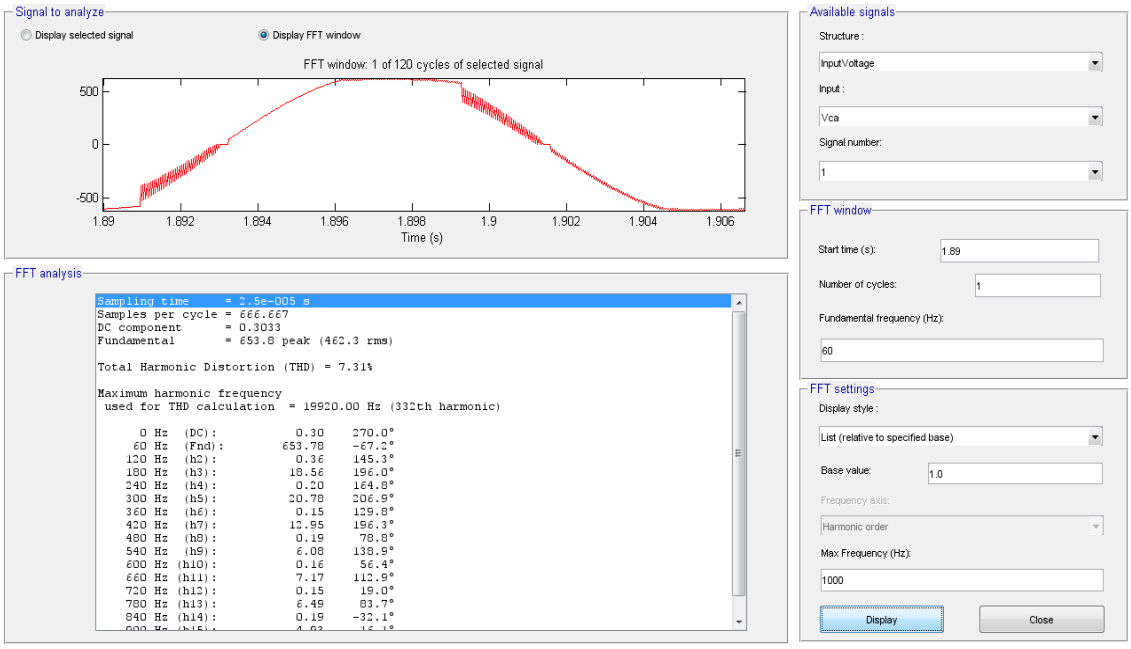

Figure 3.29: Three Phase Unbalanced Vca Harmonic Spectrum Table

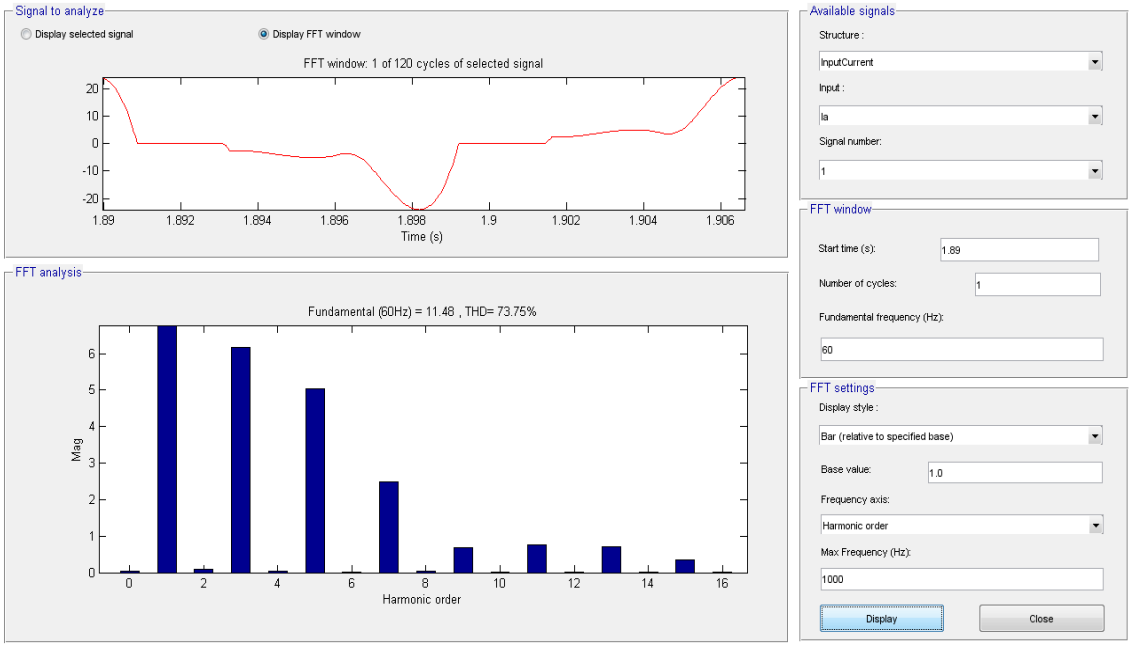

Figure 3.30: Three Phase Unbalanced Ia Harmonic Spectrum Graph

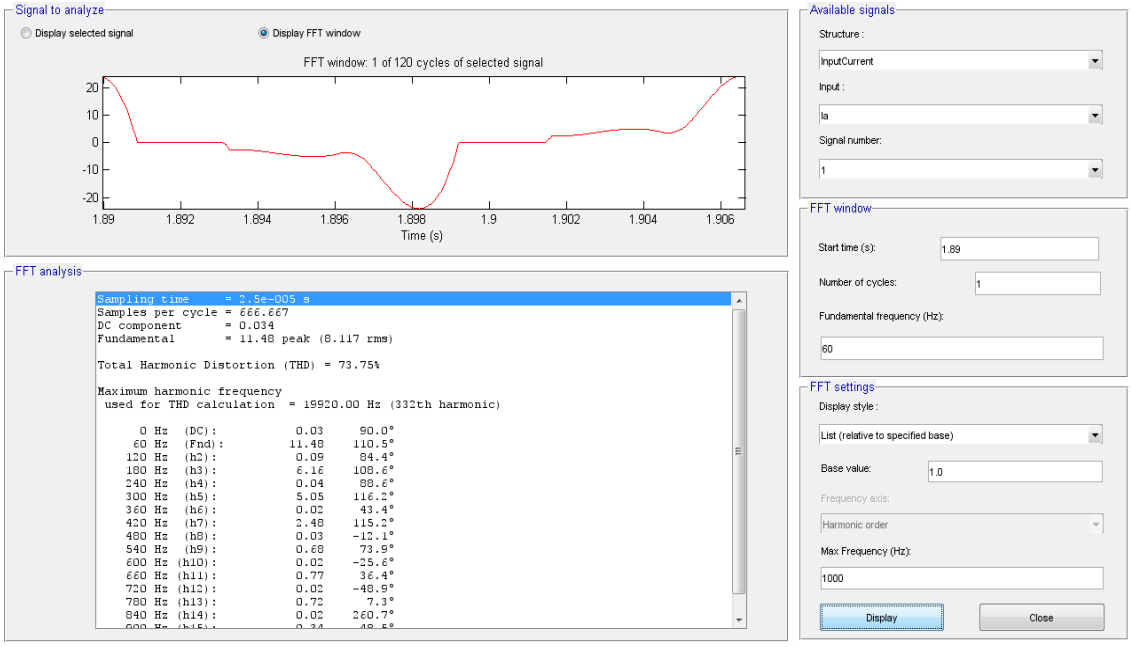

Figure 3.31: Three Phase Unbalanced Ia Harmonic Spectrum Table

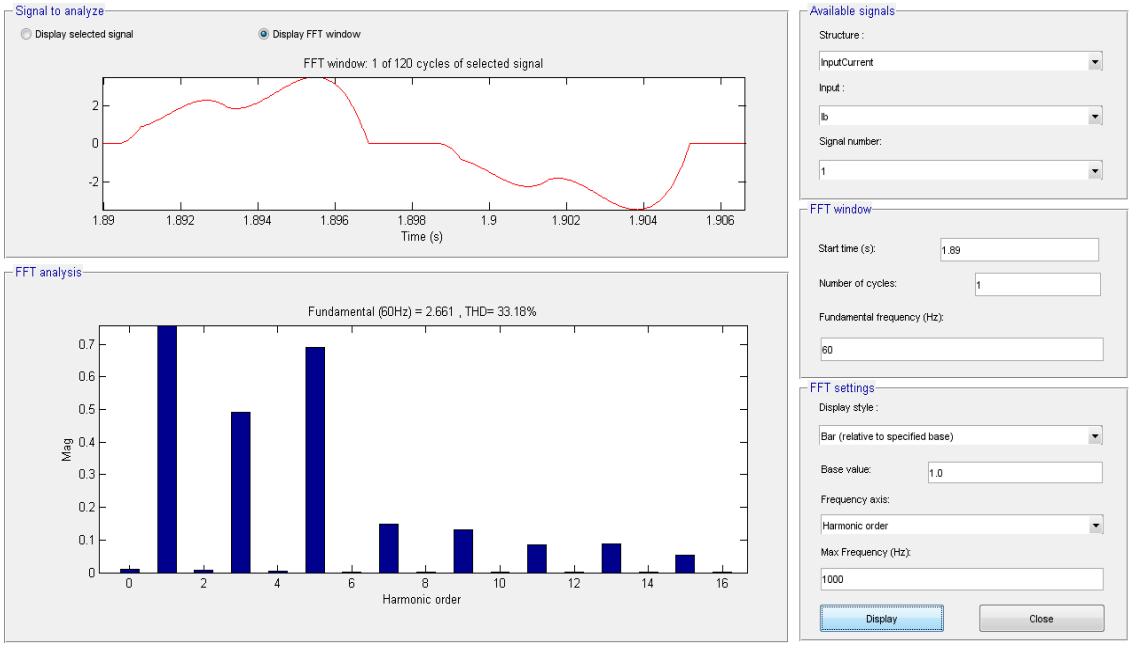

Figure 3.32: Three Phase Unbalanced Ib Harmonic Spectrum Graph

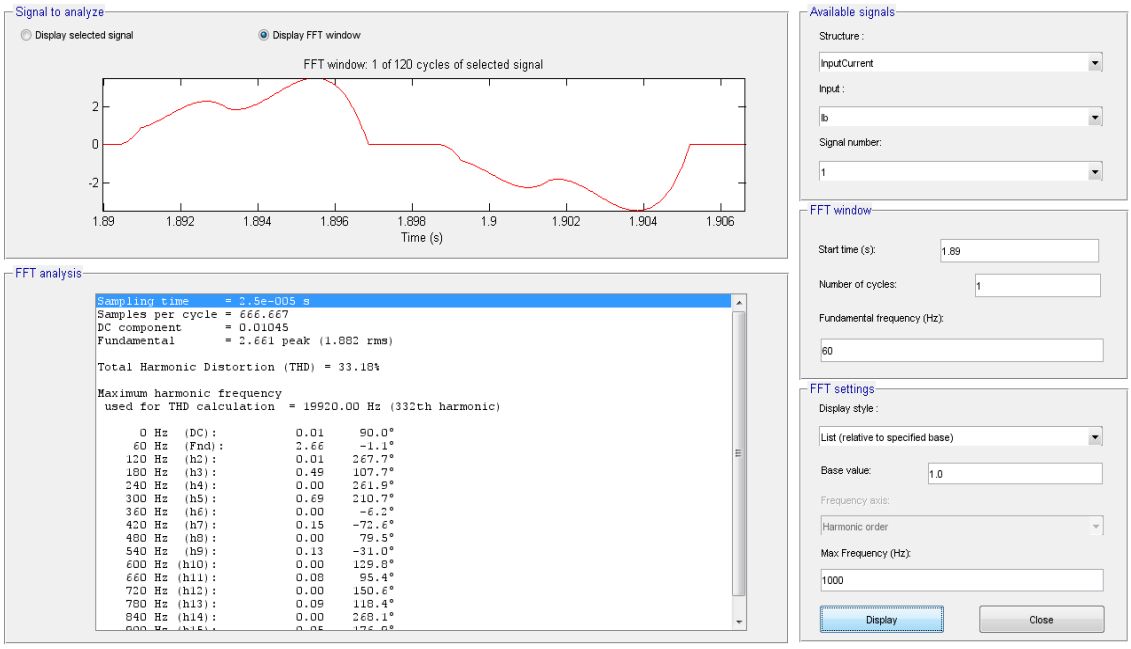

Figure 3.33: Three Phase Unbalanced Ib Harmonic Spectrum Table

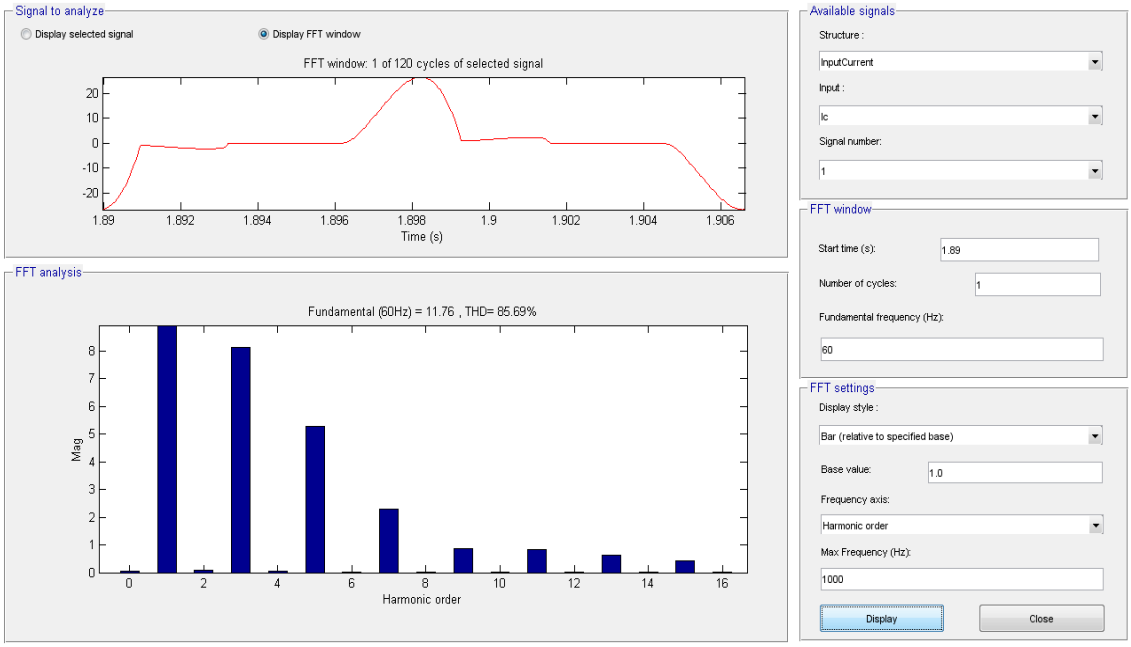

Figure 3.34: Three Phase Unbalanced Ic Harmonic Spectrum Graph

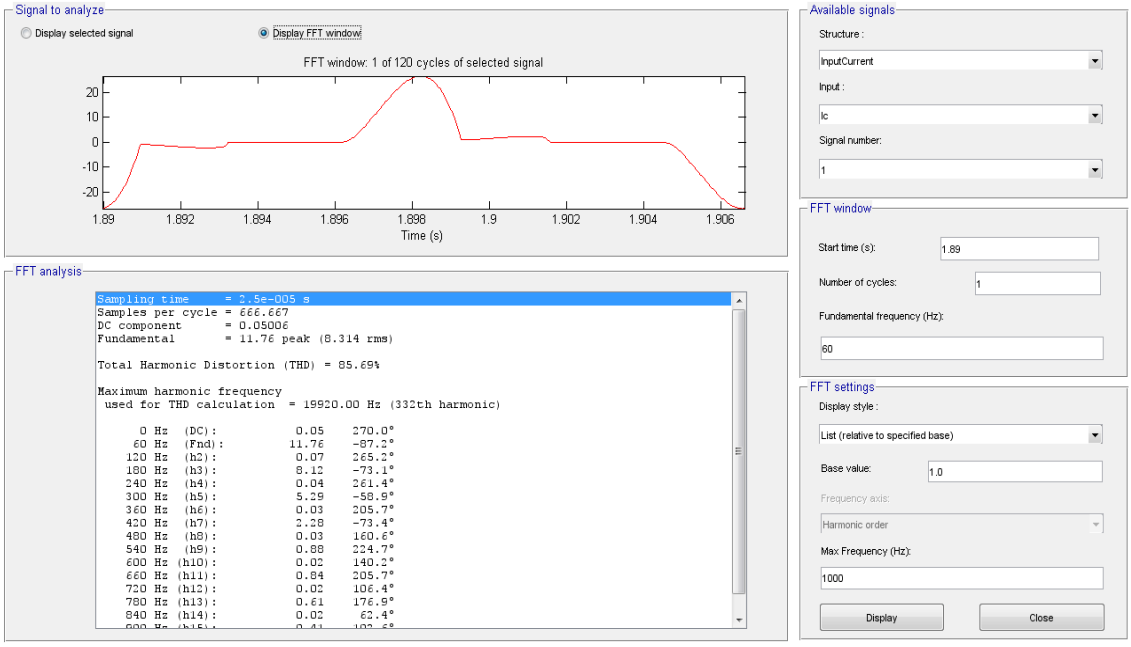

Figure 3.35: Three Phase Unbalanced Ic Harmonic Spectrum Table

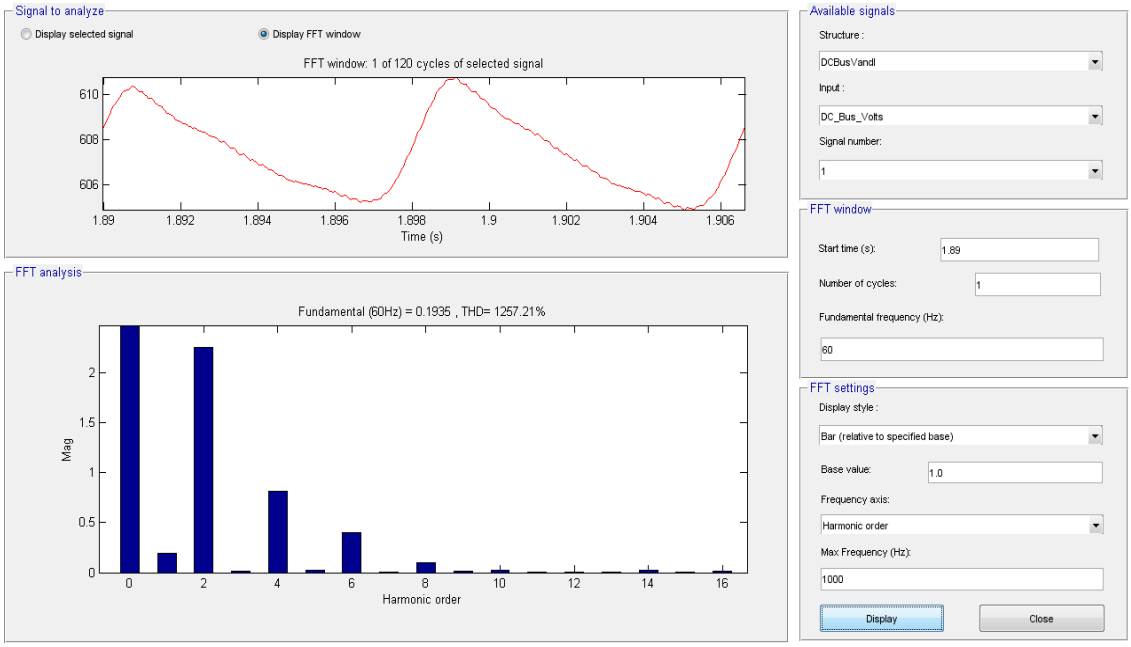

Figure 3.36: Three Phase Unbalanced DC Bus Voltage Harmonic Spectrum Graph

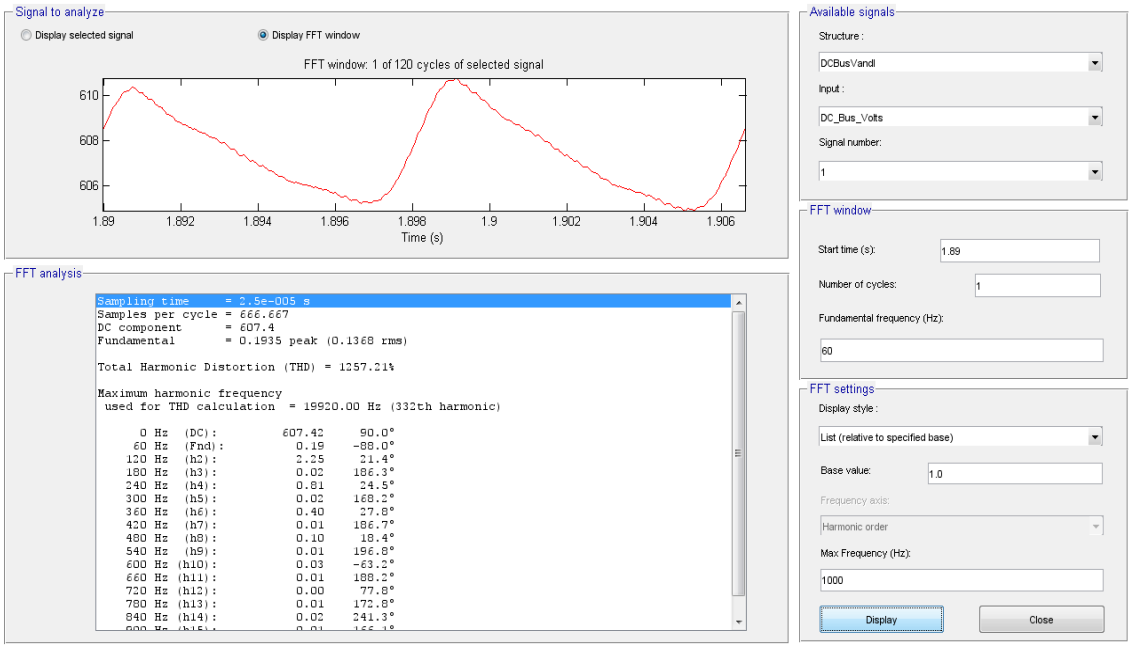

Figure 3.37: Three Phase Unbalanced DC Bus Voltage Harmonic Spectrum Table

3.3.4 Unbalanced Voltage Conditions with DC Bus Filters Simulation

Figure 3.38 shows the Simulink® circuit diagram for the variable frequency drive running a motor under unbalanced voltage conditions. Two notch filters were added to the DC minus side of the DC bus. The approximate voltage unbalance on the input is now 3.4%.

Figure 3.39 and 3.40 show the input voltage waveforms respectively. The waveforms show that the voltage and current waveforms still vary from one phase to the next. The characteristic harmonics are still present in each phase and they also vary from one phase to the next. The THD for Vab=9.00%, Vbc=9.22%, Vca=3.47%, Ia=59.15%, Ib=25.02%, and Ic=65.38%. Figure 3.41 and 3.42 show the FFT spectrum graph and table for Vab respectively. Figure 3.43 and 3.44 show the FFT spectrum graph and table for Vbc respectively. Figure 3.45 and 3.46 show the FFT spectrum graph and table for Vca respectively. Figure 3.47 and 3.48 show the FFT spectrum graph and table for Ia respectively. Figure 3.49 and 3.50 show the FFT spectrum graph and table for Ib respectively. Figure 3.51 and 3.52 show the FFT spectrum graph and table for Ic respectively. Figure 3.53 and 3.54 show the harmonic spectrum graph and table for the DC bus voltage. It is interesting to note that the voltage ripple is now about 2 volts.

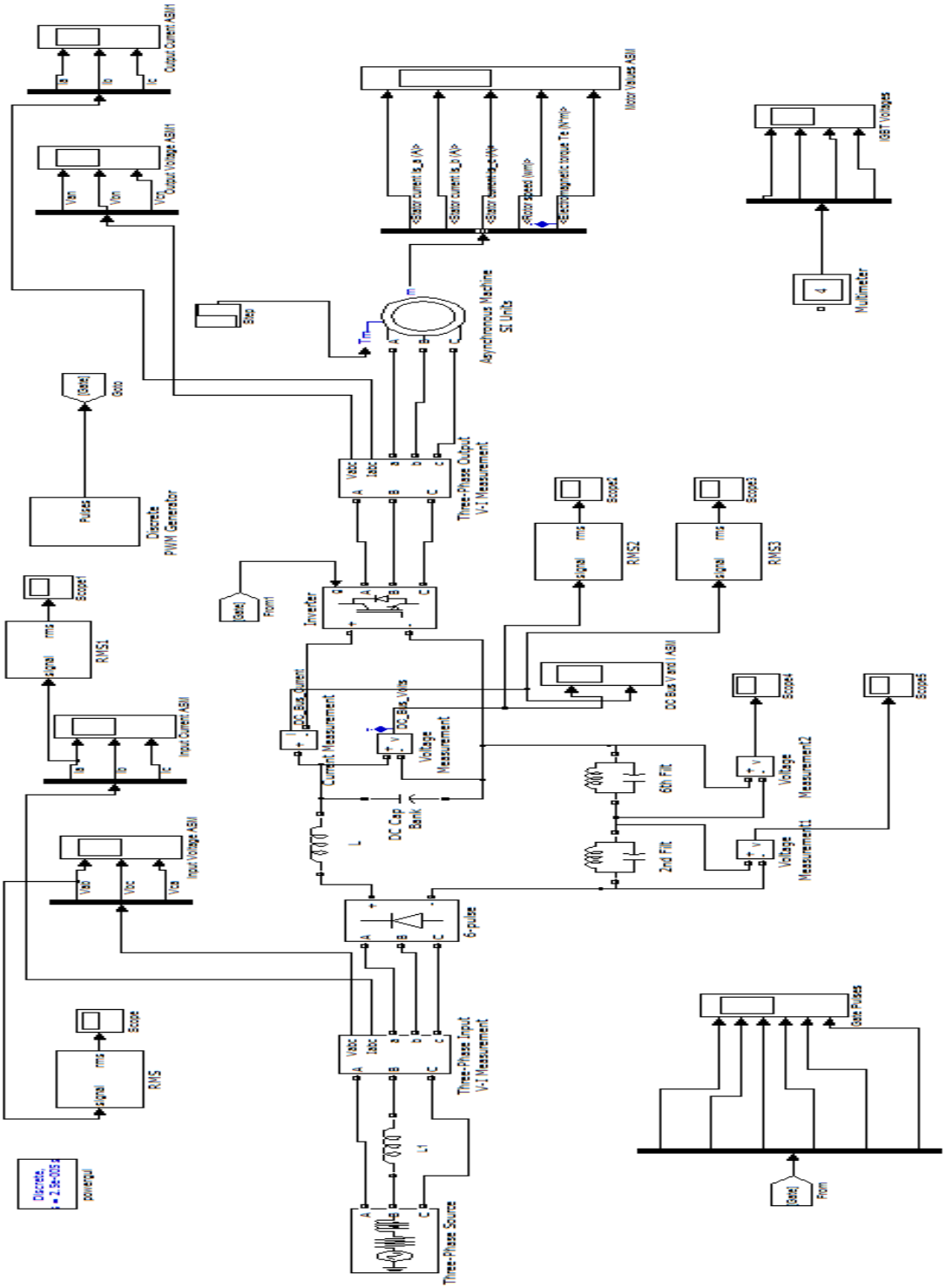

Figure 3.38: Three Phase Unbalanced Voltage Circuit with Filters Simulation

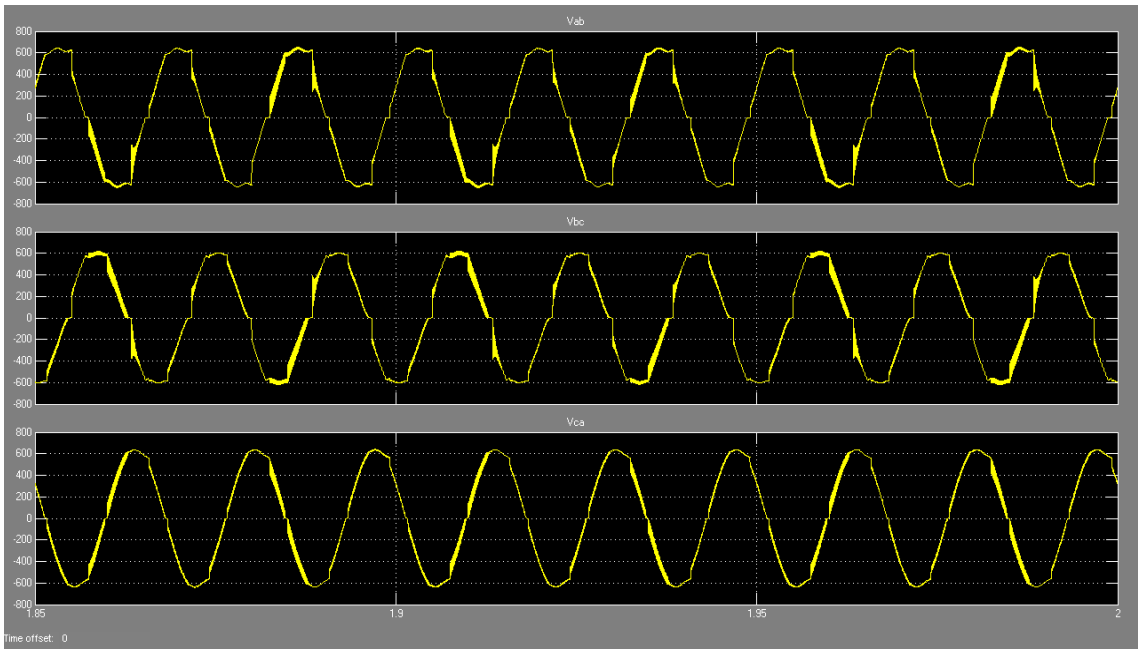

Figure 3.39: Three Phase Unbalanced Voltage with Filters Waveform

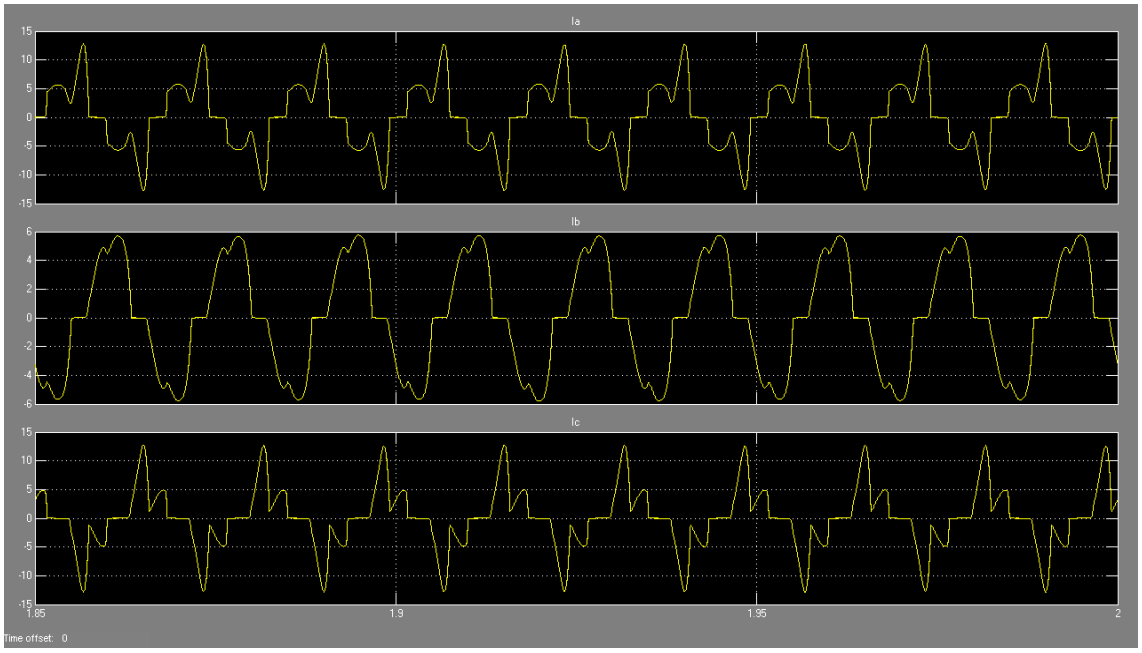

Figure 3.40: Three Phase Unbalanced Current with Filters Waveform

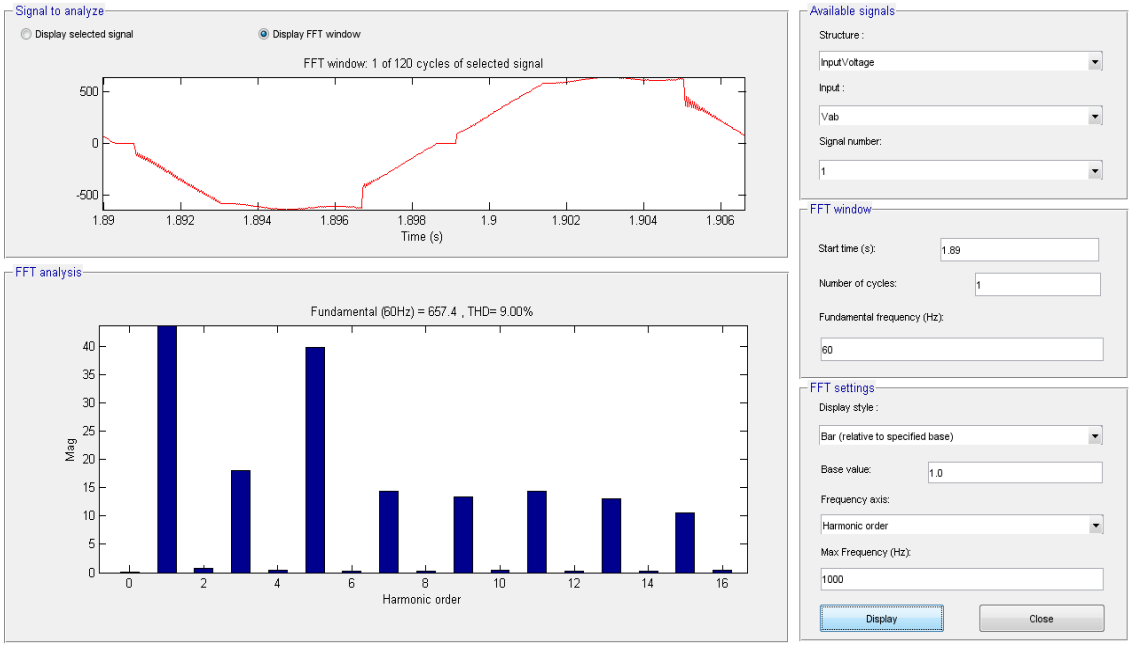

Figure 3.41: Three Phase Unbalanced Vab with Filters Harmonic Spectrum Graph

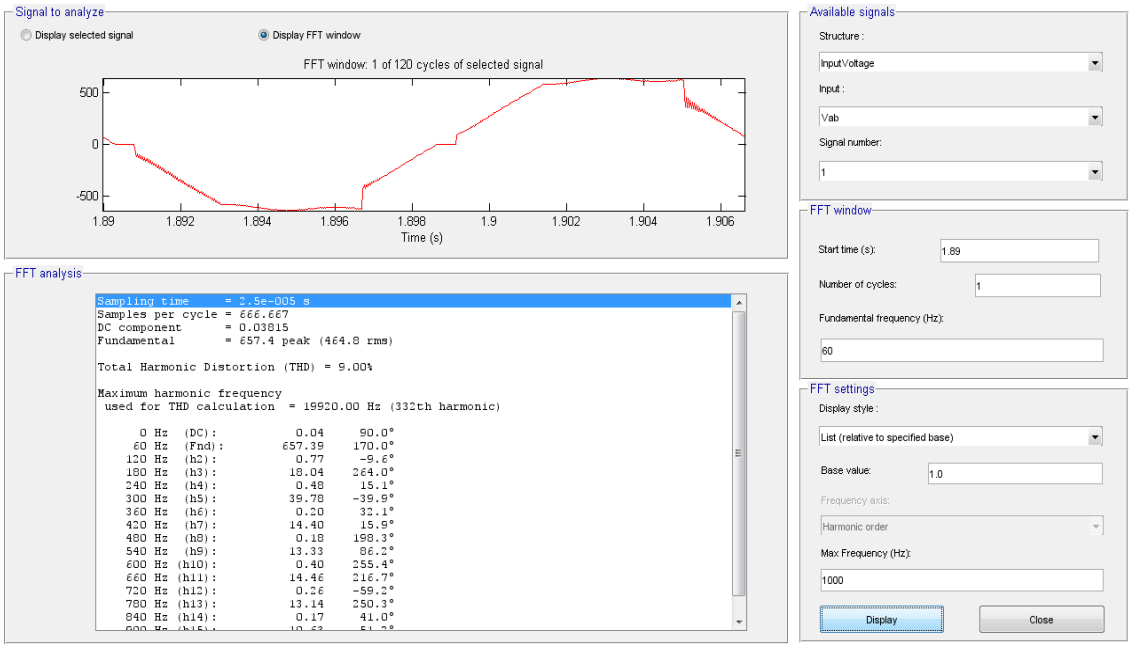

Figure 3.42: Three Phase Unbalanced Vab with Filters Harmonic Spectrum Table

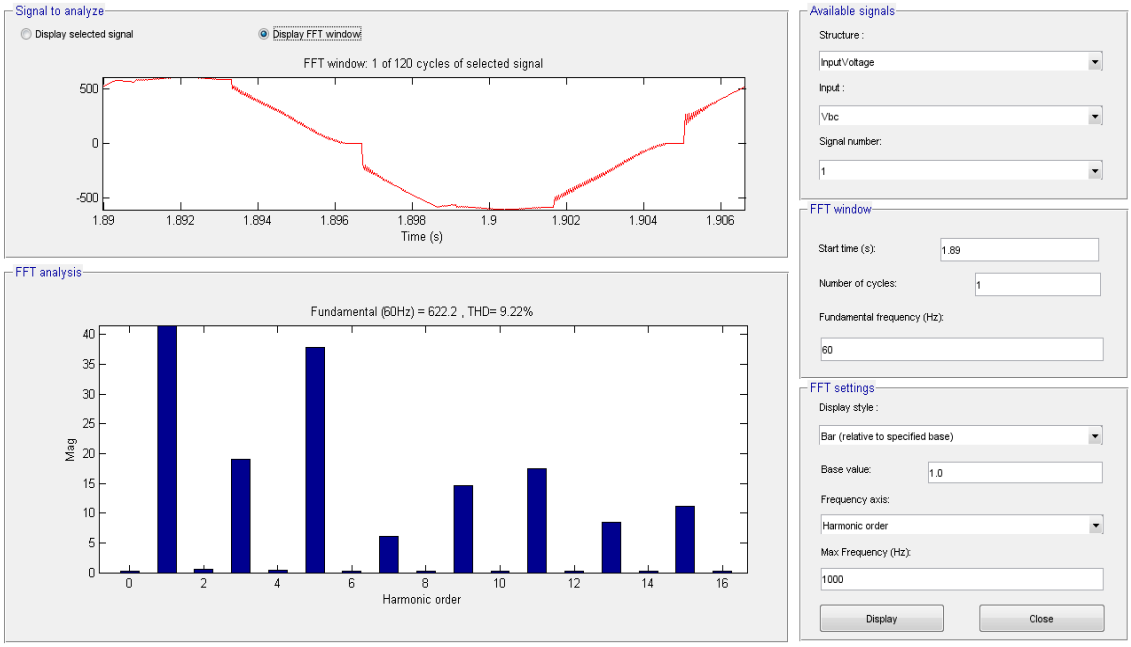

Figure 3.43: Three Phase Unbalanced Vbc with Filters Harmonic Spectrum Graph

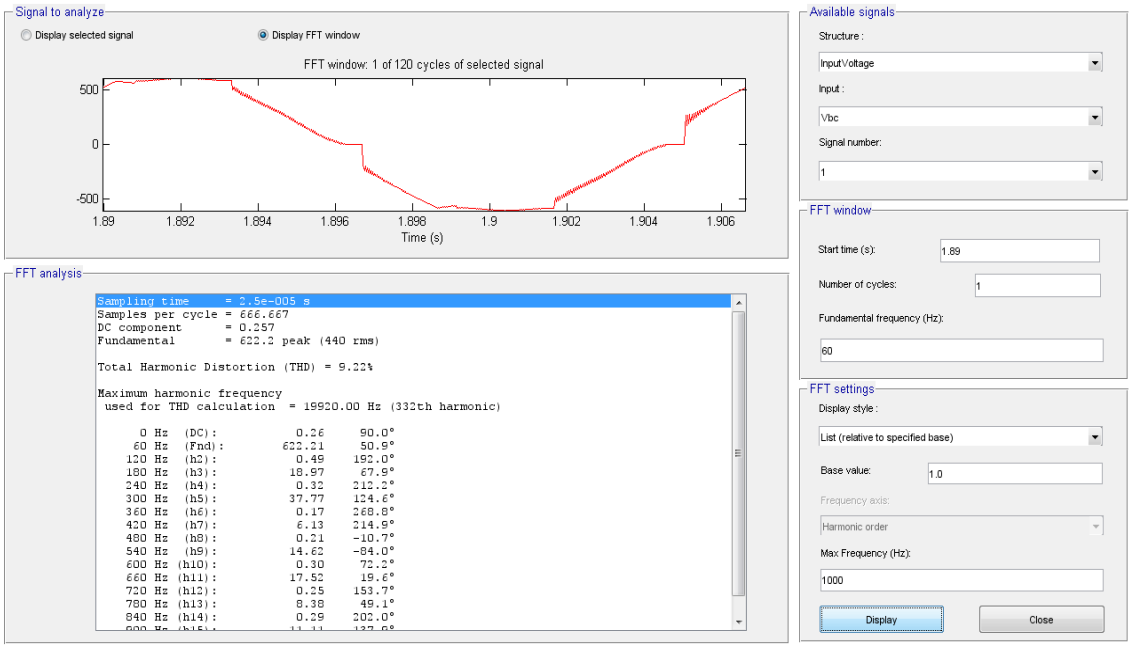

Figure 3.44: Three Phase Unbalanced Vbc with Filters Harmonic Spectrum Table

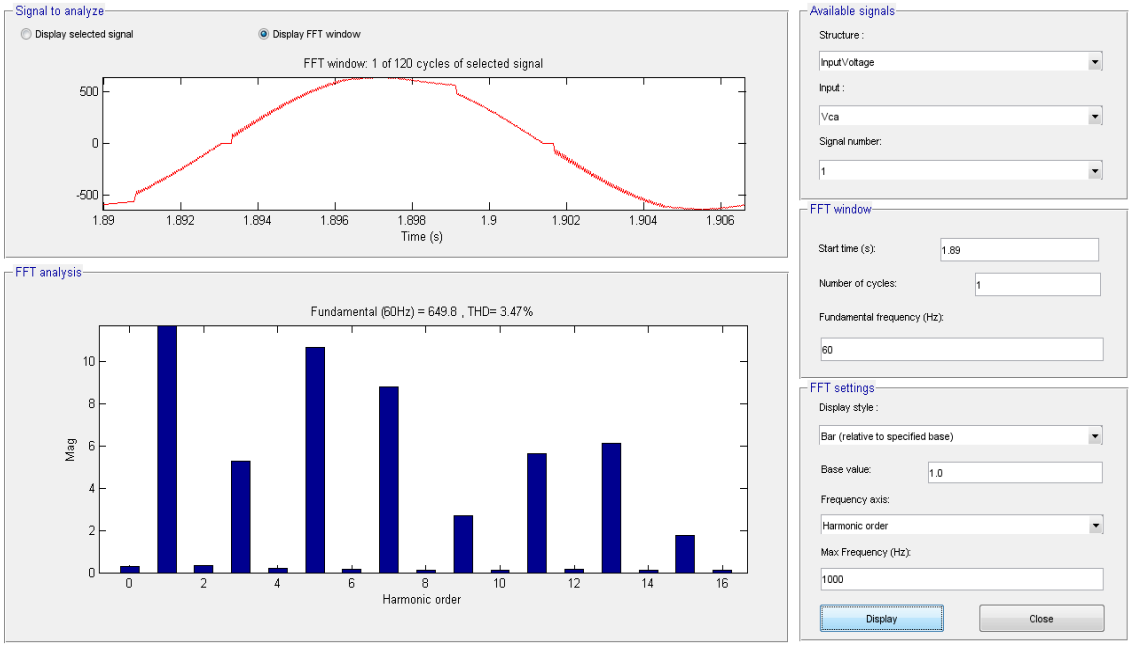

Figure 3.45: Three Phase Unbalanced Vca with Filters Harmonic Spectrum Graph

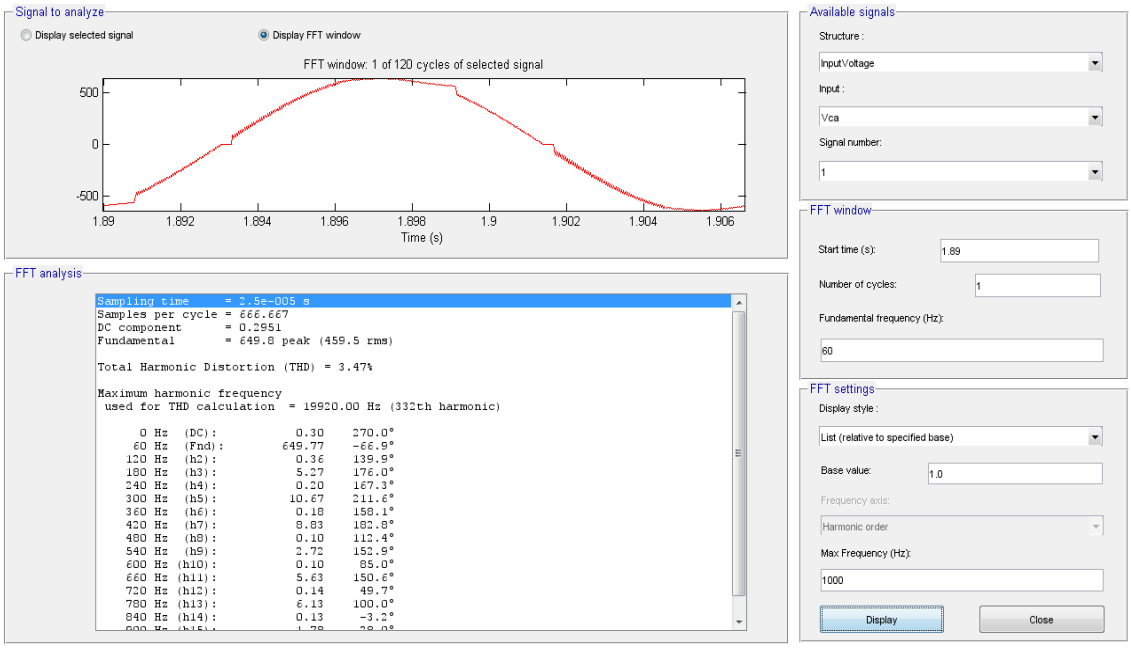

Figure 3.46: Three Phase Unbalanced Vca with Filters Harmonic Spectrum Table

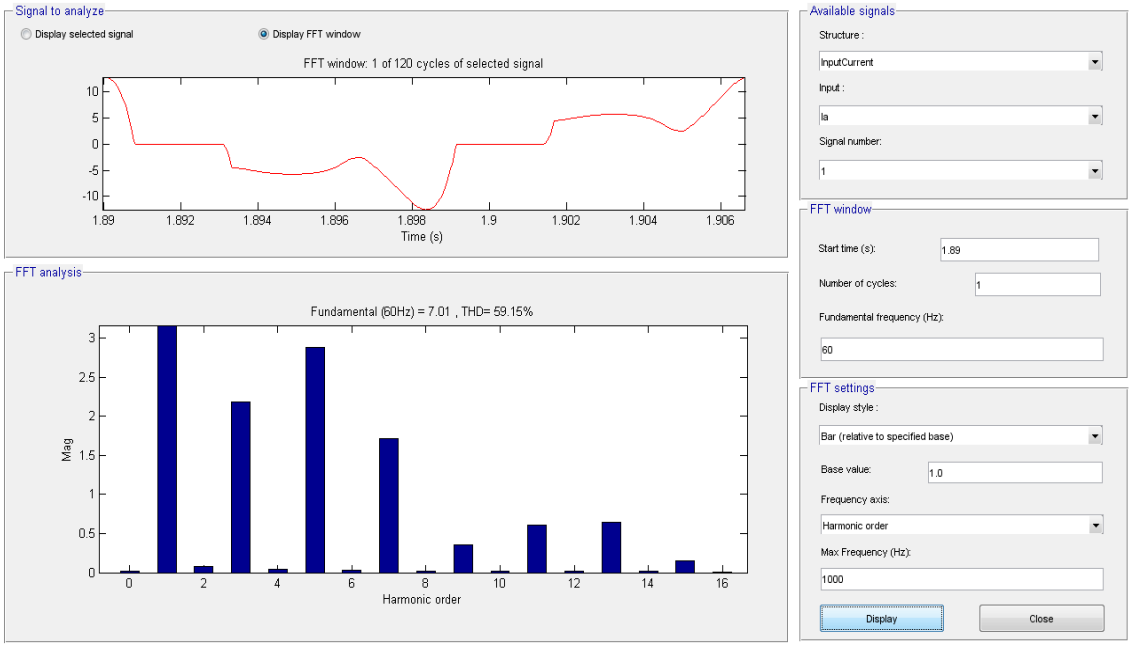

Figure 3.47: Three Phase Unbalanced Ia with Filters Harmonic Spectrum Graph

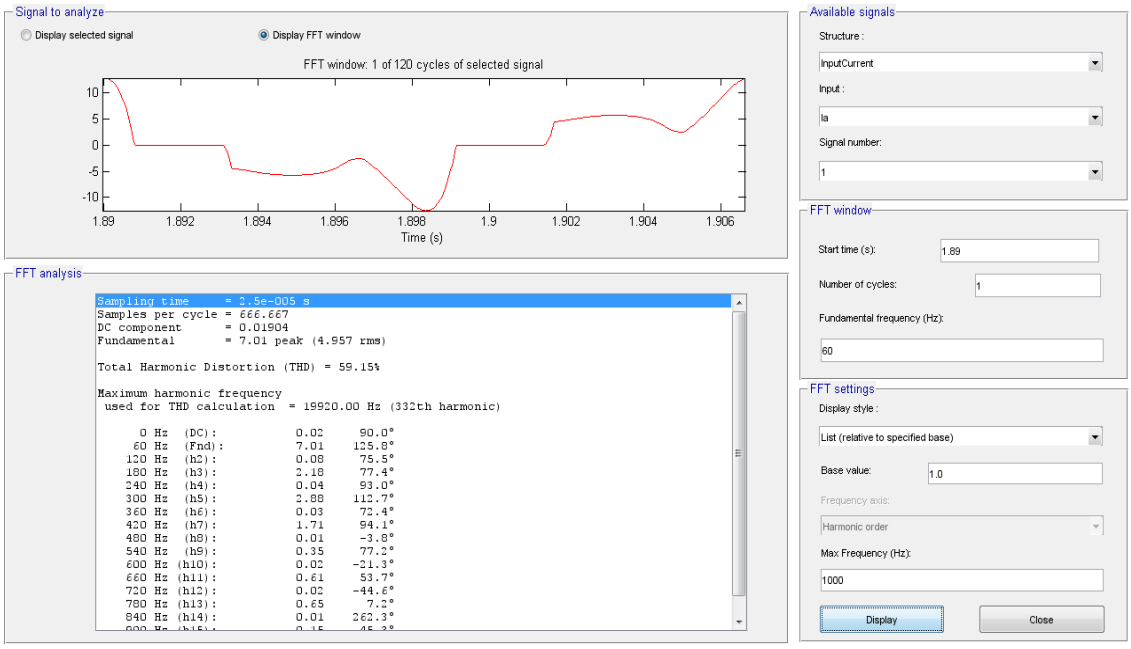

Figure 3.48: Three Phase Unbalanced Ia with Filters Harmonic Spectrum Table

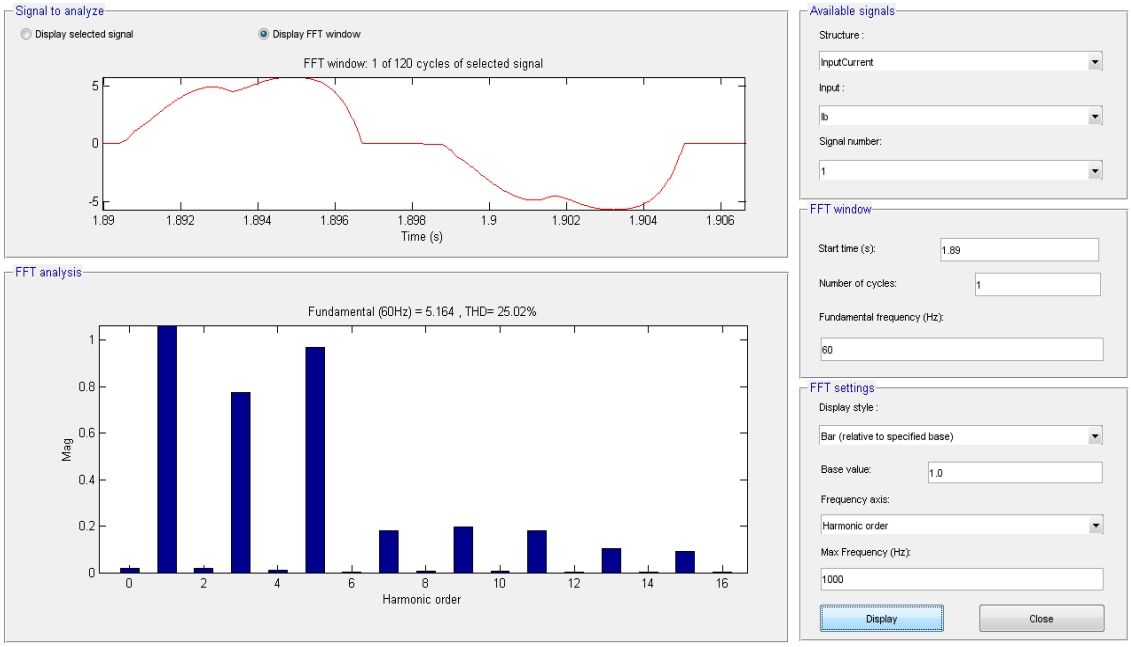

Figure 3.49: Three Phase Unbalanced Ib with Filters Harmonic Spectrum Graph

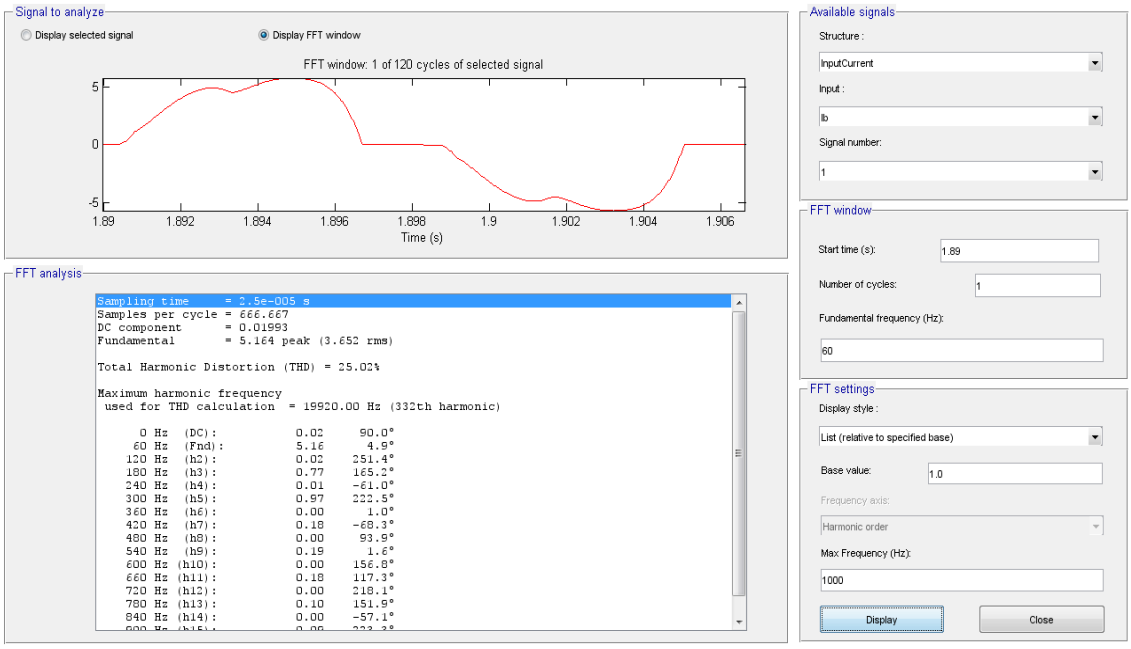

Figure 3.50: Three Phase Unbalanced Ib with Filters Harmonic Spectrum Table

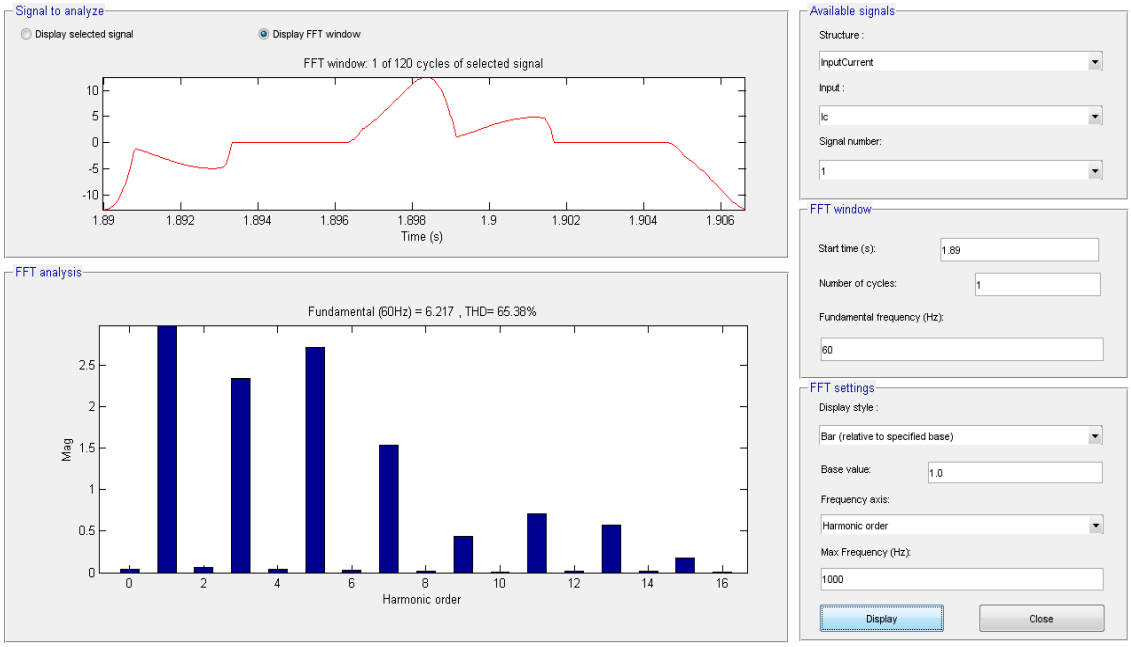

Figure 3.51: Three Phase Unbalanced Ic with Filters Harmonic Spectrum Graph

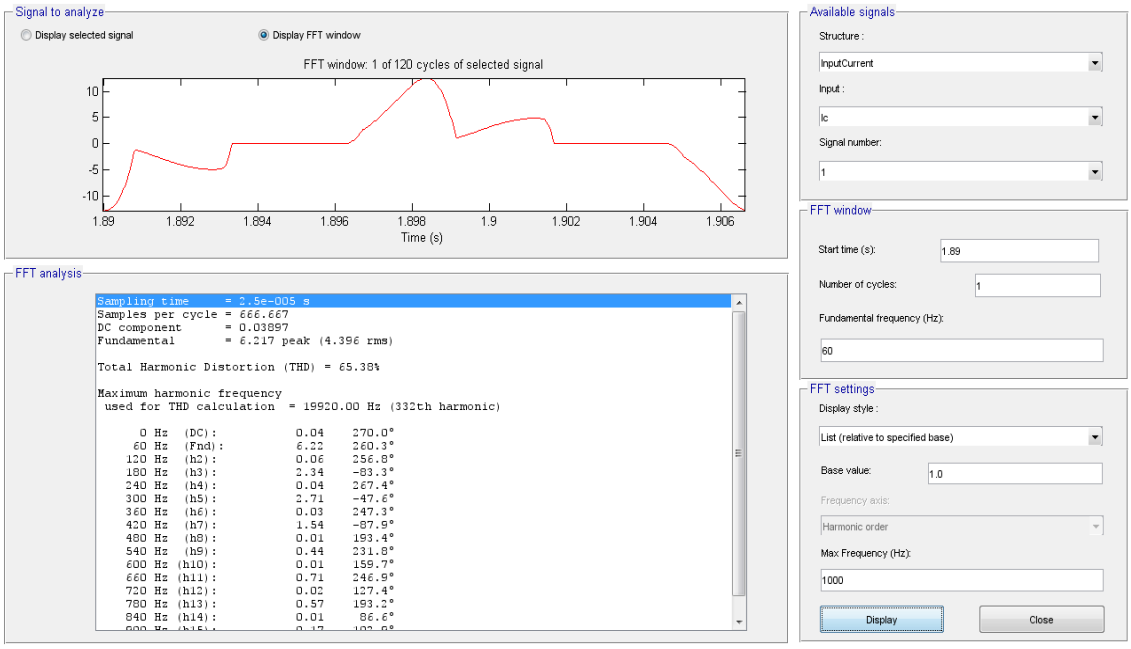

Figure 3.52: Three Phase Unbalanced Ic with Filters Harmonic Spectrum Table

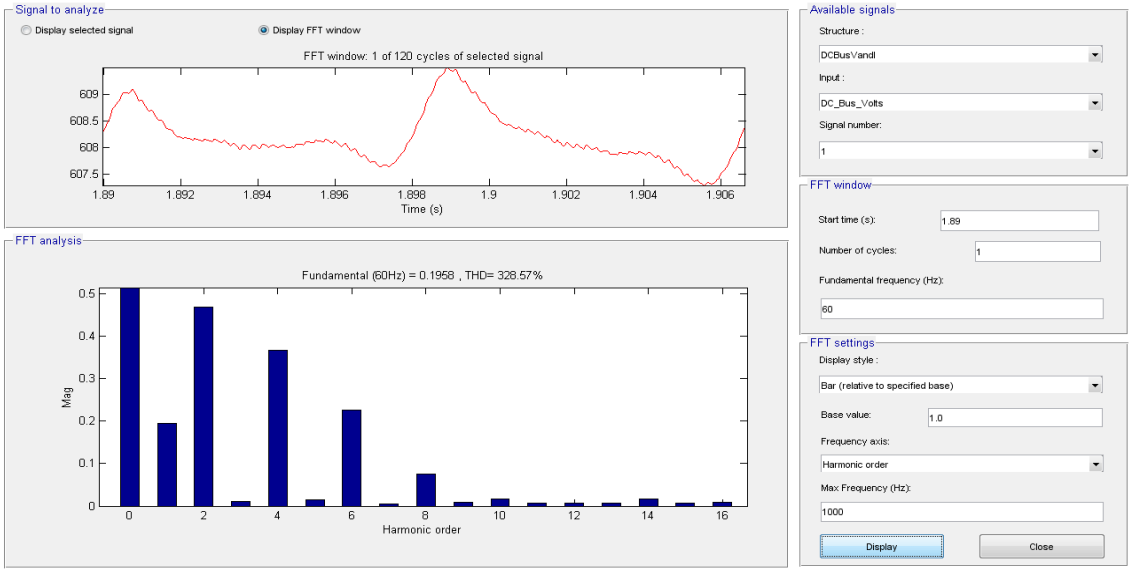

Figure 3.53: Three Phase Unbalanced DC Bus Voltage with Filters Harmonic Spectrum Graph

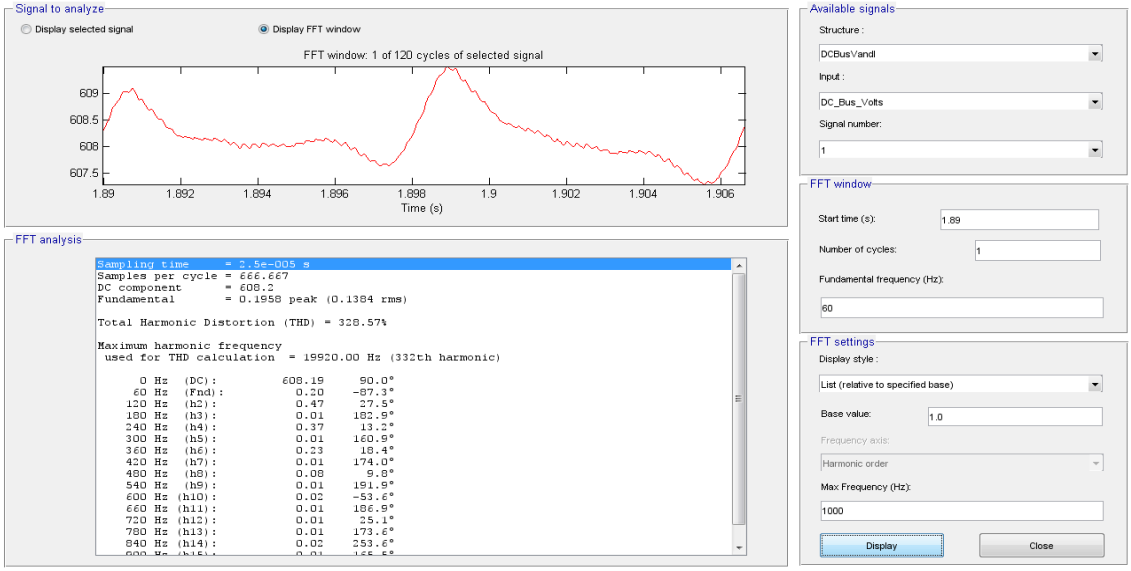

Figure 3.54: Three Phase Unbalanced DC Bus Voltage with Filters Harmonic Spectrum Table

3.4 Simulation Summary

Simulation Results														
Configuration	Input Voltage RMS (V)			Input Current RMS (A)			Input Voltage THD			Input Current THD			DC Bus 2^{nd}	DC Bus Approx
	V_{ab}	V_{bc}	V_{ca}	I_a	I_b	I_c	V_{ab}	V_{bc}	V_{ca}	I_a	I_b	I_c	Harmonic (V)	Voltage Ripple (V)
0% Unbalance no Filter	469	469	469	4.69	4.70	4.69	5.11%	4.40%	4.56%	79.94%	79.98%	79.95%	0.5	2
3.1% Unbalance no Filter	460	440	462	8.12	1.88	8.31	13.55%	11.76%	7.31%	73.75%	33.18%	85.69%	2.25	5
3.1% Unbalance with Filter	465	440	460	4.96	3.65	4.4	9.00%	9.22%	3.47%	59.15%	25.02%	65.38%	0.47	2

Table 3.3: Simulation Results Table

Table 3.3 shows the RMS values for input voltage and current, input THD for voltage and current, the voltage magnitude of the second harmonic on the DC bus, and the voltage ripple on the DC bus, for the three simulation scenarios presented in this section. Some observations can be made from Table 3.3. One observation is the introduction of voltage unbalance leads to a disproportionate distribution of current among the three phases. The second observation is the presence of voltage unbalance leads to a larger variance in THD between the three phases. Thirdly, the magnitude of the second harmonic on the DC bus increases greatly and the DC bus voltage ripple more than doubles.

With the presence of the DC bus filters, even with voltage unbalance present, the current is more evenly distributed between the three phases and the input voltage and current THD, the DC bus second harmonic voltage, and the DC bus voltage ripple all reduce. This shows the presence of the filters improve the stability of the DC bus and in turn improve the performance of the VFD under the presence of voltage unbalance.

Chapter 4

Experimentation

4.1 Experimental Set Up

An experiment was carried out based on the information presented earlier in this paper. The experimental set up mirrored the simulations presented in prior sections. in the experimental set up a 27KVA transformer was used to power a 38KVA AC drive, which would run a 3HP AC motor. The 3HP AC motor was mechanically coupled to a 3HP DC motor. The DC motor would simulate the load on the AC motor. The DC motor was then ran by a 125HP DC drive. The experimental set up was used a 6.5mH line reactor to simulate the voltage unbalance conditions.

Figure 4.1 and 4.2 show the 27KVA power transformer and power transformer nameplate respectively. Figure 4.3 shows the mechanically coupled AC and DC motor. Figure 4.4 and 4.5 show the AC motor nameplate and DC motor nameplate respectively. Figure 4.6 and 4.7 show the AC drive and AC drive nameplate respectively. Figure 4.8 and 4.9 show the DC drive and DC drive nameplate respectively. Figure 4.10 shows the line reactor used to simulate the voltage unbalance. Figure 4.11 and 4.12 show the second order filter and sixth order filter respectively.

Figure 4.1: Power Transformer

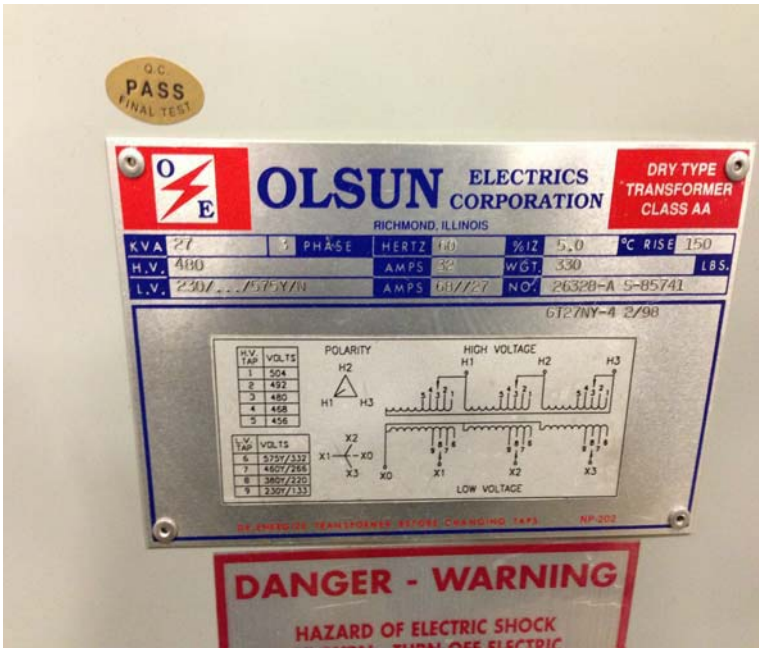

Figure 4.2: Power Transformer Data Nameplate

Figure 4.3: Coupled AC and DC motors

Figure 4.4: AC Motor Data Nameplate

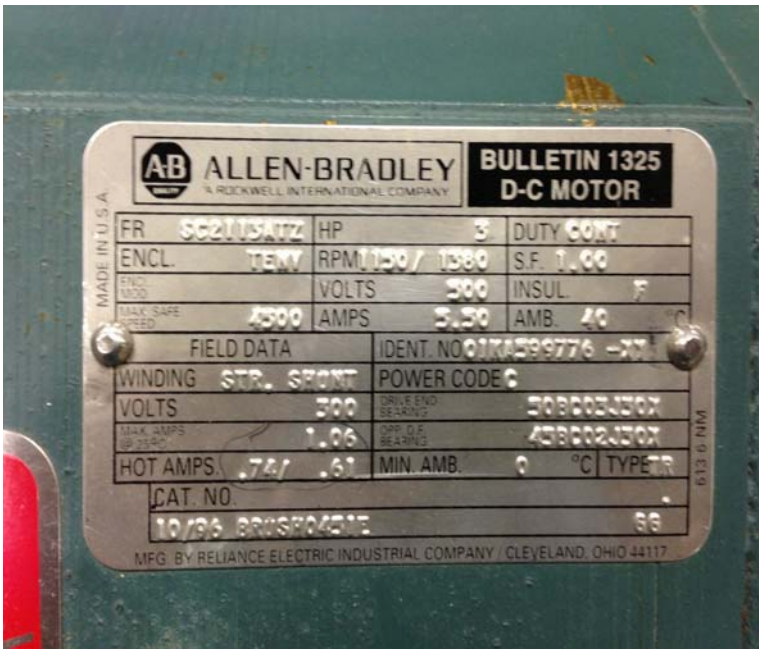

Figure 4.5: DC Motor Data Nameplate

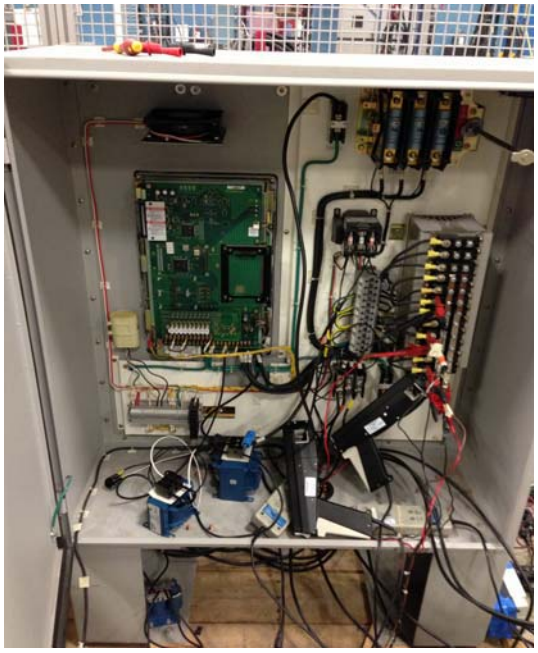

Figure 4.6: AC Drive

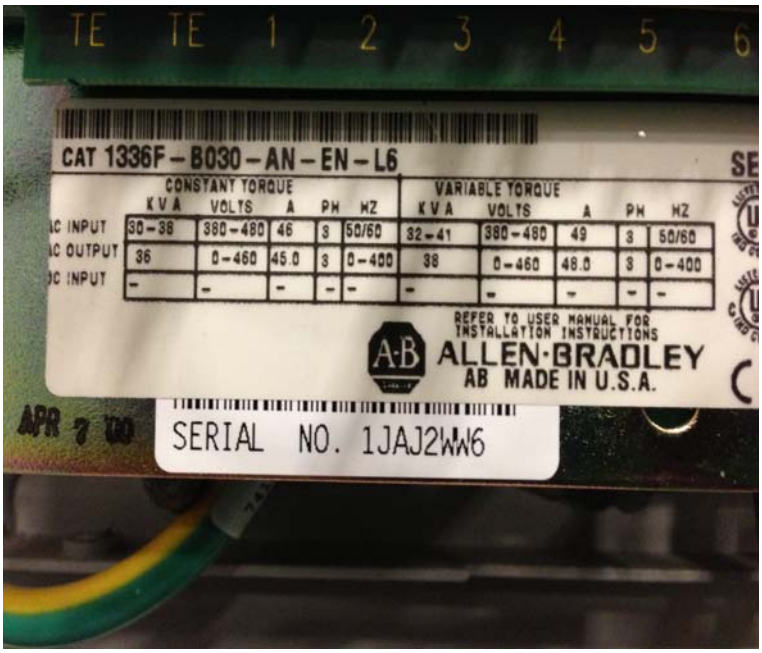

Figure 4.7: AC Drive Nameplate

Figure 4.8: DC Drive

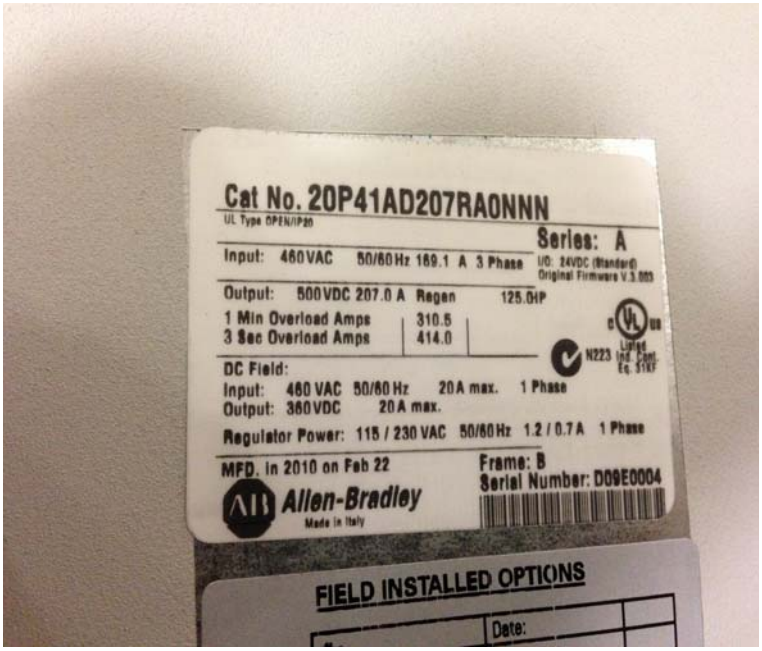

Figure 4.9: DC Drive Nameplate

Figure 4.10: Line Reactor Used to Create Voltage Unbalance

Figure 4.11: Second Order Notch Filter

Figure 4.12: Sixth Order Notch Filter

4.2 Experimentation Results

4.2.1 Balanced Voltage Conditions Experimentation

The first portion of the experiment began with signal readings under balanced voltage conditions. The following data was collected. Figure 4.13 show the voltage and current waveforms for all three phases. Figure 4.14 shows the RMS values for voltage and current on all three phases along with some other circuit parameters. Figure 4.15 shows the Vab voltage, Ib current, the DC bus voltage and DC bus current.

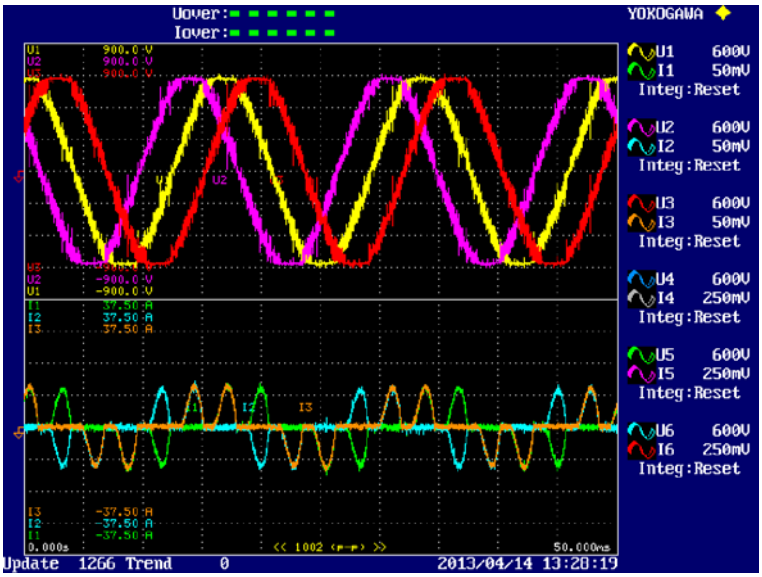

Figure 4.13: Experimental Balanced Three Phase Voltage and Current Waveforms

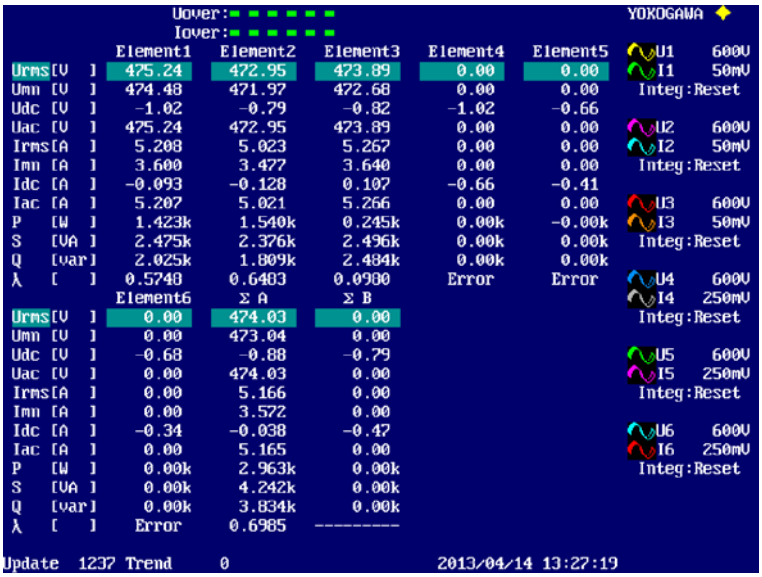

Figure 4.14: Experimental Balanced Three Phase Parameter Values

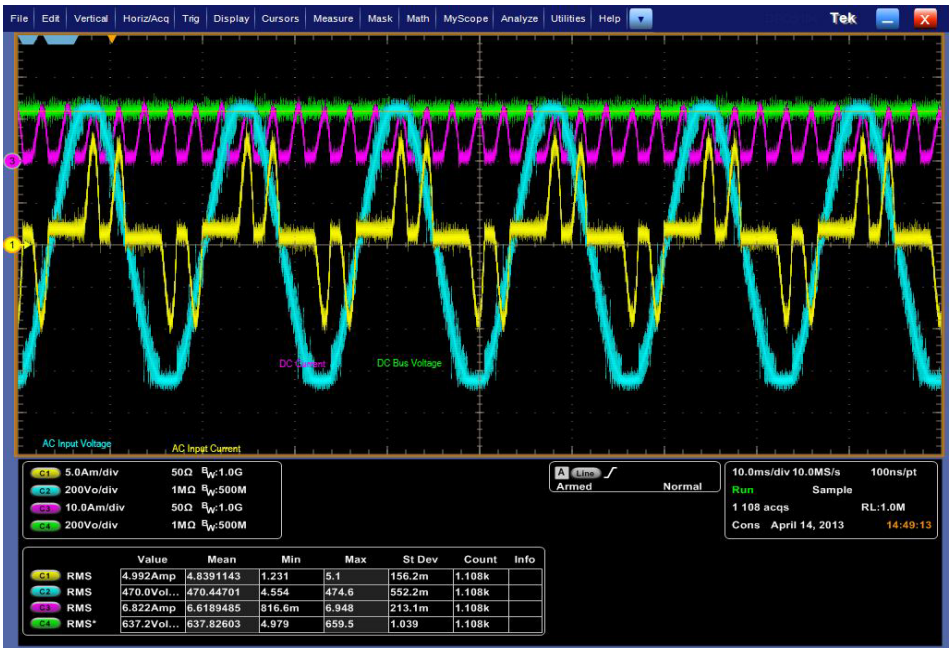

Figure 4.15: Experimental Balanced Vab, Ib, DC Bus Voltage and Current

4.2.2 Unbalanced Voltage Conditions Experimentation

The second portion of the experiment continued with signal readings under unbalanced voltage conditions. The following data was collected. Figure 4.16 show the voltage and current waveforms for all three phases. Figure 4.17 shows the RMS values for voltage and current on all three phases along with some other circuit parameters. Figure 4.18 shows the Vab voltage, Ib current, the DC bus voltage and DC bus current.

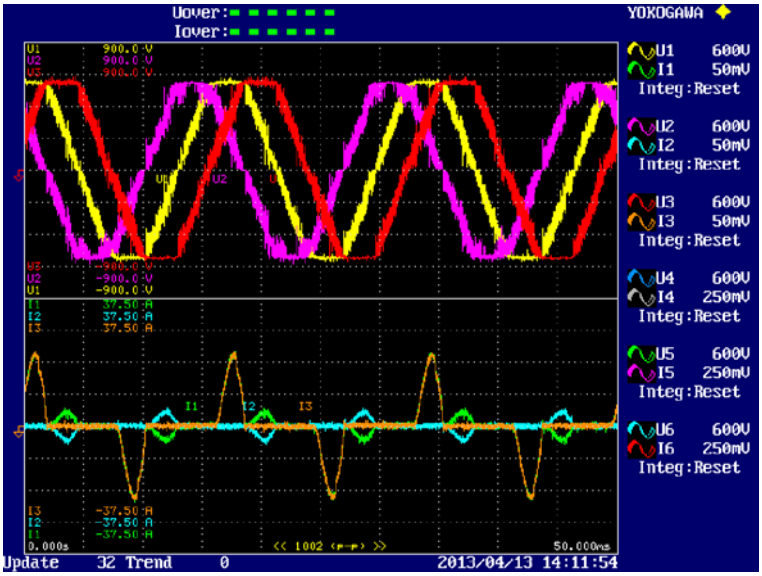

Figure 4.16: Experimental Unbalanced Three Phase Voltage and Current Waveforms

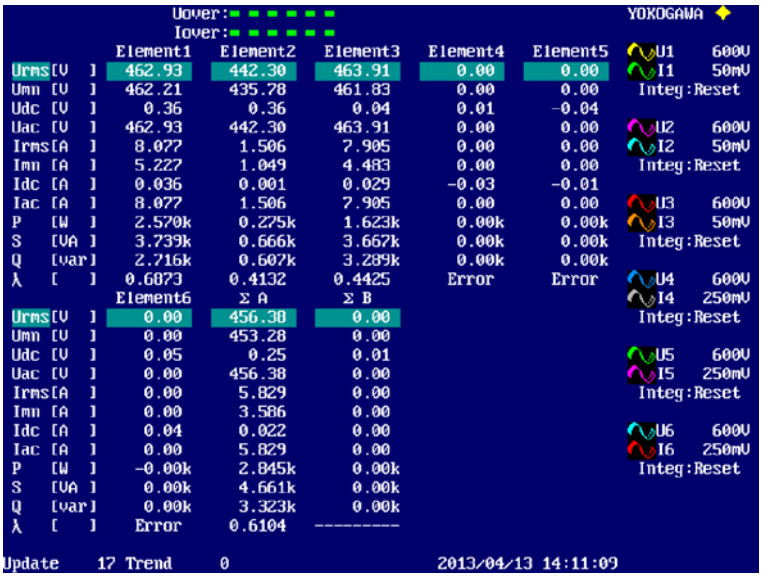

Figure 4.17: Experimental Unbalanced Three Phase Parameter Values

Figure 4.18: Experimental Unbalanced Vab, Ib, DC Bus Voltage and Current

4.2.3 Unbalanced Voltage Conditions With DC Filters Experimentation

The third portion of the experiment continued with signal readings under unbalanced voltage conditions with the passive filters on the DC bus of the AC drive. The following data was collected. Figure 4.19 show the voltage and current waveforms for all three phases. Figure 4.20 shows the RMS values for voltage and current on all three phases along with some other circuit parameters. Figure 4.21 shows the Vab voltage, Ib current, the DC bus voltage and DC bus current.

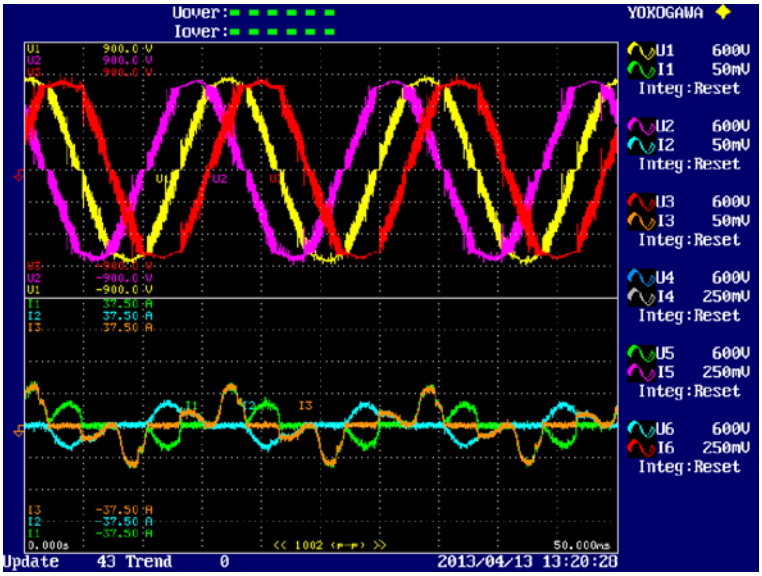

Figure 4.19: Experimental Unbalanced Three Phase With DC Filters Voltage and Current Waveforms

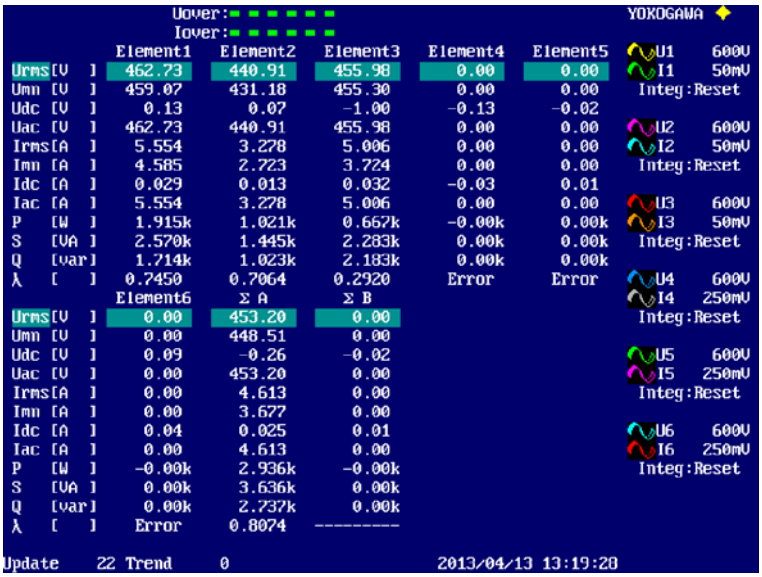

Figure 4.20: Experimental Unbalanced Three Phase With DC Filters Parameter Values

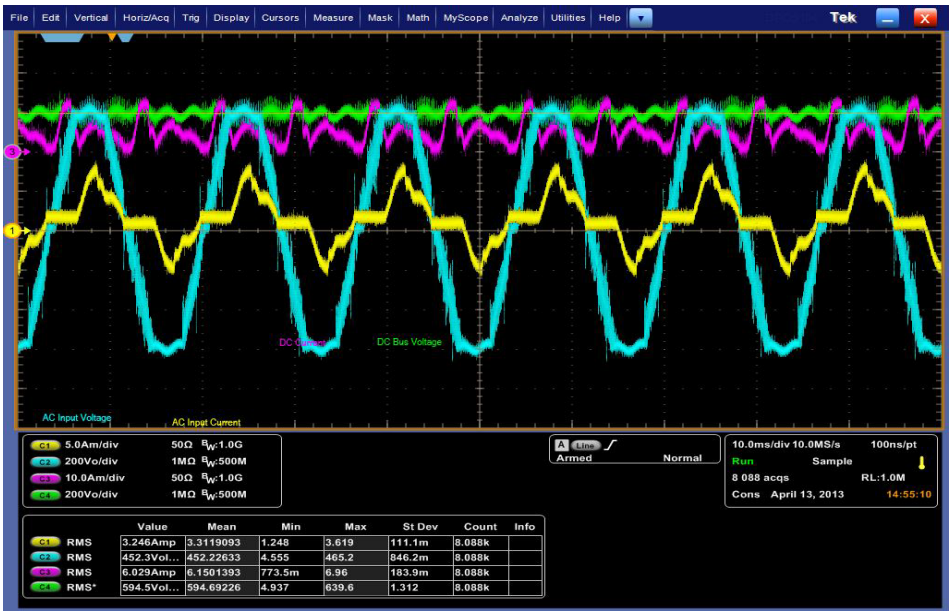

Figure 4.21: Experimental Unbalanced With DC Filters Vab, Ib, DC Bus Voltage and Current

4.3 Experimentation Summary

Experimentation Results												
Configuration	Input Voltage RMS (V)			Input Current RMS (A)			Input Voltage THD			Input Current THD		
	V_{ab}	V_{bc}	V_{ca}	I_a	I_b	I_c	V_{ab}	V_{bc}	V_{ca}	I_a	I_b	I_c
0% Unbalance no Filter	475	473	474	5.20	5.00	5.30	2.84%	2.33%	2.58%	70.44%	70.11%	69.50%
3.1% Unbalance no Filter	463	442	464	8.00	1.50	7.90	3.85%	5.00%	5.65%	68.97%	74.60%	75.30%
3.1% Unbalance with Filter	463	441	456	5.60	3.30	5.00	3.54%	4.44%	3.79%	52.12%	42.00%	66.38%

Table 4.1: Experimentation Results Table

Table 4.1 shows the RMS values for input current and voltage and the THD values for voltage and current. Some important observations can be made from Table 4.1. One is, just as in the system simulation, the introduction of voltage unbalance leads to a disproportionate distribution of current among the three phases. Also, the presence of voltage unbalance leads to a larger variance in the THD between the three phases. The experimental result in earlier sections of this paper show that the presence of voltage unbalance leads to a flat-topping effect in the voltage waveform, which indicates the presence of a third harmonic. In addition, the DC bus voltage waveform exhibits not only increased voltage ripple, but also inconsistent bus voltage stability, with some regions having less voltage ripple than others.

With the presence of the DC bus filters, even with voltage unbalance, just as in the system simulation, the current is more evenly distributed between the three phases and the input voltage and current THD, all reduce. The input voltage waveforms show reduced flat-topping, which means a reduction in the third harmonic on the input of the VFD and thus better DC bus voltage stability, which leads to improved VFD performance under the presence of voltage unbalance.

Chapter 5

Experimentation and Simulation Results Comparison

It should be noted the THD values for the input voltage and current do not exactly line up for multiple reasons. One reason is the difficulty involved in the simulation of the source in the experimental section. The actual experiment was conducted in a facility that contained unknown harmonic content on the distribution. It was difficult to determine and implement that harmonic content in Simulink®. Another reason for the value discrepancy is that Simulink® calculated the THD values based on the first 332 harmonics, while the experimentation section only used the first 100 harmonics to calculate THD. What should be taken away from the input THD values for the simulation and experimentation section is that their behaviors are very similar.

Chapter 6

Conclusion

The simulation and experimentation section of this paper conclude that a 6-pulse VFD under severe voltage unbalance conditions exhibit some notable characteristics. They include a disproportionate distribution of current among the three phases, a larger variance in the THD between the three phases, and an increase in the DC bus voltage ripple. The simulation and experimentation section of this paper then show the presence of notch filters on the DC bus improve the distribution of current among the three phases and improves DC bus voltage stability and in turn improves the VFD's capability to operate motor loads under voltage unbalance conditions.

Bibliography

[1] *Crest factor*, Tech. report, Ametek Programmable Power.

[2] Gary W. Chang and Paulo F. Ribeiro, *Harmonics theory*, Tech. report, Siemens Power T and D and BWX Technologies, Inc.

[3] D Yildirim C P Butterfield E Muljadi, T Batan, *Understanding the unbalanced-voltage problem in wind turbine generation*, "IEEE TRANSACTIONS ON INDUSTRY APPLICATIONS".

[4] Jeffrey Fessler, *Digital signal processing and analysis*, University Lecture, 2004.

[5] W. Mack Grady and Robert J. Gillskie, *Harmonics and how they relate to power factor*, EPRI Power Quality Issues and Opportunities Conference (PQA93) (San Diego, CA), November 1993.

[6] W. Mack Grady and Surya Santaso, *Understanding power system harmonics*, Tech. report, University of Texas at Austin and Electrotek Concepts, Inc.

[7] Zoher Z. Karu, *Signals and systems made ridiculously simple*, Zizi Press, Alabama, 1995.

[8] Ravindra S. Kashyap, *Waveguide resonators*, Tech. report, Indian Institute of Technology Bombay.

[9] William E. Berkopec Kevin Lee, Thomas M. Jahns and Thomas A. Lipo, *Closed-form analysis of adjustable-speed drive performance under input-voltage unbalance and sag conditions*, IEEE TRANSACTIONS ON INDUSTRY APPLICATIONS **42**.

[10] Arteche Power Quality, *Avoiding harmonic resonance with low pass harmonic filters*, Inteligent Power Quality.

[11] Maxim Raginsky, *Lecture xi: The fast fourier transform (fft) algorithm*, University Lecture, 2008.

[12] Todd Stroik, *System problems and electronic loads: harmonics, resonance, and commutation*, Netaworld.

[13] Daniel J. Carnovale Thomas M. Blooming, *Application of ieee std 519-1992 harmonic limits*, Tech. report, Eaton Electrical.

[14] Annette von Jouanne, *Assessment of voltage unbalance*, IEEE TRANSACTIONS ON POWER DELIVERY **16**.

[15] George J. Wakileh, *Power systems harmonics fundamentals, analysis, and filter design*, Springer-Verlag, New York, 2001.